

Multivalent Binding in Platinum Metal Complexes

Dissertation

Zur Erlangung des akademischen Grades
„Doktor der Naturwissenschaften“
im Fachbereich Biologie und Chemie
der Justus-Liebig-Universität Gießen



vorgelegt von

Biswa Nath Ghosh

aus Kolkata (Indien)

Gießen, im October 2011

Erstgutachter:	Prof. Dr. Sabine Schlecht
Zweitgutachter:	Prof. Dr. Siegfried Schindler
Abgabe der Dissertation im Prüfungsamt:	04.10.2011
Tag der mündlichen Prüfung:	21.11.2011

The present thesis was conducted in the period August 2008 to August 2011 at the Institute of Chemistry and Biochemistry of Freie University Berlin and at the Institute of Inorganic and Analytical Chemistry of Justus-Liebig-University Giessen, under the supervision of Prof. Dr. Sabine Schlecht.

I declare:

The present thesis was prepared by me and without illicit help from others. Any citations being included literally or by adaption from the literature or personal communications have been marked appropriately. The principles of best practice in academia, as documented in the respective charter of Justus-Liebig-University of Giessen have been applied in all investigations constituting this thesis.

Die vorliegende Arbeit wurde in der Zeit von August 2008 bis August 2011 am Institut für Chemie und Biochemie der Freien Universität Berlin und am Institut für Anorganische und Analytische Chemie der Justus-Liebig-Universität Gießen unter der Anleitung von Prof. Dr. Sabine Schlecht durchgeführt.

Ich erkläre:

Ich habe die vorgelegte Dissertation selbstständig und ohne unerlaubte fremde Hilfe und nur mit den Hilfen angefertigt, die ich in der Dissertation angegeben habe. Alle Textstellen, die wörtlich oder sinngemäß aus veröffentlichten Schriften entnommen sind, und alle Angaben, die auf mündlichen Auskünften beruhen, sind als solche kenntlich gemacht. Bei den von mir durchgeführten und in der Dissertation erwähnten Untersuchungen habe ich die Grundsätze guter wissenschaftlicher Praxis eingehalten, wie sie in der „Satzung der Justus-Liebig-Universität Gießen zur Sicherung guter wissenschaftlicher Praxis“ niedergelegt sind.

Gießen, den 04.10.2011

Biswa Nath Ghosh

Dedicated To
My Beloved
Parents

Abstract*

In this doctoral thesis, iodotrimethylplatinum(IV) complexes of different pyridine and 2,2'-bipyridine ligands are investigated. The crystal structures of both the mononuclear and dinuclear pyridine complexes reveal an octahedral coordination around the platinum(IV) and a *facial* arrangement of the methyl groups. The crystal structure of the dinuclear complexes confirms that the iodide ligand acts as a bridging ligand that holds the two platinum metal ions together.

The reaction of the mononuclear pyridine complexes with iodotrimethylplatinum(IV) in chloroform results in the formation of the corresponding dinuclear complexes (both *cis* and *trans* isomers) of pyridines. Although the pyridine substituents have no significant influence on the crystal structures of either the mononuclear or the dinuclear complexes, the equilibrium population of these complexes in solution depends largely on the electronic effect of the pyridine substituent as well as on the steric bulk of the pyridine substituent.

Iodotrimethylplatinum(IV) on treatment with 2,2'-bipyridine and its derivatives gives mononuclear 2,2'-bipyridine complexes. The crystal structure of the bipyridine complexes confirms the *fac*-octahedral coordination of the trimethylplatinum moiety and the bidentate coordination of the 2,2'-bipyridines. Bond length comparison shows that Pt-N bond distances in bipyridine complexes are slightly shorter than in the corresponding pyridine complexes, reflecting the better π -acceptor character of the 2,2'-bipyridines. In addition, the N-Pt-N bite angle in the bipyridine complexes is much lower than in the pyridine complexes. It was also observed that in the crystal packing of 4,4'-Dichloro-2,2'-bipyridine complex of iodotrimethylplatinum(IV), intermolecular non-covalent interaction between methyl hydrogen and chlorine atom leads to the formation of *zig-zag* chain structures, which are linked through weak π - π interactions to form two-dimensional layer structure.

The reaction of iodotrimethylplatinum(IV) complexes of pyridines with the corresponding 2,2'-bipyridines lead to the substitution of ligands resulting in the formation of chelate bipyridine complexes. The equilibrium for these substitution reactions strongly favours the formation of chelate products. The formation of chelate complexes in solution at equilibrium depends largely on the electronic effect of the substituent as well as on the nature of the solvent.

Abstract (in German Language)*

In dieser Arbeit wurden Iodidotrimethylplatin(IV)-Komplexe mit verschiedenen Pyridin- und 2,2'-Bipyridin-Liganden untersucht. Die Kristallstrukturen von sowohl mononuklearen und dinuklearen Pyridin-Komplexen zeigen eine oktaedrische Koordination des Platin(IV) und eine *faciale* Anordnung der Methylgruppen. Die Kristallstrukturen von dinuklearen Komplexen bestätigen, dass der Iodid-Ligand als verbrückender Ligand, der zwei Platin-Ionen zusammenhält, dient.

Die Reaktion von mononuklearen Pyridin Komplexen mit Iodidotrimethylplatin(IV) in Chloroform resultiert in der Bildung des entsprechenden dinuklearen Pyridinkomplexes (sowohl *cis*- als auch *trans*-Isomer). Obwohl die Pyridinsubstituenten keinen signifikanten Einfluss auf die Kristallstruktur sowohl von mononuklearen als auch von dinuklearen Komplexen haben, hängt das Gleichgewichtsverhältnis beider Spezies in Lösung zu einem großen Teil von den elektronischen Einflüssen der Substituenten, sowie deren sterischem Anspruch ab.

Die Reaktion von Iodidotrimethylplatin(IV) mit 2,2'-Bipyridin und dessen Derivaten erzeugt mononukleare 2,2'-Bipyridin-Komplexe. Die Kristallstrukturen der Bipyridin-Komplexe bestätigen die *fac*-oktaedrische Koordination des Trimethylplatin-Rests und die bidentale Koordination der 2,2'-Bipyridine. Ein Vergleich der Bindungslängen zeigt, dass der Pt-N Bindungsabstand in Bipyridin-Komplexen leicht kürzer ist als in den entsprechenden Pyridin-Komplexen, was die besseren π -Akzeptor Eigenschaften von 2,2'-Bipyridinen zeigt. Des Weiteren ist der N-Pt-N Winkel in Bipyridin-Komplexen wesentlich kleiner als in Pyridin-Komplexen. Zudem wurden in der Kristallpackung des 4,4'-Dichlorido-2,2'-bipyridin-Komplexes von Iodidotrimethylplatin(IV) intermolekulare, nicht kovalente Wechselwirkungen zwischen den Methyl-Wasserstoffatomen und den Chloratomen festgestellt, die zu der Ausbildung von kettenartigen Zick-Zack-Strukturen führen, die über schwache π - π -Wechselwirkungen verbunden sind und eine zweidimensionale Schichtstruktur erzeugen.

Die Reaktion von Iodidotrimethylplatin(IV)-Pyridinkomplexen mit den entsprechenden 2,2'-Bipyridinen führt zu einer Substitution der Liganden, die in der Bildung von Chelat-Bipyridin-Komplexen resultiert. Im Gleichgewicht ist die Bildung des Chelatprodukts bei dieser Substitutionsreaktion stark bevorzugt. Die Bildung von Chelat-Komplexen in Lösung

hängt im Gleichgewicht zu einem großen Teil von den elektronischen Effekten der Substituenten sowie von der Natur des Lösungsmittels ab.

Table of Contents

1	Introduction.....	1
1.1	The Element Platinum.....	1
1.2	The Platinum(II) Chemistry.....	2
1.3	The Platinum(IV) Chemistry.....	3
1.4	The Chelate Effect.....	7
1.5	Nuclear Magnetic Resonance (NMR) Spectroscopy.....	9
1.6	X-ray Crystallography.....	11
1.7	Aim of the Thesis.....	12
2	Iodotrimethylplatinum(IV) Complexes of Pyridines.....	15
2.1	A Comparative Study of the Solution Behaviour of Iodotrimethylplatinum(IV) Complexes of Pyridines.....	15
2.1.1	Introduction.....	15
2.1.2	Syntheses and characterization of the complexes.....	16
2.1.3	X-ray crystallographic characterization of [PtMe ₃ (4-DMAP) ₂ I] (1) and [PtMe ₃ (3-BrPy) ₂ I] (2).....	16
2.1.4	Solution behaviour of [PtMe ₃ L ₂ I] (L = 4-DMAP, 3-BrPy, 4-CNPy) complexes in CDCl ₃	19
2.1.5	Conclusion.....	27
2.2	Substituent Effects on the Reaction of Iodotrimethylplatinum(IV) Complexes of Pyridines with Tetranuclear Iodotrimethylplatinum(IV).....	28
2.2.1	Introduction.....	28
2.2.2	Syntheses and characterization of the complexes.....	29
2.2.3	X-ray crystallographic characterization of [PtMe ₃ L ₂ I] complexes (L = 4-MePy, 4-EtPy, 4-OMePy and 3-OMePy).....	29
2.2.4	¹ H NMR studies for the reaction of [PtMe ₃ I] ₄ with [PtMe ₃ L ₂ I] complexes (L = 4-MePy, 4-EtPy, 4-OMePy, 4-DMAP, 4- ¹ BuPy, 4-CNPy, 3-MePy, 3-EtPy, 3-OMePy, 3-ClPy).....	33
2.2.5	Conclusion.....	43

2.3	Crystallographic Investigation of Dinuclear Iodotrimethylplatinum(IV) Complexes of Pyridines.....	44
2.3.1	Introduction.....	44
2.3.2	Crystal structures of <i>trans</i> -[PtMe ₃ (py)I] ₂ , <i>cis</i> -[PtMe ₃ LI] ₂ (L = 4-EtPy, 4-OMePy, 4-CNPY, 3-CIPY).....	44
3	Iodotrimethylplatinum(IV) Complexes of 2,2'-Bipyridines.....	50
3.1	Introduction.....	50
3.2	Syntheses and characterization of the complexes.....	51
3.2.1	¹ H NMR studies of the complexes.....	52
3.3	X-ray crystallographic characterization of the complexes, [PtMe ₃ (L-L)I] (L-L = bipy, 4Me-bipy, 5Me-bipy, OMe-bipy and Me ₂ N-bipy).....	54
3.4	X-ray crystallographic characterization of [PtMe ₃ (Cl-bipy)I].....	60
3.5	Conclusion.....	63
4	Ligand-Exchange Study on Iodotrimethylplatinum(IV) Complexes.....	64
4.1	Introduction.....	64
4.2	Result and Discussion.....	65
4.2.1	Syntheses and characterization of the complexes.....	65
4.2.2	Reaction of [PtMe ₃ L ₂ I] (L = py, 4-MePy and 4-OMePy) complexes with corresponding 2,2'-bipyridines (bipy, 4Me-bipy and OMe-bipy).....	65
4.2.3	Reaction of [PtMe ₃ (4-DMAP) ₂ I] with Me ₂ N-bipy.....	67
4.3	Conclusion.....	71
5	Experimental Section.....	72
5.1	Characterization Methods.....	72
5.1.1	¹ H NMR Spectroscopy.....	72
5.1.2	IR Spectroscopy.....	72
5.1.3	Elemental Analysis.....	72
5.1.4	EI-Mass Spectroscopy.....	72
5.2	Materials and Working Conditions.....	73
5.3	Syntheses.....	74
5.3.1	Synthesis of iodotrimethylplatinum(IV).....	74
5.3.2	Syntheses of 4,4'-disubstituted-2,2'-bipyridine ligands.....	75

5.3.2.1	Synthesis of 4,4'-bis(dimethylamino)-2,2'-bipyridine (Me ₂ N-bipy).....	75
5.3.2.2	Synthesis of 4,4'-dichloro-2,2'-bipyridine (Cl-bipy).....	76
5.3.3	Syntheses of mononuclear iodotrimethylplatinum(IV) complexes of pyridines.....	77
5.3.2.1	Synthesis of [PtMe ₃ (py) ₂ I].....	77
5.3.2.2	Synthesis of [PtMe ₃ (4-MePy) ₂ I].....	77
5.3.2.3	Synthesis of [PtMe ₃ (3-MePy) ₂ I].....	78
5.3.2.4	Synthesis of [PtMe ₃ (4-EtPy) ₂ I].....	78
5.3.2.5	Synthesis of [PtMe ₃ (3-EtPy) ₂ I].....	79
5.3.2.6	Synthesis of [PtMe ₃ (4-OMePy) ₂ I].....	79
5.3.2.7	Synthesis of [PtMe ₃ (3-OMePy) ₂ I].....	80
5.3.2.8	Synthesis of [PtMe ₃ (4-DMAP) ₂ I].....	81
5.3.2.9	Synthesis of [PtMe ₃ (4- ^t BuPy) ₂ I].....	81
5.3.3.10	Synthesis of [PtMe ₃ (4-CNPy) ₂ I].....	82
5.3.3.11	Synthesis of [PtMe ₃ (3-BrPy) ₂ I].....	82
5.3.3.12	Synthesis of [PtMe ₃ (3-ClPy) ₂ I].....	83
5.3.4	Syntheses of iodotrimethylplatinum(IV) complexes of 2,2'-bipyridines.....	83
5.3.4.1	Synthesis of [PtMe ₃ (bipy)I].....	83
5.3.4.2	Synthesis of [PtMe ₃ (4Me-bipy)I].....	84
5.3.4.3	Synthesis of [PtMe ₃ (5Me-bipy)I].....	84
5.3.4.4	Synthesis of [PtMe ₃ (OMe-bipy)I].....	85
5.3.4.5	Synthesis of [PtMe ₃ (Me ₂ N-bipy)I].....	86
5.3.4.6	Synthesis of [PtMe ₃ (Cl-bipy)I].....	86
5.4	Crystallography.....	88
6	Summary.....	106
7	Zusammenfassung.....	111
8	Appendix.....	116
8.1	References.....	116
8.2	Abbreviations.....	121
8.3	Table of Figures.....	124
8.4	Tables.....	128
8.5	Table of Schemes.....	130

8.6 Acknowledgements.....132
8.7 Publications & Presentations.....133

1 Introduction

1.1 The Element Platinum

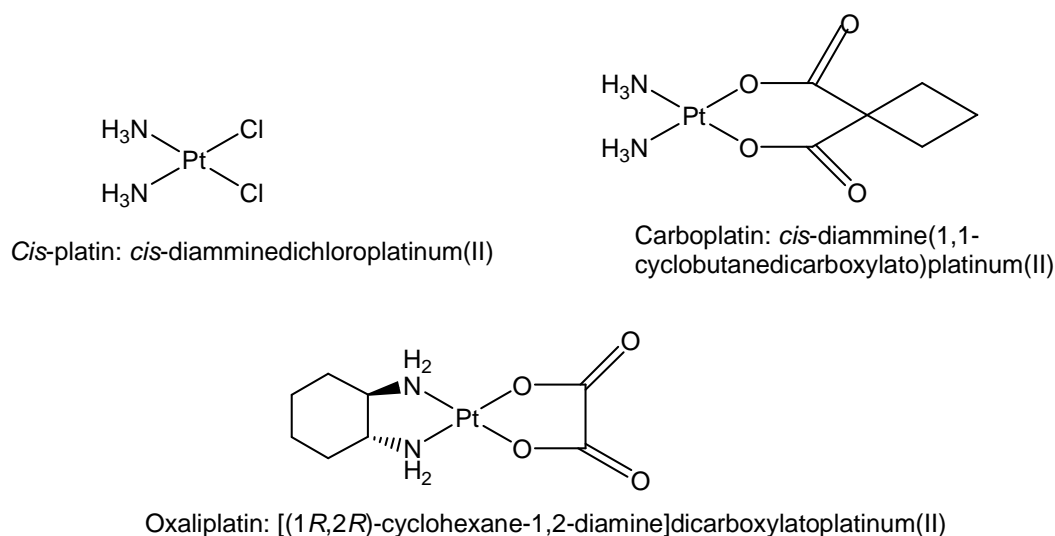
Platinum is a chemical element with the symbol Pt and is classified as a “Transition Metal”. The atomic number of platinum is 78 and the electron configuration is $[\text{Xe}] 4f^{14} 5d^9 6s^1$. The name platinum originates from the Spanish word *platina del Pinto*, meaning “little silver of the Pinto River”.^[1] Platinum is an extremely rare metal, occurring at a concentration of only 0.005 ppm in the Earth’s crust. It occurs in native form, accompanied by small amounts of other metals belonging to the same group (osmium, iridium, ruthenium, palladium, and rhodium). Another source of platinum is sperrylite (PtAs_2).^[2] Platinum is a beautiful silvery-white metal, when pure, and is malleable and ductile. Platinum has six naturally occurring isotopes: ^{190}Pt , ^{192}Pt , ^{194}Pt , ^{195}Pt , ^{196}Pt , and ^{198}Pt . The most abundant of these is ^{195}Pt , comprising 33.83% of all platinum and it is the only stable isotope with a non-zero spin ($I = \frac{1}{2}$). The most common oxidation states of platinum are +2 and +4. The +1 and +3 oxidation states are less common, and often stabilized by metal bonding in bimetallic (or polymetallic) species. The predominant geometry for +2 oxidation state is square planar, while for the +4 oxidation state it is octahedral.^[3,4]

Platinum is generally unreactive and is remarkably resistant to corrosion, even at high temperatures, and thus is considered a noble metal. It is insoluble in hydrochloric acid and in nitric acid but dissolves in aqua regia to form hexachloroplatinic acid, H_2PtCl_6 .^[5]

Platinum is used in a variety of different applications, the largest amount being used in the car industry. It is also used in electronics, laboratory equipment, spark plugs, turbine engines and oxygen sensors.^[6] Another common use of platinum is as a catalyst for chemical reactions such as the decomposition of hydrogen peroxide into water and oxygen gas,^[7] ignition of hydrogen. As a precious metal, large amounts of platinum are also consumed in jewellery. Being a heavy metal, it leads to health issues upon exposure to its salts, but due to its corrosion resistance, it is not toxic as a metal.

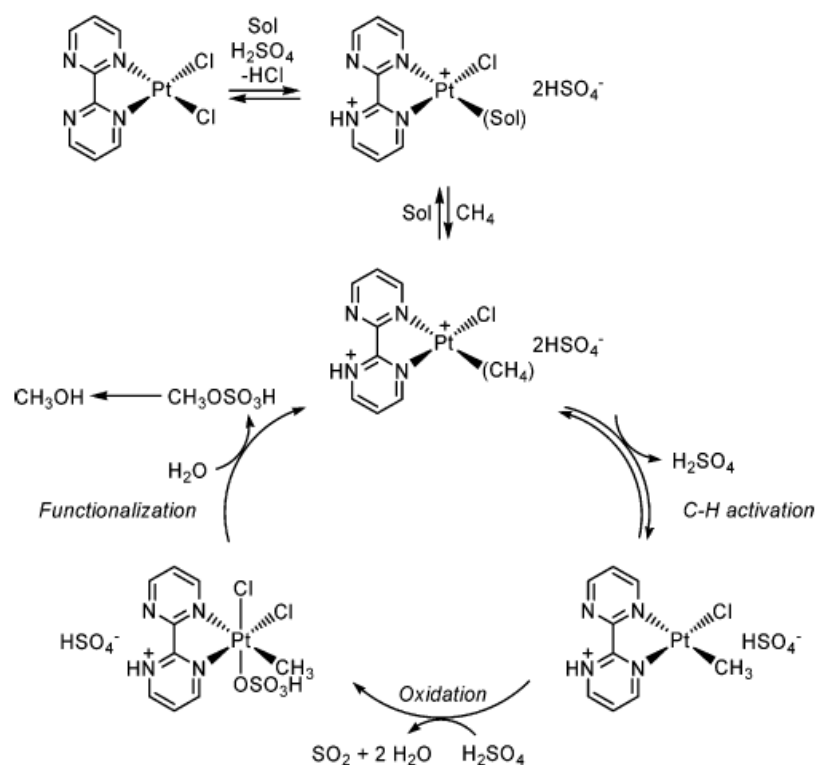
1.2 The Platinum(II) Chemistry

One of the most important platinum(II) complexes, *cis*-[Pt(NH₃)₂Cl₂] (*cis*-platin) was described by Michele Peyrone (known as Peyrone's chloride).^[8] It is a chemotherapy drug as shown by Rosenberg *et al.*^[9] and is used to treat various types of cancers, including small cell lung cancer, ovarian cancer and germ cell tumours. It was the first member of a class of platinum-containing anti-cancer drugs. Along with *cis*-platin, carboplatin^[10] and oxaliplatin^[11] are also used as chemotherapy drugs.



Scheme 1.1 Platinum(II) compounds exhibit anti-cancer activity.

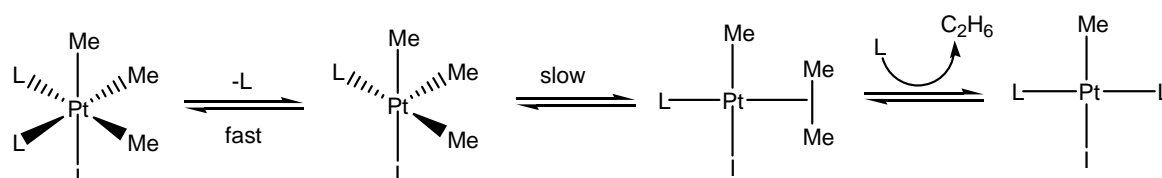
Platinum(II) complexes also play a catalytic role in synthesizing different organic compounds from the hydrocarbon. Periana *et al.*^[12] reported the direct, low temperature, oxidative conversion of methane to methanol in the presence of concentrated sulfuric acid catalyzed by (2,2'-bipyrimidine)platinum(II), [Pt(bpym)Cl₂] at greater than 70% one-pass yield with 81% selectivity. Johansson *et al.*^[13] also reported the benzene and methane C-H activation under mild and neutral conditions in hydroxylic solvent, 2,2,2-trifluoroethanol (TFE) at a cationic platinum(II) diimine aqua complex.



Scheme 1.2 Proposed mechanism for the oxidation of methane to methanol.^[12,14b]

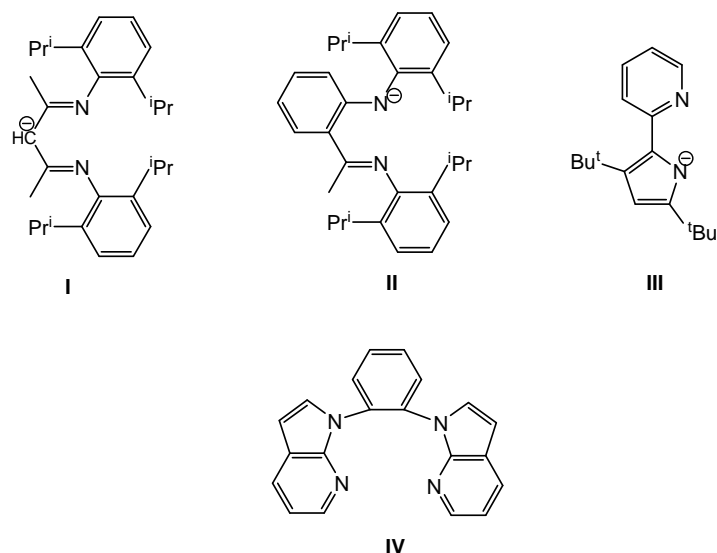
1.3 The Platinum(IV) Chemistry

Like platinum(II) chemistry, platinum(IV) chemistry has attracted tremendous attention over the last few decades due to their involvement in the Shilov Process.^[14,15] It was shown experimentally that five-coordinated unsaturated platinum(IV) complexes are involved as key intermediates in the platinum(IV)/platinum(II)-mediated C-X (X = H, halide, OR, etc.) bond-breaking or -making processes.^[15-20]



Scheme 1.3 Mechanism for the reductive elimination of ethane from $[PtMe_3L_2I]$ (L = tertiary phosphane ligand).^[15a,15c]

These five-coordinated unsaturated platinum(IV) complexes can be isolated when bulky anionic or neutral N,N-chelating ligands^[19-21] are attached to the platinum(IV) metal ion which provides enough steric protection to the vacant platinum(IV) coordination site.



Scheme 1.4 Bulky anionic N,N-chelating ligands (I-III) and neutral N,N-chelating ligand (IV) which stabilize five-coordinate platinum(IV) species.

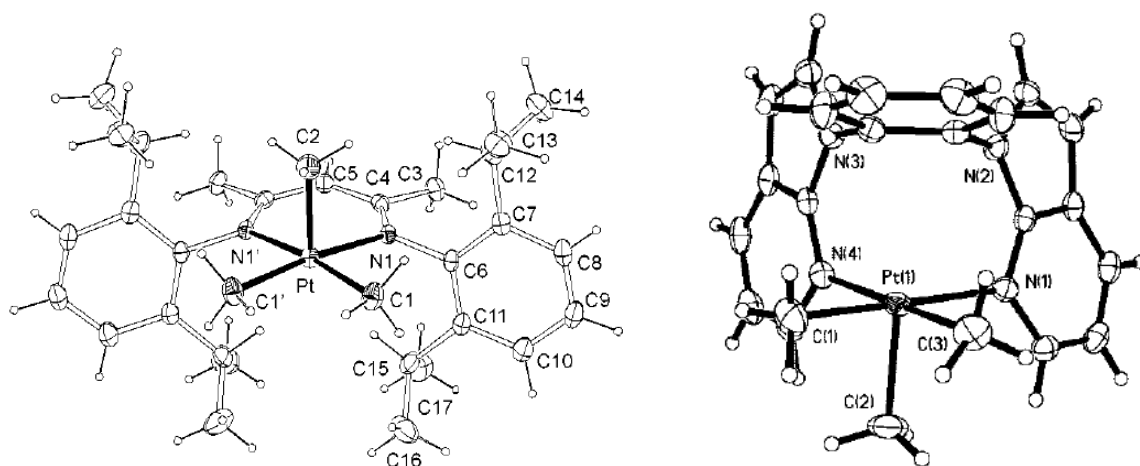


Figure 1.1 Crystal structures of $[\{(o\text{-}^i\text{Pr}_2\text{C}_6\text{H}_3)\text{NC}(\text{CH}_3)_2\text{CH}\}\text{PtMe}_3]$ (left);^[19c] (BAB)PtMe₃ [BAB = 1,2-bis(*N*-7-azaindoly)benzene] (right).^[21]

Platinum(IV) chemistry also has some applications in biology. Like platinum(II) complexes such as *cis*-platin, carboplatin, oxaliplatin, platinum(IV) complexes such as CHIP [*cis*-dichloro-*trans*-dihydroxy-bis-isopropylamineplatinum(IV)], JM216 [*cis*-dichloro-*trans*-diacetato-ammine-cyclohexylamineplatinum(IV)], *cis*-1,4-diaminocyclohexane complexes of platinum(IV) have been a subject of several clinical trials for cancer treatment.^[22-26]

The first organic compound of platinum, iodotrimethylplatinum(IV), was prepared by Pope and Peachy by the reaction of anhydrous platinum tetrachloride with methyl magnesium iodide in 1909.^[27] Later in 1975, Baldwin *et al.* developed the synthetic route of this compound.^[28] X-ray investigations^[29-31] have shown that in iodotrimethylplatinum(IV) four platinum atoms describe a tetrahedron, as do the four iodine atoms, and the two tetrahedra are interpenetrating so as to give a heterocubane structure of platinum and iodine atoms. Each platinum atom is hexa-coordinated by the three terminal methyl groups and three bridged iodine atoms (Figure 1.2). It is soluble in most non-polar solvents and essentially insoluble in polar media such as water and acetone. The related trimethylplatinum(IV) derivatives $[\text{PtMe}_3\text{X}]_4$ (where X = chlorine,^[32] bromine,^[33] SCH_3 ,^[29] SCN ,^[34] azide,^[35] triflate^[36]) also form heterocubane structures where Pt and X atoms occupy alternate corners of slightly distorted cubes.

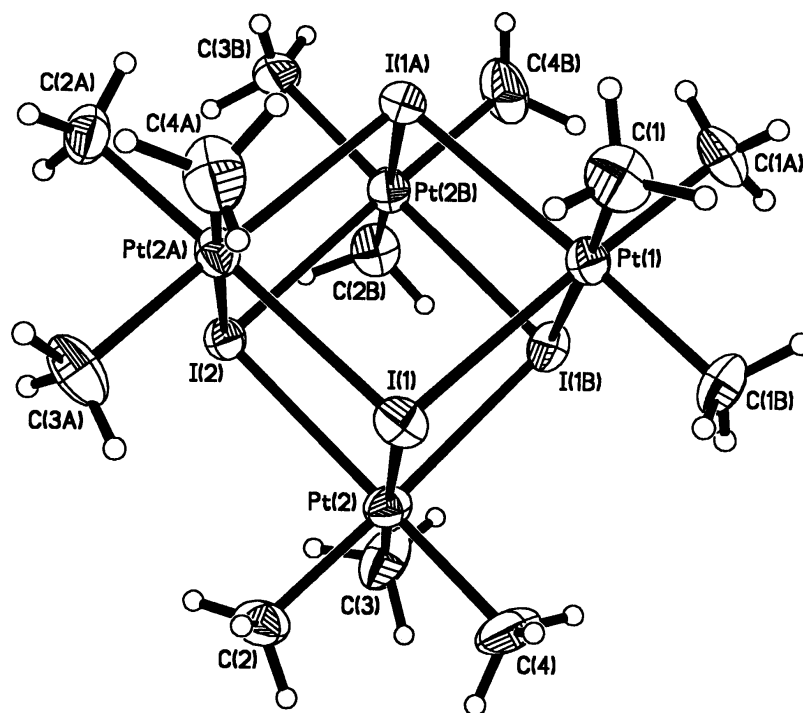
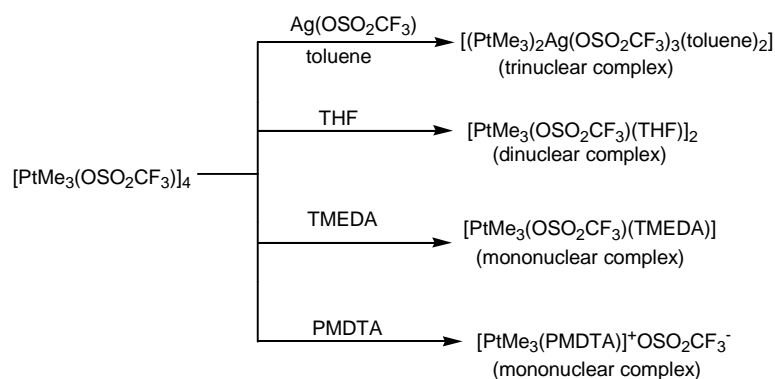
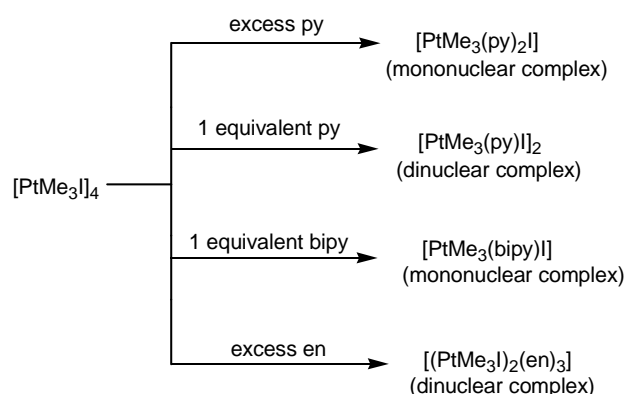


Figure 1.2 Molecular structure of iodotrimethylplatinum(IV).^[29]

The trimethylplatinum(IV) cation, PtMe_3^+ is highly versatile and forms wide variety of complexes with both neutral and anionic ligands. Schlecht *et al.*^[36] showed that tetranuclear trimethylplatinum(IV) triflate converts to trinuclear, dinuclear and mononuclear complexes by treatment with various bases (Scheme 1.5). Tetranuclear iodotrimethylplatinum also converts to corresponding mononuclear and dinuclear complexes depending on the coordination nature and amount of nitrogen ligand (Scheme 1.6).

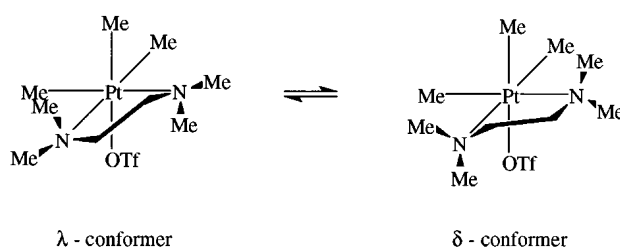


Scheme 1.5 Effect of different bases on trimethylplatinum(IV) triflate complex. TMEDA = *N,N,N',N'*-tetramethylethylenediamine, PMDTA = *N,N,N',N'',N''*-pentamethyldiethylenetriamine).^[36]

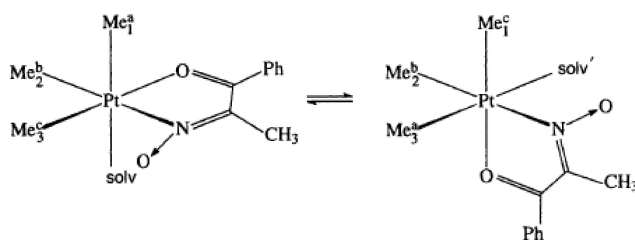


Scheme 1.6 Effect of nitrogen ligands on iodotrimethylplatinum(IV) complex. py = pyridine, bipy = 2,2'-bipyridine, en = ethylenediamine.^[37-39]

Many of the trimethylplatinum(IV) complexes containing neutral chelating nitrogen donor ligands such as 2,6-bis[1-(phenylimino)ethyl]pyridine (BIP),^[40] TMEDA^[41] exhibit dynamic behaviour in solution. Also trimethylplatinum(IV) complexes of organochalcogen ligands such as thio and seleno ethers,^[42-45] anionic nitrogen/oxygen or oxygen/oxygen ligands^[46-49] have been a subject of dynamic investigation because of their fluxional behaviour in solution.

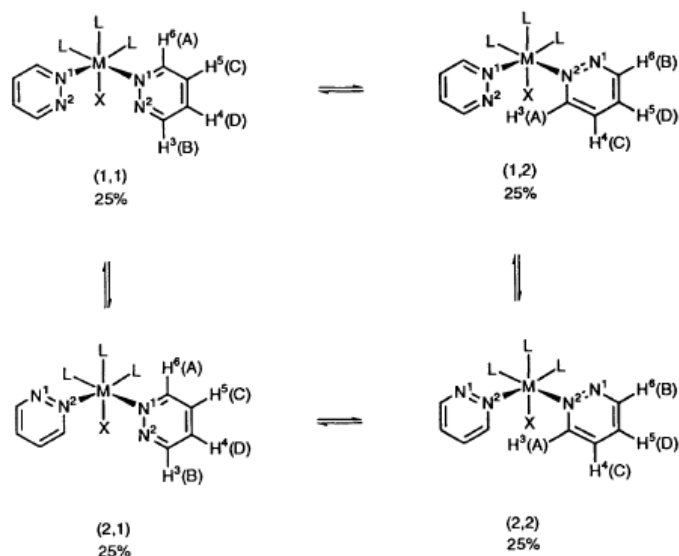


Scheme 1.7 The fluxional behaviour of $[\text{PtMe}_3(\text{TMEDA})\text{OTf}]$ (OTf = OSO_2CF_3).^[41]



Scheme 1.8 The fluxional behaviour of $[\text{PtMe}_3(\text{ppdm})(\text{H}_2\text{O})]$ where ppdm = 1-phenylpropane-1,2-dione 2-oximate.^[47]

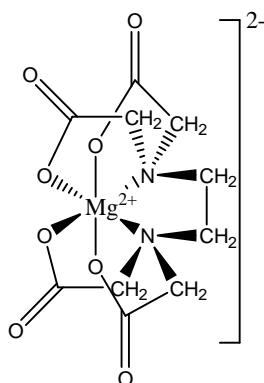
It was also shown that some trimethylplatinum(IV) complexes containing pyridazine and its derivatives such as 4-methylpyridazine and 3-methylpyridazine display a 1,2-metallotropic shift in the solution phase due to the presence of a contiguous pair of nitrogen atoms in the pyridazine ligands.^[50-52]



Scheme 1.9 Effect of 1,2-metallotropic shift in $[\text{PtMe}_3(\text{pydz})_2\text{X}]$ (where X = Cl, Br, I; pydz = pyridazine) complexes.^[51]

1.4 The Chelate Effect

When a multidentate ligand coordinates to a metal ion from more than one donor site forming a ring with the metal, it is said to be a chelating ligand and the resulting compound is said to be a chelate complex. Chelate complexes are usually found to be more stable than the comparable non-chelate complexes with the same donor atoms. This extra stability of a coordination complex containing chelate rings is known as “*the chelate effect*”. Scheme 1.10 illustrates the example of a chelate complex of Mg^{2+} .



Scheme 1.10 $[\text{Mg}(\text{EDTA})]^{2-}$ chelate complex.

The increased stability of the chelate complexes can be explained by the thermodynamic approach. The equilibrium constant, K_{eq} for a chemical reaction is related to the standard Gibbs free energy (ΔG°) according to equation 1.1.

$$\Delta G^\circ = -RT \ln K_{\text{eq}} \quad (1.1)$$

Here, R is the universal gas constant and T is the temperature in Kelvin.

For chelation reaction K_{eq} is usually positive, i.e., $\Delta G^\circ =$ negative.

Now, ΔG° is related to ΔH° and ΔS° according to equation 1.2.

$$\Delta G^\circ = \Delta H^\circ - T\Delta S^\circ \quad (1.2)$$

Here, ΔH° is the standard enthalpy change of the reaction; ΔS° is the standard entropy change.

Now, consider the following chelation reaction:



Since the bonding characteristics of ammonia and ethylenediamine (en) are very similar, the change in enthalpy for the above reaction is negligible. However, positive entropy changes for the forward reaction make the reaction thermodynamically favourable, which explains the stability of the chelate complex. This is supported by Spike *et al.*^[53] (who showed experimentally that the enthalpy change for the above chelation reaction is very small and the increase in the stability of the cadmium chelates is purely an entropy factor).

1.5 Nuclear Magnetic Resonance (NMR) Spectroscopy

Nuclear Magnetic Resonance (NMR) spectroscopy is an extremely important technique used to determine the content and purity of a sample as well as the molecular structure of the compounds. NMR spectroscopy is based on the principle of energy difference between the two states. The two states of a nucleus with a nuclear spin quantum number of $\frac{1}{2}$ [commonly named as α (the lower energy state) and β (the higher energy state)], and hence the energy difference, are generated in the presence of an external magnetic field (B_0) by the magnetic moment of the electrically charged atomic nucleus (for example, ^1H , ^{13}C , ^{15}N , etc.). Thus, an energy transfer takes place between the two states at a wavelength that corresponds to radio frequency. The signal that matches this transfer is measured and processed in order to yield an NMR spectrum for the nucleus concerned.

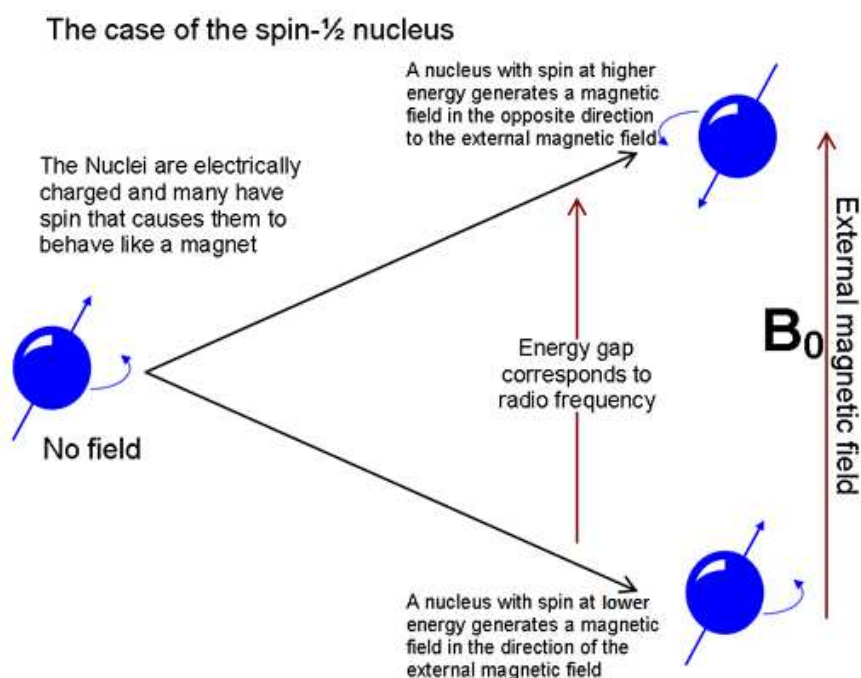


Figure 1.3 The basis of NMR in the case of spin $\frac{1}{2}$ nuclei such as ^1H , ^{13}C , ^{15}N , ^{31}P , ^{195}Pt , etc.^[54]

The energy difference (ΔE) between the two states is

$$\Delta E = \gamma \hbar B_0 \quad (1.4)$$

Where γ is the gyromagnetic ratio for a given nucleus and \hbar is the reduced Planck's constant.

The relative population of a state is given by the *Boltzmann distribution*:

$$N_{\beta}/N_{\alpha} = e^{-\Delta E/kT} = e^{-\gamma\hbar B_0/kT} \approx 1 - \gamma\hbar B_0/kT \quad (1.5)$$

Where N_{β} , N_{α} represents the number of nuclei in the β and α states, respectively; k is the Boltzmann constant and T is the temperature in Kelvin. The equation (1.5) shows that the population of the states is affected by several factors. Nuclei that have large gyromagnetic ratio are more sensitive than nuclei with lower gyromagnetic ratio. Proton has the largest gyromagnetic ratio among the naturally abundant nuclei, and thus, is the most sensitive nucleus. The sensitivity can also be increased by decreasing the temperature or by increasing the magnetic field.

Each nucleus in a molecule has different molecular surroundings, and thus, different electronic environments. Electrons around the nucleus shield it from the external magnetic field, and thus their resonance frequencies will be different. The resonant frequency is strongly dependent on the electronegativity of the nucleus. The ring current (anisotropy) and bond strain also affect the frequency shift. The difference between the frequency of the reference signal and the frequency of the signal is divided by the frequency of the reference signal to give the chemical shift. In ^1H NMR spectroscopy, chemical shifts are usually referenced to TMS (tetramethylsilane), whose chemical shift is set to zero ppm.

The energy state of a nucleus is also affected by the orientation of the neighbouring nuclei. In such cases, the nuclei are said to be spin-spin-coupled to each other and the phenomenon is known as spin-spin coupling. The magnitude of the splitting (coupling constant J) depends on the strength of the coupling; however, it is independent of the strength of the magnetic field. The multiplicity of the splitting depends on the number of chemically bonded nuclei in the vicinity of the observed nucleus.

The most important parameter in NMR spectroscopy is the area of NMR signal. The area under each signal arising from non-exchangeable proton is directly proportional to the number of equivalent nucleus responsible for that signal, or in other words, is directly proportional to the molar amount of the detected isotope.

Quantitative one-dimensional NMR spectroscopy of complex mixtures is usually hindered due to severe overlap of signals. This can be circumvented with higher magnetic fields or by

expanding the proton spectrum to another dimension, running a two-dimensional experiment. Types of two-dimensional NMR include correlation spectroscopy (COSY), exchange spectroscopy (EXSY), nuclear overhauser effect spectroscopy (NOESY), and diffusion ordered spectroscopy (DOSY).

NMR DOSY technique is a method for separating compounds in a multicomponent mixture based on the translational diffusion coefficients of each chemical species in solution. Therefore, the technique depends on the size and shape of the molecule, as well as the physical properties of the surrounding environment such as viscosity, temperature, etc.

The measurement of diffusion is carried out by observing the attenuation of the NMR signals during a pulsed field gradient experiment. The degree of attenuation is a function of the magnetic gradient pulse amplitude (G) and occurs at a rate proportional to the diffusion coefficient (D) of the molecule. Assuming that a line at a given (fixed) chemical shift δ belongs to a single sample component A with a diffusion coefficient D_A , we have

$$S(\delta, z) = S_A(\delta) \exp(-D_A Z) \quad (1.6)$$

Where $S_A(\delta)$ is the spectral intensity of component A in zero gradient ('normal' spectrum of A), D_A is its diffusion coefficient and Z encodes different gradient amplitudes used in the experiment.^[55]

1.6 X-ray Crystallography

X-ray crystallography is the most commonly used method for determining the three dimensional structure of molecules. The most precise method of X-ray crystallography is single-crystal X-ray diffraction. It is based on constructive interference of monochromatic X-rays and a crystalline sample. When X-rays are beamed at the crystal, the interaction of the X-rays with the sample produces constructive interference (and a diffracted ray) when conditions satisfy Bragg's law ($n\lambda = 2d\sin\theta$, where θ is the scattering angle, λ is the X-ray wavelength, d is the interplanar distance), thereby causing a diffraction pattern. This diffraction pattern converted to electron density map using the mathematical Fourier transformation. Since electrons more or less surround atomic nucleus uniformly, it is possible

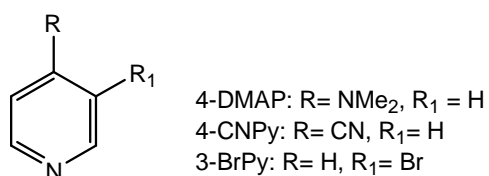
to determine the location of atoms; however, due to the presence of only one electron, it is difficult to map hydrogen. As the crystal is gradually rotated, multiple sets of electron density maps were obtained for each angle of rotation. These data are combined computationally with complementary chemical information to produce and refine the crystal structure of the crystalline sample.

1.7 Aim of the Thesis

The central aim of this thesis is the study of the chelate effect in platinum(IV) complexes containing aromatic nitrogen ligands. This requires a systematic analysis of binding and exchange of monovalent pyridine based ligands with the bivalent 2,2'-bipyridine based ligands in the molecular complexes of trimethylplatinum(IV). As described in Section 1.3, the trimethylplatinum(IV) cation is highly versatile and forms complexes with both the monovalent and bivalent nitrogen donor ligands, and hence this is a good system for the study of the chelate effect. In view of this, several pyridine and 2,2'-bipyridine complexes of iodotrimethylplatinum(IV) were studied throughout this thesis.

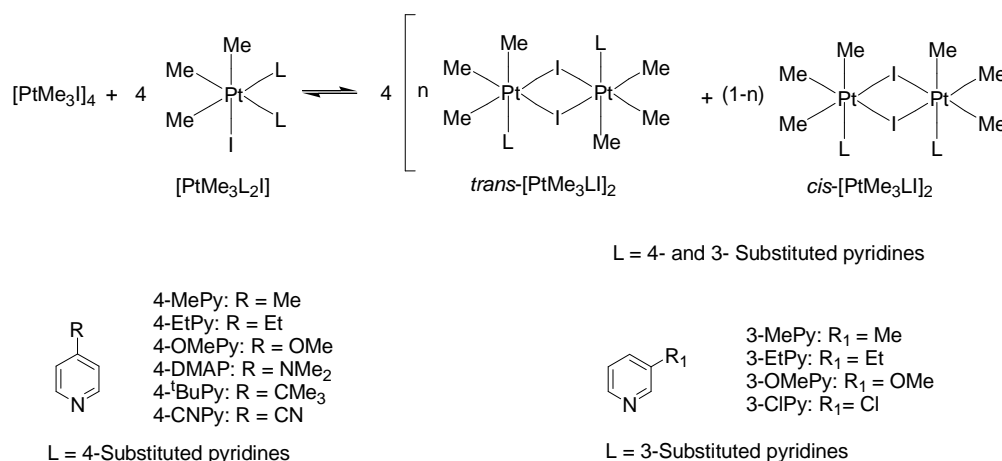
Chapter 2 describes the results of investigations in regard to the iodotrimethylplatinum(IV) complexes obtained with several pyridine ligands. In detail, the following results are discussed:

- Solution behaviour of mononuclear iodotrimethylplatinum(IV) complexes containing strongly electron donating pyridine (4-DMAP) and electron withdrawing pyridines (4-CNPy and 3-BrPy) were investigated in order to examine the effect of pyridines on the solution phase. Furthermore, the X-ray crystallographic studies of $[\text{PtMe}_3(4\text{-DMAP})_2\text{I}]$ and $[\text{PtMe}_3(3\text{-BrPy})_2\text{I}]$ were carried out to establish the solid state structure of these mononuclear pyridine complexes (Chapter 2.1).



Scheme 1.11 Different pyridines used for the solution behaviour study of $[\text{PtMe}_3\text{L}_2\text{I}]$ (L = pyridines) complexes.

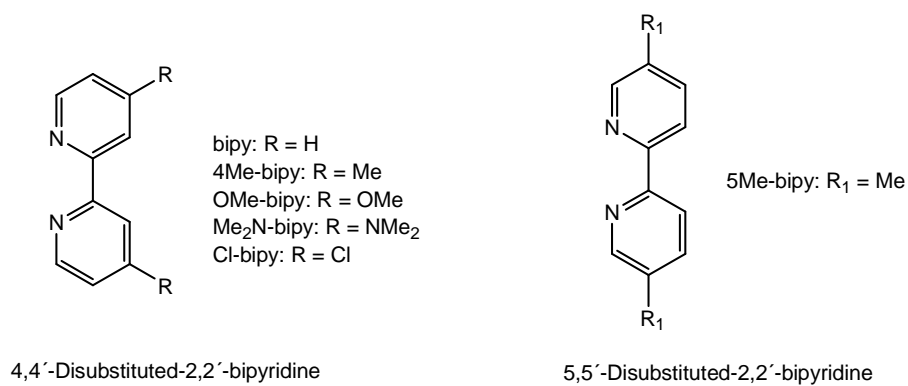
- The influence of the nucleophilicity and the steric bulk of the pyridine substituent on the reaction of mononuclear iodotrimethylplatinum(IV) complexes of pyridines with tetranuclear iodotrimethylplatinum(IV) leading to the formation of the dinuclear complexes were explored. This study also includes the crystal structures of four mononuclear iodotrimethylplatinum(IV) complexes of pyridines $[\text{PtMe}_3\text{L}_2\text{I}]$ ($\text{L} = 4\text{-MePy}, 4\text{-EtPy}, 4\text{-OMePy}$ and 3-OMePy) (Chapter 2.2).



Scheme 1.12 Different pyridines (4- and 3-substituted) used for the reaction of $[\text{PtMe}_3\text{L}_2\text{I}]$ with iodotrimethylplatinum(IV).

- The crystal structures of five dinuclear pyridine complexes of iodotrimethylplatinum $\{trans\text{-}[\text{PtMe}_3(\text{py})\text{I}]_2, cis\text{-}[\text{PtMe}_3\text{LI}]_2$ ($\text{L} = 4\text{-EtPy}, 4\text{-OMePy}, 4\text{-CNPy}$ and 3-ClPy) were investigated to verify the molecular structure of these dinuclear complexes (Chapter 2.3).

Chapter 3 deals with the complexation of iodotrimethylplatinum(IV) with 2,2'-bipyridine ligands which gives rise to mononuclear $[\text{PtMe}_3(\text{L-L})\text{I}]$ (where L-L = bipy, 4Me-bipy, 5Me-bipy, OMe-bipy, Me₂N-bipy, Cl-bipy) complexes. The complexes were characterized by ¹H NMR, EI-MS, IR spectroscopy, elemental analyses, and X-ray crystallography. X-ray structural investigations of these complexes reveal the expected *facial* octahedral coordination geometry of the PtMe₃ moiety and bidentate coordination of the bipyridine ligand. Moreover, the crystal packing of $[\text{PtMe}_3(\text{Cl-bipy})\text{I}]$ shows the intermolecular non-covalent interaction between methyl hydrogen and a chlorine atom leading to the formation of one-dimensional *zig-zag* chain structures which are linked through weak $\pi\text{-}\pi$ interactions to generate a two-dimensional layer structure.



Scheme 1.13 Different 2,2'-bipyridines.

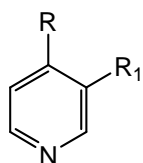
Chapter 4 describes the substitution of pyridine ligands with the 2,2'-bipyridine ligands in the molecular complexes of iodotrimethylplatinum(IV). Four different pyridines (py, 4-MePy, 4-OMePy and 4-DMAP) and corresponding 2,2'-bipyridines (bipy, 4Me-bipy, OMe-bipy and Me₂N-bipy) were used for the substitution reaction to determine the influence of rigidity and the electronic effect of the substituent on the chelation reaction. The ligand-exchange reaction was conducted in two different solvents (CDCl₃ and nitrobenzene-d₅) in order to examine the dependence of the exchange equilibria on the solvent in iodotrimethylplatinum(IV) system.

2 Iodotrimethylplatinum(IV) Complexes of Pyridines

2.1 A Comparative Study of the Solution Behaviour of Iodotrimethylplatinum(IV) Complexes of Pyridines

2.1.1 Introduction

As described in the introduction the chemistry of trimethylplatinum(IV) complexes has received considerable interest in the last few decades. Among the iodotrimethylplatinum(IV) complexes the study of the mononuclear $[\text{PtMe}_3(\text{py})_2\text{I}]$ (py = pyridine) complex was found to be quite interesting. This complex was reported to be mononuclear^[39] and have a concentration-dependent molecular weight due to the dissociation into the dinuclear complex $[\text{PtMe}_3(\text{py})\text{I}]_2$ and pyridine.^[38] In order to investigate whether the solution behaviour of iodotrimethylplatinum(IV) complex is influenced by the coordinated pyridine or not, it was decided to extend the study to iodotrimethylplatinum(IV) complexes involving substituted pyridines having different electron density on the pyridine ring nitrogen. In this context the ligands 4-dimethylaminopyridine (4-DMAP), 4-cyanopyridine (4-CNPy), 3-bromopyridine (3-BrPy) (Scheme 2.1.1) having different electron density on the pyridine nitrogen are well suited for the study. In this chapter the syntheses of $[\text{PtMe}_3\text{L}_2\text{I}]$ (L = 4-DMAP, 4-CNPy, 3-BrPy) complexes are reported and the investigation of several features of their solution behaviour by ^1H NMR study discussed. The crystal structures of $[\text{PtMe}_3\text{L}_2\text{I}]$ (L = 4-DMAP, 3-BrPy) complexes are also reported here.

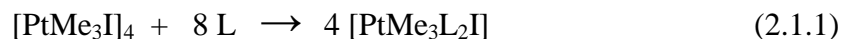


4-DMAP: R= NMe₂, R₁ = H
4-CNPy: R= CN, R₁= H
3-BrPy: R= H, R₁= Br

Scheme 2.1.1 Different substituted pyridines.

2.1.2 Syntheses and characterization of the complexes

Tetranuclear iodotrimethylplatinum(IV), $[\text{PtMe}_3\text{I}]_4$ reacts with substituted pyridines to give six-coordinate mononuclear trimethylplatinum(IV) complexes, $[\text{PtMe}_3\text{L}_2\text{I}]$ (where L = 4-DMAP, 3-BrPy, 4-CNPy) according to equation 2.1.1.



These synthesized mononuclear complexes are pale yellow to yellow crystalline solids, being stable in the solid state and soluble in chloroform. The C-H stretching region in the infrared spectra of all three complexes comprised three bands: two due to C-H stretching modes and one due to the overtone of the asymmetric C-H deformation mode. The C-H stretching modes and Pt-C modes are consistent with the PtMe_3 moiety having *facial* octahedral coordination geometry.^[39] The complexes were also characterized by elemental analyses. Full synthetic and analytical data of the complexes are reported in Chapter 5.3.3.

2.1.3 X-ray crystallographic characterization of $[\text{PtMe}_3(4\text{-DMAP})_2\text{I}]$ (**1**) and $[\text{PtMe}_3(3\text{-BrPy})_2\text{I}]$ (**2**)

The yellow crystals of complexes **1** and **2** were obtained by slow diffusion of n-hexane into their chloroform solution. Both the complexes crystallize in $P2_1/n$ space group with a monoclinic crystal system and contain four molecules in their unit cell. The crystal structures of both complexes consist of a discrete monomeric unit in which the central platinum atom is hexa-coordinated by the three methyl groups in a *facial* arrangement, two pyridine ligands and an iodine atom (see Figures 2.1.1-2.1.2). Selected bond lengths and bond angles of the complexes are given in Tables 2.1.1-2.1.2, while X-ray diffraction parameters and crystallographic data are reported in Tables 5.4.1-5.4.2.

The Pt-C bond lengths vary according to the *cis/trans* influences,^[56,57] i.e., the methyl group *trans* to the π -donating iodide ligand exhibits a longer bond to the metal in **2** while this effect appears less pronounced for **1**. The Pt-I bond distance (2.79 Å in **1** and 2.78 Å in **2**) in both structures is essentially identical and is only slightly shorter than the corresponding value (2.83 Å) for the bridging iodides in the reported complex $[\text{PtMe}_3\text{I}]_4$.^[29] Also, the Pt-I bond distance in both complexes is significantly longer than the Pt^{IV} -I bond distance that has been

observed in several octahedral platinum(IV) complexes, e.g., 1,6-[Pt(en)₂I₂]₂·2H₂O (2.68 Å),^[58] [PtI₆(phen)] (2.66, 2.67 Å),^[59] [PtI₅(phen)] (2.67, 2.67 Å),^[59] [PtMe₂I₂(Pz₂CH₂)] (2.65, 2.65 Å),^[60] [PtMe₂I₂{(Me₂Pz)₂CH₂}] (2.65, 2.65 Å),^[60] [PtMe₂I(O₂C₃H₇)(C₁₂H₈N₂)] (2.62 Å),^[61] *trans*-bis(acetylacetonato)di-iodoplatinum(IV) (2.67 Å).^[62] The Pt-N bond distances in **1** (2.17 and 2.18 Å) are only marginally shorter than in **2** (2.17 and 2.21 Å) and are close to the values found for the Pt-N bonds in [PtMe₃(pydz)₂Cl] (2.18, 2.19 Å),^[51] [PtMe₂I₂(Pz₂CH₂)] (2.18 Å).^[60] The Pt-N bond distances in both complexes are somewhat longer than the Pt-N bond distances reported for a number of platinum(IV) complexes, e.g., *trans*-[Pt(NH₃)₂(2,4-pentanediiiminate)₂](ClO₄)₂ (2.00 Å),^[63] [PtI₆(phen)] and [PtI₅(phen)] (range 2.06-2.12 Å).^[59] Longer Pt-N bond distances are also observed in several platinum(IV) complexes such as [PtMe₂I₂{(Me₂Pz)₂CH₂}] (2.24 Å),^[60] [PtMe₃(OSO₂CF₃)(TMEDA)] (2.24 Å).^[36] The N1-Pt1-N2 angle (89.2°) in **1** only slightly deviates from regular octahedral geometry which opens up the N1-Pt1-C2 and N2-Pt1-C1 *cis* angles to 93.0° and 91.2° respectively, and narrows down the N1-Pt1-C1 and N2-Pt1-C2 *trans* angles to 177.9° and 176.4° respectively. Similarly, the N1-Pt1-N2 angle (92.9°) in **2** also deviates from regular octahedral geometry which opens up the N1-Pt1-C2 and N2-Pt1-C3 *cis* angles to 90.8° and 92.8° respectively, and narrows down the N1-Pt1-C1 and N2-Pt1-C2 *trans* angles to 176.8° and 176.1° respectively. Other angular distortions are consistent with the minimum interligand non-bonded interactions. The dimensions of the ring systems are as expected.

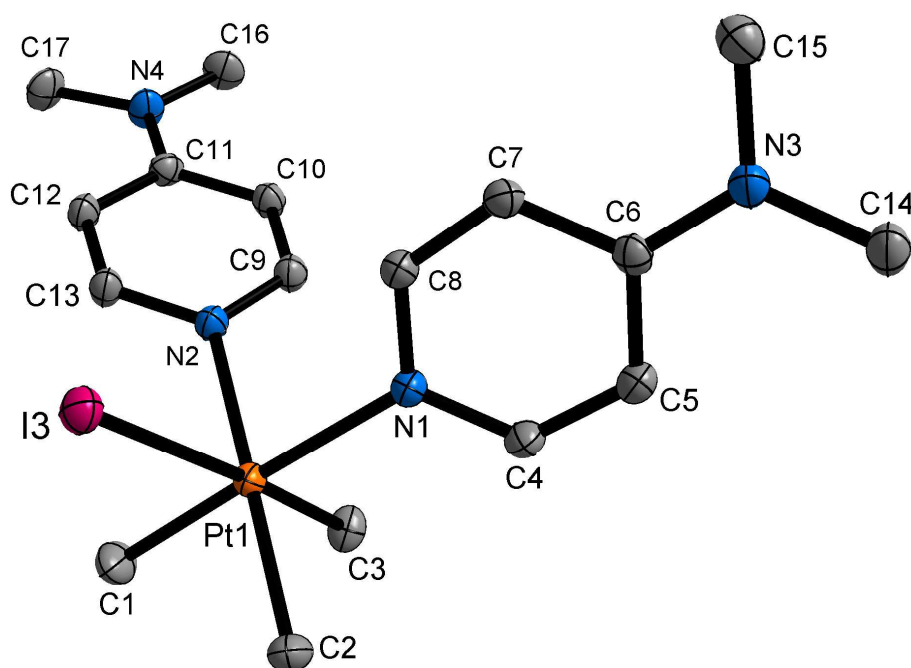


Figure 2.1.1 Molecular structure of [PtMe₃(4-DMAP)₂I] (**1**) showing the atom labelling scheme. Thermal ellipsoids are at the 50% probability level. Hydrogen atoms are omitted for clarity.

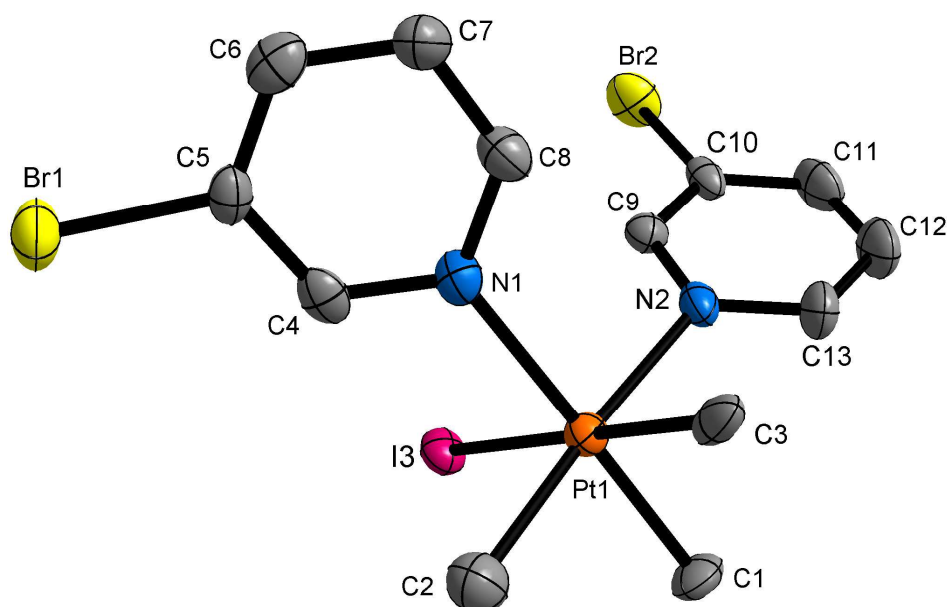


Figure 2.1.2 Molecular structure of $[\text{PtMe}_3(3\text{-BrPy})_2\text{I}]$ (**2**) showing the atom labelling scheme. Thermal ellipsoids are at the 50% probability level. Hydrogen atoms are omitted for clarity.

Table 2.1.1 Selected bond lengths [\AA] and angles [$^\circ$] for $[\text{PtMe}_3(4\text{-DMAP})_2\text{I}]$ (**1**)

Pt1-C1	2.050(2)	Pt1-N2	2.173(2)
Pt1-C2	2.051(2)	Pt1-N1	2.1804(19)
Pt1-C3	2.065(2)	Pt1-I3	2.7953(4)
C1-Pt1-C2	86.43(11)	C1-Pt1-I3	91.00(8)
C1-Pt1-C3	86.31(11)	C2-Pt1-I3	91.61(7)
C2-Pt1-C3	87.11(10)	C3-Pt1-I3	177.09(7)
N2-Pt1-N1	89.20(7)	N2-Pt1-I3	91.20(5)
C1-Pt1-N2	91.24(9)	N1-Pt1-I3	91.01(5)
C2-Pt1-N2	176.38(9)	C2-Pt1-N1	93.03(9)
C3-Pt1-N2	89.97(9)	C3-Pt1-N1	91.68(9)
C1-Pt1-N1	177.93(9)		

Table 2.1.2 Selected bond lengths [\AA] and angles [$^\circ$] for $[\text{PtMe}_3(3\text{-BrPy})_2\text{I}]$ (**2**)

Pt1-C1	2.025(10)	Pt1-N1	2.171(8)
Pt1-C2	2.036(12)	Pt1-N2	2.211(9)
Pt1-C3	2.180(13)	Pt1-I3	2.7796(8)
C1-Pt1-C2	86.7(5)	C1-Pt1-N1	176.8(4)
C1-Pt1-C3	89.0(4)	C2-Pt1-N1	90.8(4)
C2-Pt1-C3	86.1(5)	C3-Pt1-N1	88.9(3)
N1-Pt1-N2	92.9(3)	C1-Pt1-N2	89.5(4)
N1-Pt1-I3	89.2(2)	C2-Pt1-N2	176.1(4)
N2-Pt1-I3	89.9(2)	C3-Pt1-N2	92.8(4)
C1-Pt1-I3	92.8(3)	C3-Pt1-I3	176.8(3)
C2-Pt1-I3	91.3(4)		

2.1.4 Solution behaviour of [PtMe₃L₂I] (L = 4-DMAP, 3-BrPy, 4-CNPy) complexes in CDCl₃

[PtMe₃(4-DMAP)₂I] (1)

The ambient-temperature (300 K) solution ¹H NMR spectrum of [PtMe₃(4-DMAP)₂I] (**1**) at a concentration of 0.06 M in CDCl₃ exhibited well resolved signals, consistent with 4-DMAP acting as a monodentate ligand. The spectrum comprised three regions: (i) the platinum-methyl region (δ = 1.05-1.44 ppm); (ii) the N,N-dimethylamine region (δ = 3.02 ppm) and (iii) the aromatic (ligand) region (δ = 6.40-8.31 ppm). The ¹H NMR spectrum of **1** is shown in Figure 2.1.3.

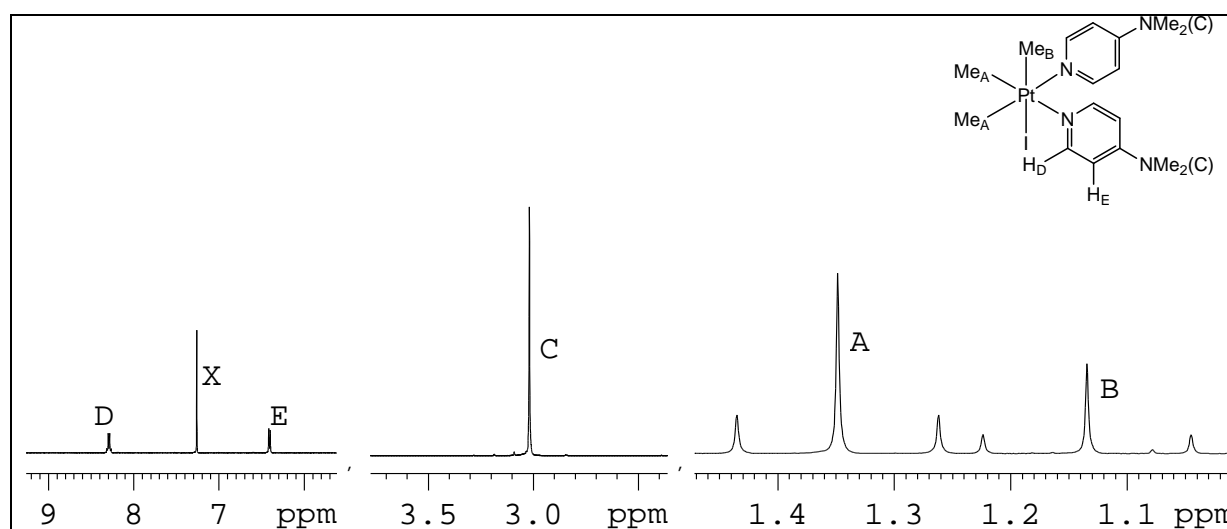


Figure 2.1.3 The 400 MHz ¹H NMR spectrum of [PtMe₃(4-DMAP)₂I] (**1**) in CDCl₃ at a concentration of 0.06 M. For labelling, see inset. X is the solvent peak.

The platinum-methyl region of the ¹H NMR spectrum of **1** comprised two signals, with satellites due to ¹⁹⁵Pt-H scalar coupling, in a 1:2 intensity ratio. The relative intensities of the signals were assigned to the *trans* I (signal B) and *trans* 4-DMAP (signal A) platinum-methyl environments, respectively. ²J_{Pt-H} scalar coupling constant observed for signal B is higher than for signal A, indicating that 4-DMAP exerts a stronger *trans* influence than iodide.

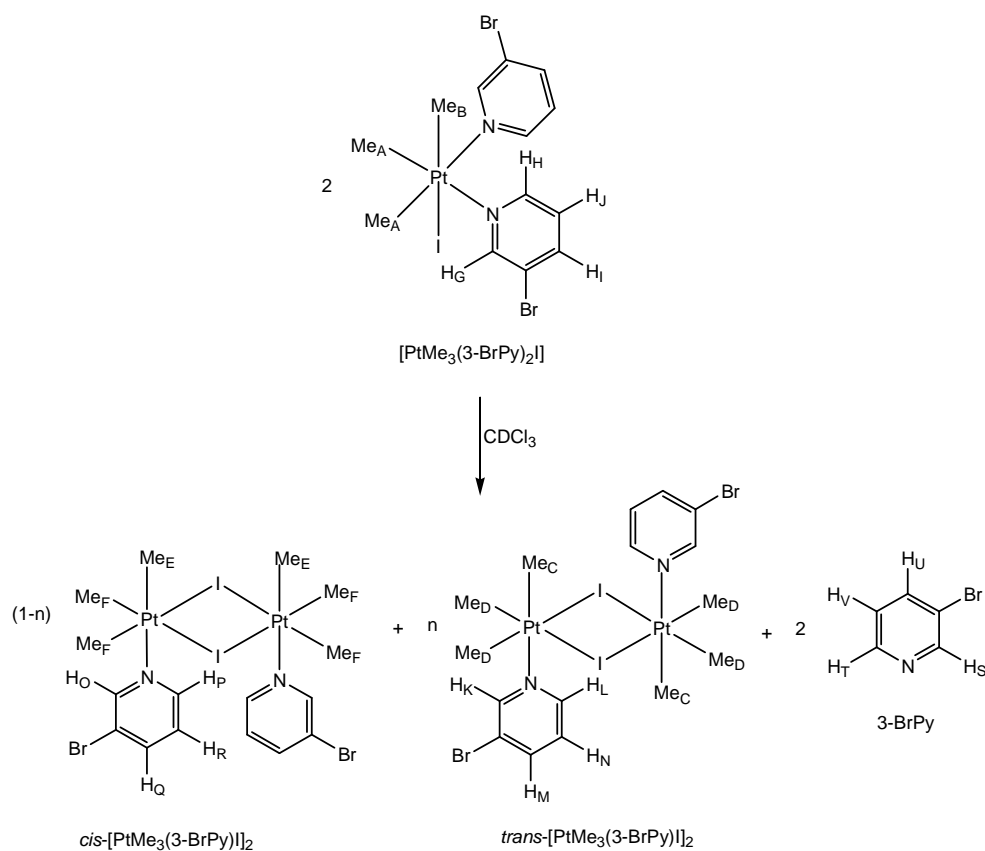
The aromatic region of the ¹H NMR spectrum displayed two signals (D and E), assigned to H_D and H_E of the 4-DMAP ligand respectively. H_D and H_E were distinguished by the coupling of H_D to ¹⁹⁵Pt (see Table 2.1.3) which allowed an assignment to the hydrogen atom adjacent to the coordinated nitrogens. The coordinated ligand sub-spectra were assigned on the basis of

their scalar coupling networks and by comparison with the ^1H NMR spectrum of the free 4-DMAP ligand.

The signal due to the N,N-dimethylamine group comprised an intense singlet (C) in the ^1H NMR spectrum of **1**.

[PtMe₃(3-BrPy)₂I] (2) and [PtMe₃(4-CNPy)₂I] (3)

The solution behaviour of both complexes, [PtMe₃(3-BrPy)₂I] (**2**) and [PtMe₃(4-CNPy)₂I] (**3**) proved very interesting. Unlike complex **1**, which exists only as a monomer in solution, it was found that even highly concentrated solution of both complexes **2** and **3** dissociates in CDCl₃ resulting in the formation of a mixture of *cis* and *trans* dinuclear complexes [PtMe₃LI]₂ and the free pyridine ligand L (L = 3-BrPy in the case of **2**, 4-CNPy in the case of **3**) (see Schemes 2.1.2-2.1.3). However, the *cis* isomer formed only to a very small degree relative to the *trans* isomer in the case of **3**. The ^1H NMR spectra of **2** and **3** in CDCl₃ at 0.06 M at 300 K are illustrated in Figures 2.1.4-2.1.5 respectively.



Scheme 2.1.2 The dissociation of [PtMe₃(3-BrPy)₂I] (**2**) into *cis* and *trans*-[PtMe₃(3-BrPy)I]₂ and 3-bromopyridine (3-BrPy) in CDCl₃ (showing the labelling).

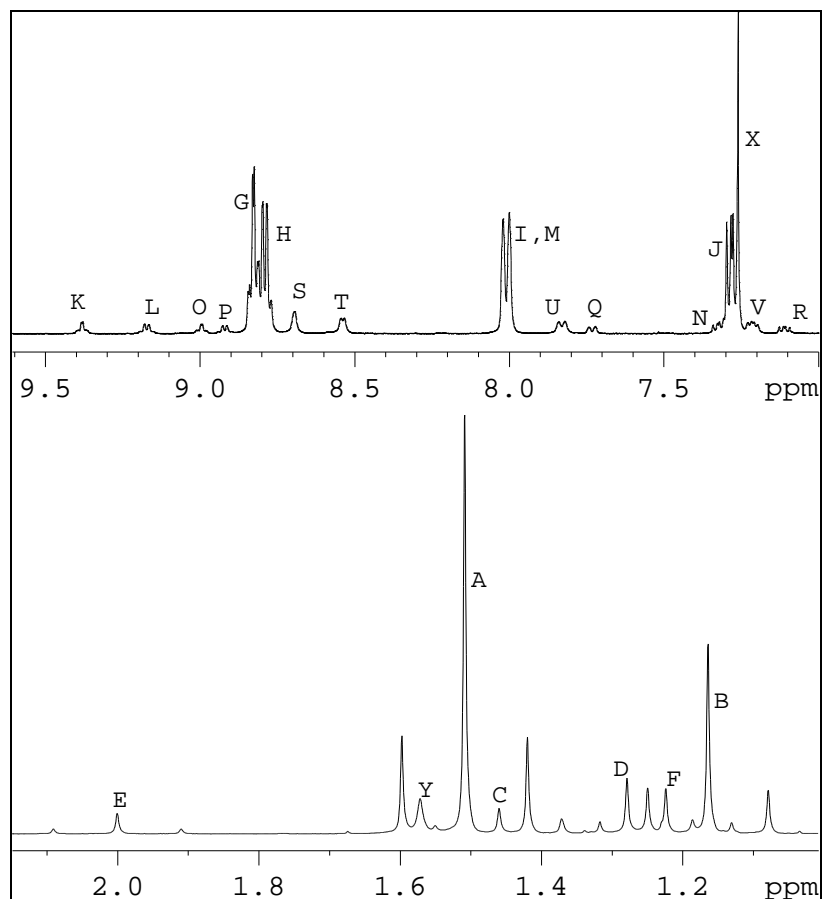
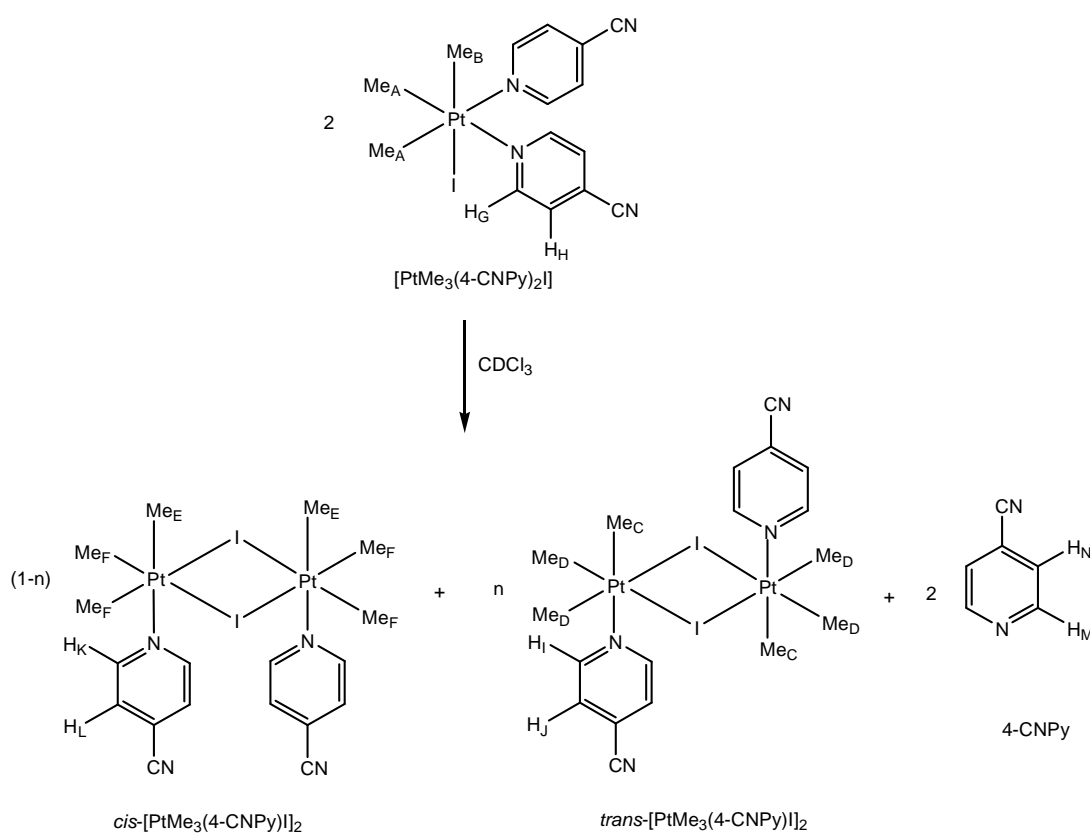


Figure 2.1.4 The 400 MHz ^1H NMR spectrum of $[\text{PtMe}_3(3\text{-BrPy})_2\text{I}]$ (**2**) in CDCl_3 at 0.06 M at 300 K. X is the solvent peak and Y is the peak for water present in CDCl_3 . For labelling, see Scheme 2.1.2. Due to close proximity, the signals G and H were not fully resolved and not assigned unambiguously. The signals I and M have virtually identical chemical shifts and not assigned unambiguously.

The platinum-methyl regions of the spectra each comprised three sets of signals, one set due to the mononuclear complex while other two sets of signals correspond to the *cis* and *trans* dinuclear complexes. The signals A and B with intensity ratio of 2:1 were assigned to *trans* pyridine ligand (3-BrPy in the case of **2**, 4-CNPy in the case of **3**) and *trans* I platinum-methyl environments, respectively for the mononuclear complex. For both *cis* and *trans* dinuclear complexes, the environment of the methyl groups *trans* to bridging iodide would be almost identical so that little, if any, difference in chemical shifts would be expected. Thus, the signals D and F were assigned to *trans* and *cis* isomer respectively. On the other hand, the methyl groups *trans* to pyridine ligand would be expected to have markedly different chemical shifts for the two isomers, since the shielding effect of the pyridine ring would be significant for *trans* isomer and insignificant for *cis* isomer. Thus, the signal at higher field (C) assigned to *trans* isomer and the one at much lower field (E) to *cis* dinuclear form.

The aromatic regions of the spectra each displayed four sets of signals, one set due to the mononuclear complex $[\text{PtMe}_3\text{L}_2\text{I}]$, two sets due to the *cis* and *trans* dinuclear complexes $[\text{PtMe}_3\text{LI}]_2$, and the one set due to the free pyridine ligand L. In the case of the 3-BrPy system, each set comprised four signals while it is two for the 4-CNPy system. Because of the influence of the aromatic ring current, aromatic ring protons for the *cis* isomer is slightly more shielded relative to the *trans* isomer. The signal for the *trans* isomer thus appears at higher frequency relative to the *cis* isomer in both complexes. The hydrogen atoms adjacent to the coordinated nitrogen exhibit ^{195}Pt scalar coupling in each of the mononuclear and dinuclear complexes.



Scheme 2.1.3 The dissociation of $[\text{PtMe}_3(4\text{-CNPy})_2\text{I}]$ (**3**) into *cis* and *trans*- $[\text{PtMe}_3(4\text{-CNPy})\text{I}]_2$ and 4-cyanopyridine (4-CNPy) in CDCl_3 (showing the labelling).

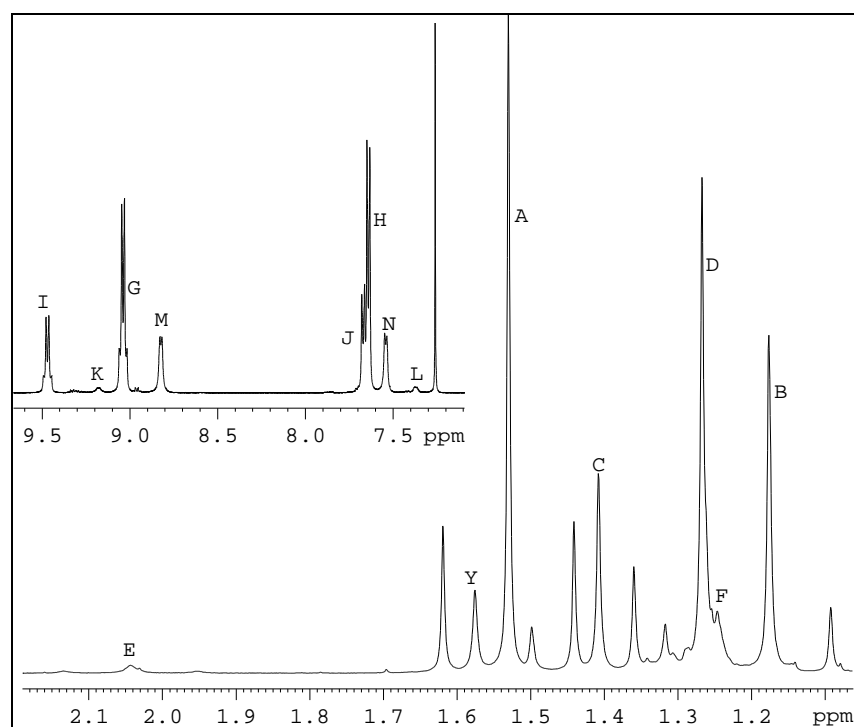


Figure 2.1.5 The 400 MHz ^1H NMR spectrum of $[\text{PtMe}_3(4\text{-CNPY})_2\text{I}]$ (**3**) in CDCl_3 at 300 K at 0.06 M. Signals X, Y are the peak for the solvent and water present in CDCl_3 , respectively. For labelling, see Scheme 2.1.3. Signals K and L were not fully resolved and not assigned unambiguously.

While it is clear from the ^1H NMR spectra of both the complexes **2** and **3** that there are indeed different Pt(IV) species present in CDCl_3 , their assignment cannot be made on the basis of this one-dimensional data alone. Therefore, these signals were distinguished by a ^1H DOSY experiment. The advantage of the DOSY technique is its ability to fully resolve multi-component mixtures arraying resonances based on their molecular weights along the diffusion axis. As shown in Figure 2.1.6 for **2**, the ^1H DOSY spectrum provides a direct observation about which of the Pt(IV) species diffuses more quickly, and therefore a fast determination of which signal originates from the free ligand and which are the dinuclear Pt(IV) species. The ^1H DOSY spectrum of **2** shows the expected diffusion order, with the free ligand 3-bromopyridine (signals S, T) having the largest diffusion coefficient and diffusing most quickly, followed by the mononuclear complex **2** (signals G, H) and dinuclear *cis*- $[\text{PtMe}_3(3\text{-BrPy})\text{I}]_2$ (signals O, P) and finally *trans*- $[\text{PtMe}_3(3\text{-BrPy})\text{I}]_2$ (signals K, L) having smallest diffusion coefficients and moving slowest. Since both the *cis* and *trans* dinuclear complexes have equal molecular weight, the DOSY peaks are not well resolved along the diffusion axis. The small modification in the diffusion values of mononuclear complex **2** and dinuclear *cis*- $[\text{PtMe}_3(3\text{-BrPy})\text{I}]_2$ compared to *trans*- $[\text{PtMe}_3(3\text{-BrPy})\text{I}]_2$ can be interpreted in terms of enlargement of the spheric size and changes in the hydrodynamic radius and shape by the

trans arrangement of the ligand molecules. Similarly, the signals which appeared in the one-dimensional ^1H spectrum of **3** were also analyzed with the help of ^1H DOSY spectroscopy (see Figure 2.1.7).

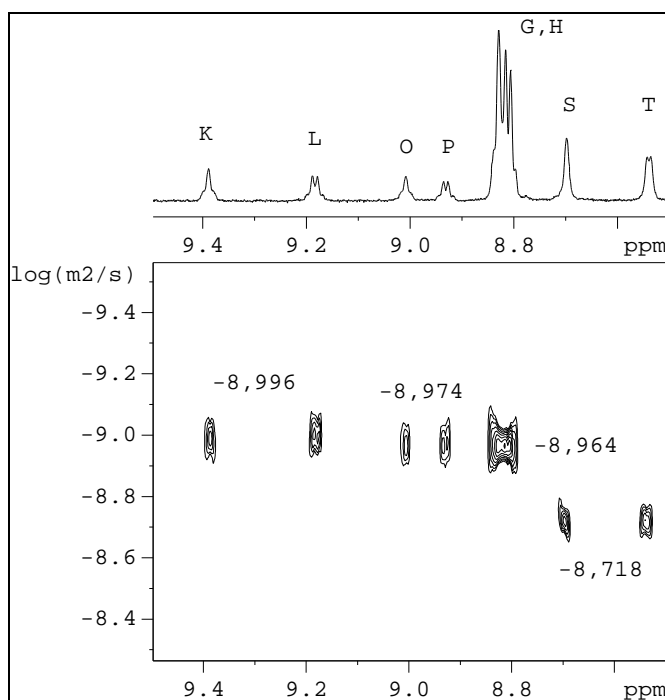


Figure 2.1.6 Part of aromatic ligand region of the 600 MHz ^1H DOSY spectrum of $[\text{PtMe}_3(3\text{-BrPy})_2]\text{I}$ (**2**) in CDCl_3 at 0.06 M showing the presence of $[\text{PtMe}_3(3\text{-BrPy})_2]\text{I}$ (**2**), *cis* and *trans*- $[\text{PtMe}_3(3\text{-BrPy})\text{I}]_2$ and 3-bromopyridine (3-BrPy). For labelling, see Scheme 2.1.2.

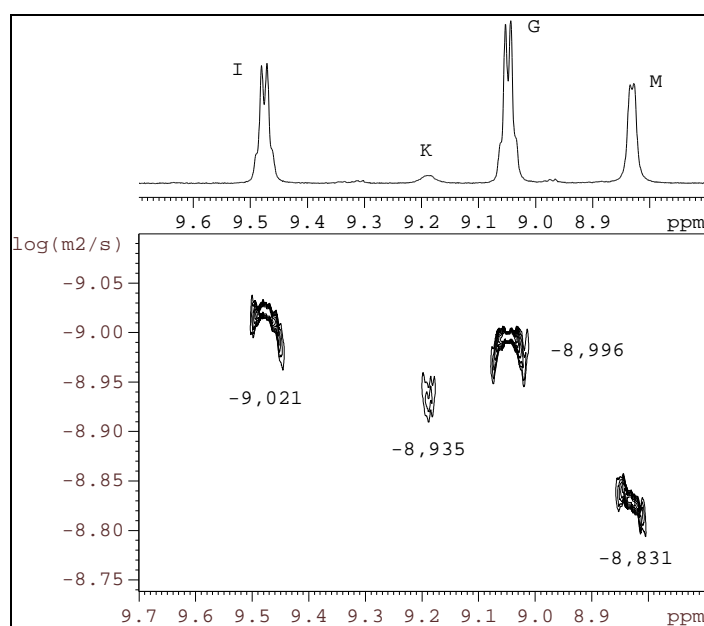


Figure 2.1.7 Part of aromatic ligand region of the 600 MHz ^1H DOSY spectrum of $[\text{PtMe}_3(4\text{-CNPy})_2]\text{I}$ (**3**) in CDCl_3 at 0.02 M showing the presence of $[\text{PtMe}_3(4\text{-CNPy})_2]\text{I}$ (**3**), *cis* and *trans*- $[\text{PtMe}_3(4\text{-CNPy})\text{I}]_2$ and 4-cyanopyridine (4-CNPy). For labelling, see Scheme 2.1.3.

Table 2.1.3 ^1H NMR data^a of 4-DMAP, 3-BrPy and 4-CNPY complexes of iodotrimethylplatinum(IV) in CDCl_3 at 300 K

Pt(IV) species	Species present in solution	$\delta(\text{Pt-CH}_3)^{b, e}$	<i>Trans</i> ligand	$\delta(\text{aromatic ligand H})^{c, e}$
[PtMe ₃ (4-DMAP) ₂ I] (Figure 2.1.3)	[PtMe ₃ (4-DMAP) ₂ I]	A 1.35 (69.3) B 1.14 (71.5)	4-DMAP I	C 3.02 D 8.29 (7.2) (19.6) ^d E 6.40 (7.2)
[PtMe ₃ (3-BrPy) ₂ I] (Figure 2.1.4)	[PtMe ₃ (3-BrPy) ₂ I]	A 1.51 (71.1) B 1.17 (68.3)	3-BrPy I	G 8.83 H 8.79 I 8.01 J 7.28
	<i>trans</i> -[PtMe ₃ (3-BrPy)I] ₂	C 1.46 (72.4) D 1.28 (74.3)	3-BrPy I	K 9.38 L 9.17 (5.8) (17.9) ^d M 8.01 N 7.32
	<i>cis</i> -[PtMe ₃ (3-BrPy)I] ₂	E 2.00 (72.2) F 1.23 (74.6)	3-BrPy I	O 8.99(13.9) ^d P 8.92 (5.4) (17.7) ^d Q 7.73 (8.0) R 7.11 (13.5)
	Free 3-BrPy			S 8.70 T 8.54 (4.0) U 7.83 (8.1) V 7.21
[PtMe ₃ (4-CNPY) ₂ I] (Figure 2.1.5)	[PtMe ₃ (4-CNPY) ₂ I]	A 1.53 (71.2) B 1.18 (67.3)	4-CNPY I	G 9.04 (6.4) (17.9) ^d H 7.64 (6.5)
	<i>trans</i> -[PtMe ₃ (4-CNPY)I] ₂	C 1.41 (72.5) D 1.27 (73.9)	4-CNPY I	I 9.47 (6.4) (18.5) ^d J 7.67 (6.5)
	<i>cis</i> -[PtMe ₃ (4-CNPY)I] ₂	E 2.04 (72.6) F 1.25	4-CNPY I	K 9.18 L 7.37
	Free 4-CNPY			M 8.82 (4.9) N 7.54 (5.0)

^a Chemical shifts quoted in ppm are relative to an internal solvent peak (CDCl_3 , $\delta = 7.26$ ppm). ^b $^2J_{\text{Pt-H}}$ /Hz in parentheses. ^c $^3J_{\text{H-H}}$ /Hz in parentheses. ^d $^3J_{\text{Pt-H}}$ /Hz in parentheses. ^e labelling refers to inset in Figure 2.1.3 and Schemes 2.1.2 and 2.1.3; not all scalar couplings resolved.

Table 2.1.4 Concentration-dependent solution behaviour of [PtMe₃L₂I] complexes (L = 4-DMAP, 3-BrPy, 4-CNPy)

Pt(IV) species	Concentration (in M)	Population of Monomer / Population of Dimer
[PtMe ₃ (4-DMAP) ₂ I] (1)	6.0 x 10 ⁻²	∞ ^a
	5.4 x 10 ⁻³	∞ ^a
[PtMe ₃ (3-BrPy) ₂ I] (2)	6.0 x 10 ⁻²	7.33
	5.4 x 10 ⁻³	3.0
[PtMe ₃ (4-CNPy) ₂ I] (3)	6.0 x 10 ⁻²	2.23
	5.4 x 10 ⁻³	1.08

^a In the case of [PtMe₃(4-DMAP)₂I], only monomer is present in solution (both in high and low concentration).

The population ratios of the mononuclear form to the dinuclear form for the [PtMe₃L₂I] (L= 4-DMAP, 3-BrPy, 4-CNPy) complexes at different concentration in CDCl₃ are reported in Table 2.1.4. This shows that complex [PtMe₃(4-DMAP)₂I] (**1**) is highly stable in solution and exists only as a monomer. However, the other two complexes [PtMe₃(3-BrPy)₂I] (**2**) and [PtMe₃(4-CNPy)₂I] (**3**) are not very stable in solution and both undergo dissociation which increases with dilution. Dissociation of **3** is much more pronounced than for **2**. This relationship may be rationalised in terms of a decrease in the Pt-N interaction in the mononuclear complexes, and would therefore be expected to be in accordance with the electron density present on the pyridine ring nitrogen. The relative electron densities present on the pyridine ring nitrogen are in the order: 4-DMAP > 3-BrPy > 4-CNPy. This implies that electron density on the pyridine ring N decreases from 4-DMAP to 4-CNPy. As the electron density on the pyridine ring N decreases, the Pt-N interaction weakens, thereby leading to a destabilisation of the mononuclear complexes. The resulting dissociation of the mononuclear complexes in solution leads to the formation of the iodide bridged dinuclear complexes. The increase in the extent of dissociation of the mononuclear complexes with dilution is most likely due to increasing stabilization of the free pyridine ligand by the solvent molecules.

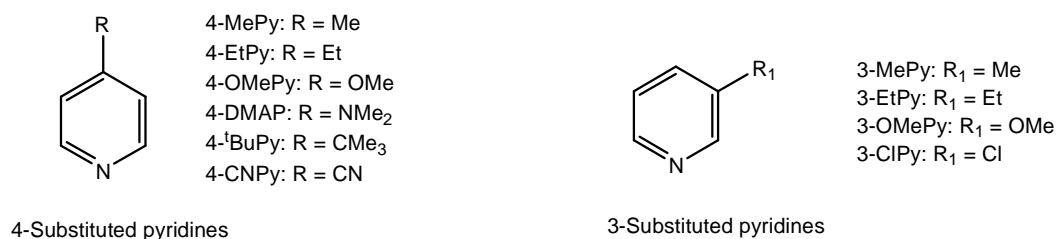
2.1.5 Conclusion

Three mononuclear iodotrimethylplatinum(IV) complexes of pyridines, $[\text{PtMe}_3\text{L}_2\text{I}]$ [where L= 4-dimethylaminopyridine (4-DMAP), 3-bromopyridine (3-BrPy), 4-cyanopyridine (4-CNPy)] were successfully synthesized and fully characterized. The crystal structures of $[\text{PtMe}_3(4\text{-DMAP})_2\text{I}]$ (**1**) and $[\text{PtMe}_3(3\text{-BrPy})_2\text{I}]$ (**2**) reveal the expected *fac*-octahedral coordination of the PtMe_3 moiety in these trimethylplatinum(IV) complexes of pyridines. Although the pyridine substituents have no significant influence on the crystal structures of the trimethylplatinum complexes of pyridines, solution behaviour of these mononuclear complexes depends largely on the coordinated pyridines and on the concentration of the mononuclear complexes. For strongly electron donating pyridines, the complexes do not undergo dissociation in solution while increasing electron deficiency in the pyridine ring nitrogen leads to the increasing dissociation of the complexes in solution. As a result of the dissociation of the mononuclear complexes, iodide bridged dinuclear complexes $[\text{PtMe}_3\text{LI}]_2$ (L= 3-BrPy and 4-CNPy) are formed in solution. ^1H NMR spectra exhibit evidence of two isomers (*cis* and *trans*- $[\text{PtMe}_3\text{LI}]_2$) present in solution. Dissociation of the mononuclear complexes also leads to the formation of free pyridine ligands (3-BrPy in the case of **2** and 4-CNPy in the case of **3**) along with the corresponding dinuclear complexes, thereby equilibrium between these species is formed in solution. The dissociation of the mononuclear complexes also increases with the dilution of the complexes.

2.2 Substituent Effects on the Reaction of Iodotrimethylplatinum(IV) Complexes of Pyridines with Tetranuclear Iodotrimethylplatinum(IV)

2.2.1 Introduction

The solution phase investigation of mononuclear iodotrimethylplatinum(IV) complexes of substituted pyridines as described in Chapter 2.1 reveals that the formation of aggregation equilibrium depends on the type of pyridine substituent attached to the trimethylplatinum(IV) moiety and also on the concentration of the mononuclear complexes. Furthermore, the influence of pyridine substituent on the solution dynamics proved more significant than the influence on the crystal structure of these mononuclear trimethylplatinum(IV) complexes of pyridines. In extending the studies on the aggregation behaviour of trimethylplatinum(IV) system, we hereby describe the reaction of mononuclear iodotrimethylplatinum(IV) complexes of pyridines with tetranuclear iodotrimethylplatinum(IV) in chloroform. Iodotrimethylplatinum reacts with mononuclear $[\text{PtMe}_3\text{L}_2\text{I}]$ ($\text{L} = \text{pyridines}$) complexes in equimolar ratio in chloroform to form a mixture of dinuclear complexes, *cis* and *trans*- $[\text{PtMe}_3\text{LI}]_2$. Two types of pyridines were chosen for this reaction, namely 4-substituted pyridines [4-methylpyridine (4-MePy), 4-ethylpyridine(4-EtPy), 4-methoxypyridine (4-OMePy), 4-dimethylaminopyridine (4-DMAP), 4-cyanopyridine (4-CNPy), and 4-^tbutylpyridine (4-^tBuPy)] and 3-substituted pyridines [3-methylpyridine (3-MePy), 3-ethylpyridine (3-EtPy), 3-methoxypyridine (3-OMePy), and 3-chloropyridine (3-CIPy)] (Scheme 2.2.1). The reaction has been followed by ¹H NMR spectroscopy. The effects of the electron density on the pyridine nitrogen, influenced by the nature of the substituent present on the pyridine ring, on the equilibrium population of the dinuclear form and the mononuclear form for this reaction are discussed. The steric influences of the pyridine substituent are also investigated here. The crystal structures of $[\text{PtMe}_3\text{L}_2\text{I}]$ ($\text{L} = 4\text{-MePy}$, 4-EtPy , 4-OMePy and 3-OMePy) are also reported here.



Scheme 2.2.1 Different substituted pyridines used for the reaction of $[\text{PtMe}_3\text{L}_2\text{I}]$ with $[\text{PtMe}_3\text{I}]_4$.

2.2.2 Syntheses and characterization of the complexes

The pale yellow to yellow crystalline mononuclear iodotrimethylplatinum(IV) complexes, $[\text{PtMe}_3\text{L}_2\text{I}]$ (L= 3- and 4-substituted pyridines) were synthesized in a similar way by the reaction of iodotrimethylplatinum(IV) with different substituted pyridines as described in Chapter 2.1. All the synthesized complexes are soluble in chloroform and characterized by IR, ^1H NMR spectroscopy and elemental analyses (see Chapter 5.3.3).

2.2.3 X-ray crystallographic characterization of $[\text{PtMe}_3\text{L}_2\text{I}]$ complexes (L = 4-MePy, 4-EtPy, 4-OMePy and 3-OMePy)

Single crystals of the complexes $[\text{PtMe}_3\text{L}_2\text{I}]$ complexes (L = 4-MePy, 4-EtPy, 4-OMePy and 3-OMePy) were obtained by slow diffusion of n-hexane into their chloroform solution. X-ray diffraction parameters and crystallographic data of the complexes are given in Tables 5.4.3-5.4.6. The molecular structures of the complexes are depicted in Figures 2.2.1-2.2.4, while selected bond lengths and bond angles are summarized in Table 2.2.1.

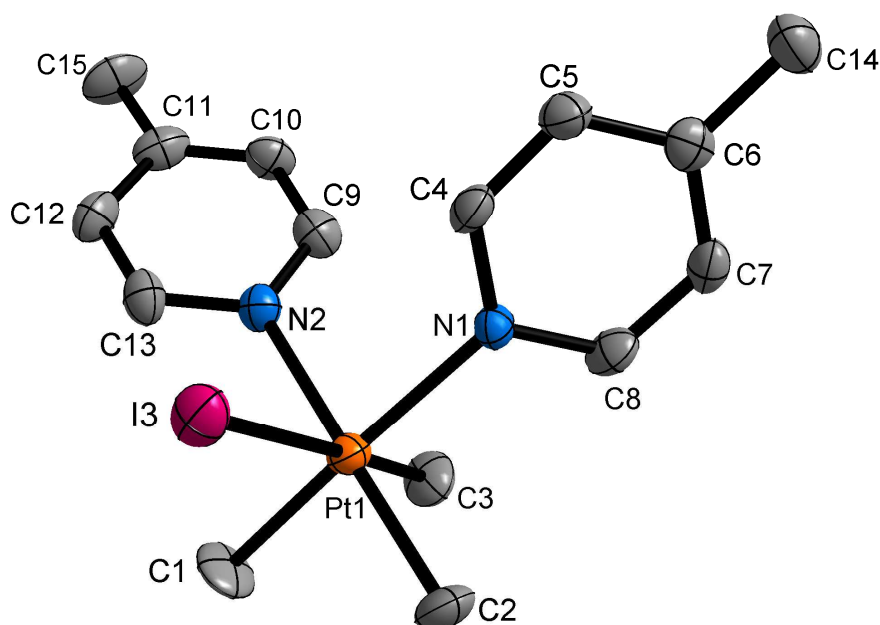


Figure 2.2.1 Molecular structure of $[\text{PtMe}_3(4\text{-MePy})_2\text{I}]$ showing the atom labelling scheme. Thermal ellipsoids are at the 50% probability level. Hydrogen atoms are omitted for clarity.

Each of the three complexes $[\text{PtMe}_3(4\text{-MePy})_2\text{I}]$, $[\text{PtMe}_3(4\text{-EtPy})_2\text{I}]$ and $[\text{PtMe}_3(3\text{-OMePy})_2\text{I}]$ has four, whereas $[\text{PtMe}_3(4\text{-OMePy})_2\text{I}]$ has eight molecules in the unit cell. $[\text{PtMe}_3(4\text{-MePy})_2\text{I}]$ crystallized in the monoclinic $P2_1/n$ space group, $[\text{PtMe}_3(4\text{-EtPy})_2\text{I}]$ in monoclinic $P2_1/c$, $[\text{PtMe}_3(3\text{-OMePy})_2\text{I}]$ in monoclinic $P2_1/a$, and $[\text{PtMe}_3(4\text{-OMePy})_2\text{I}]$ in orthorhombic $Pbca$. All the structures consist of a discrete monomeric unit in which the platinum atom is six-fold coordinated by the three methyl groups in a *facial* arrangement, two pyridine ligands and an iodine atom.

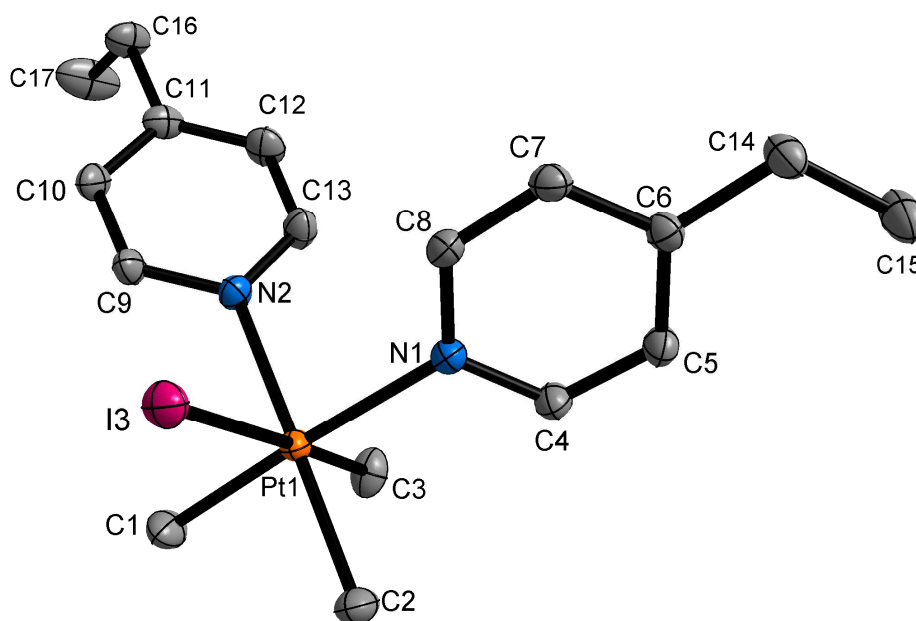


Figure 2.2.2 Molecular structure of $[\text{PtMe}_3(4\text{-EtPy})_2\text{I}]$ showing the atom labelling scheme. Thermal ellipsoids are at the 50% probability level. Hydrogen atoms are omitted for clarity.

The Pt-N bond distances in all the four structures do not differ significantly (2.17-2.20 Å) and are essentially identical to those found in the complexes $[\text{PtMe}_3(4\text{-DMAP})_2\text{I}]$ (2.17, 2.18 Å) and $[\text{PtMe}_3(3\text{-BrPy})_2\text{I}]$ (2.19 and 2.21 Å). The Pt-I bond distance in all the structures is almost the same (2.77-2.78 Å). Except $[\text{PtMe}_3(4\text{-MePy})_2\text{I}]$, where one of the two Pt- $C_{\text{trans N}}$ bonds is marginally longer than the Pt- $C_{\text{trans I}}$ bond, in all the other three complexes Pt- $C_{\text{trans N}}$ bonds are shorter than the Pt- $C_{\text{trans I}}$ bond as observed in the complexes $[\text{PtMe}_3(4\text{-DMAP})_2\text{I}]$ and $[\text{PtMe}_3(3\text{-BrPy})_2\text{I}]$. Little distortion from the regular octahedral geometry in all complexes is revealed. Adjacent 4-ethylpyridine ligands in $[\text{PtMe}_3(4\text{-EtPy})_2\text{I}]$ open up the N1-Pt1-N2 angle to 90.7° , thereby reducing the angles of the *trans* related bonds, namely N1-Pt1-C1 and N2-Pt1-C2 from 180° to 176.8° and 178.5° respectively. Similarly adjacent 4-methoxypyridine ligands in $[\text{PtMe}_3(4\text{-OMePy})_2\text{I}]$ open up the N1-Pt1-N2 angle to 90.7° ,

thereby reducing the angles of the *trans* related bonds, namely N1-Pt1-C1 and N2-Pt1-C2 from 180° to 176.3° and 179.3° respectively. N1-Pt1-N2 bond angle (88.9°) in [PtMe₃(4-MePy)₂I] narrows down the N1-Pt1-C1 and N2-Pt1-C2 *trans* angles to 177.0° and 178.4° respectively. Also, adjacent 3-methoxypyridine ligands in [PtMe₃(3-OMePy)₂I] open up the N1-Pt1-N2 angle to 90.5° , thereby reducing N1-Pt1-C1 and N2-Pt1-C2 angles to 177.6° and 176.5° respectively.

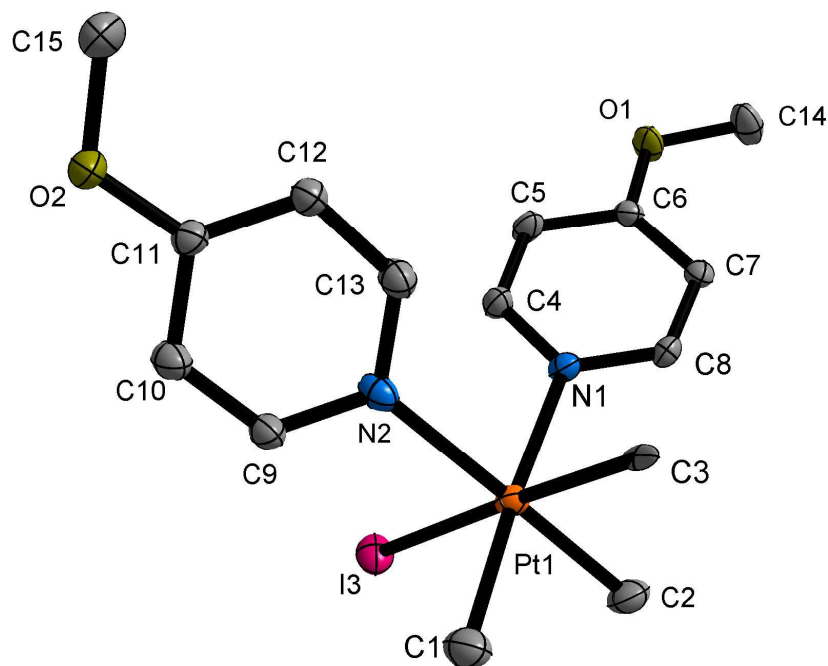


Figure 2.2.3 Molecular structure of [PtMe₃(4-OMePy)₂I] showing the atom labelling scheme. Thermal ellipsoids are at the 50% probability level. Hydrogen atoms are omitted for clarity.

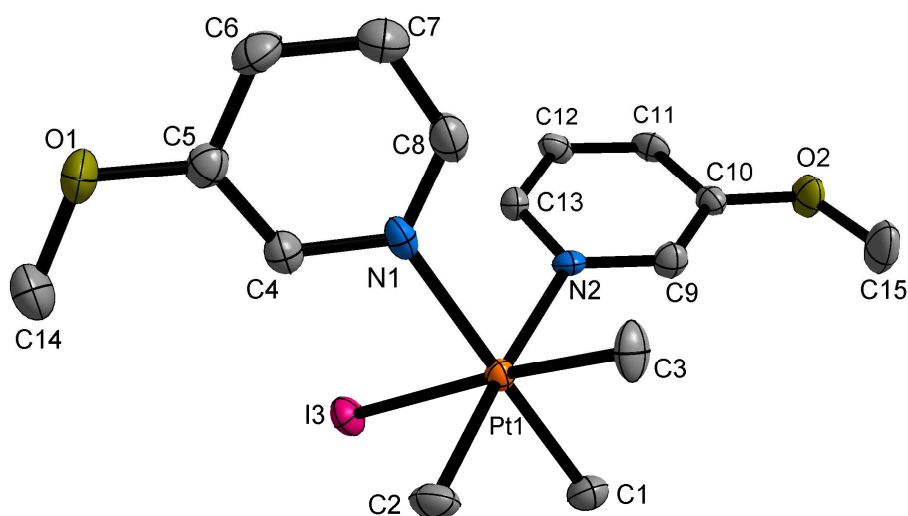


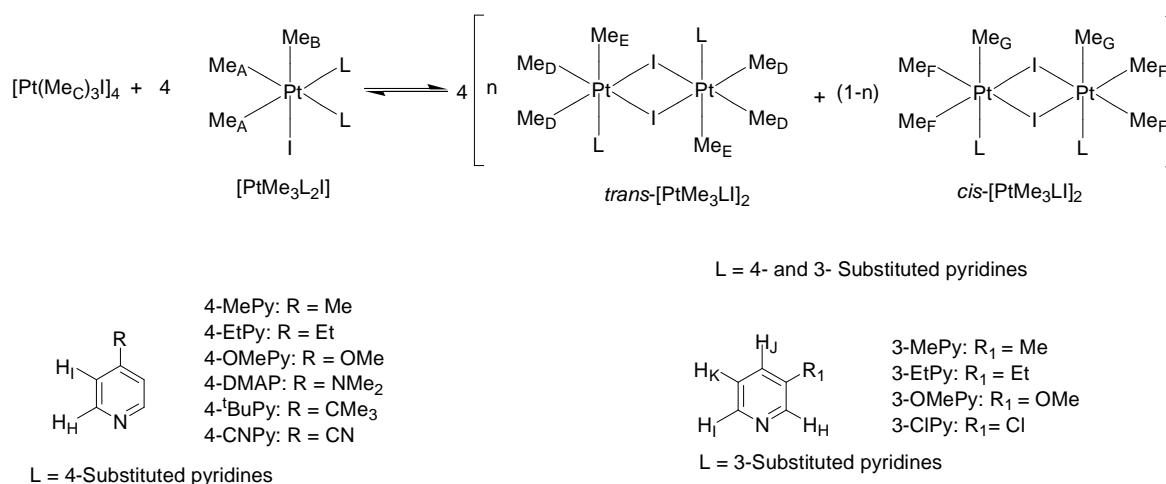
Figure 2.2.4 Molecular structure of [PtMe₃(3-OMePy)₂I] showing the atom labelling scheme. Thermal ellipsoids are at the 50% probability level. Hydrogen atoms are omitted for clarity.

Table 2.2.1 Selected bond lengths [\AA] and angles [$^\circ$] for $[\text{PtMe}_3\text{L}_2\text{I}]$ (L = 4-MePy, 4-EtPy, 4-OMePy, 3-OMePy) complexes

	$[\text{PtMe}_3(4\text{-MePy})_2\text{I}]$	$[\text{PtMe}_3(4\text{-EtPy})_2\text{I}]$	$[\text{PtMe}_3(4\text{-OMePy})_2\text{I}]$	$[\text{PtMe}_3(3\text{-OMePy})_2\text{I}]$
Pt1-C1	2.049(8)	2.053(2)	2.087(6)	2.030(6)
Pt1-C2	2.031(7)	2.054(2)	2.053(6)	2.024(6)
Pt1-C3	2.041(8)	2.067(2)	2.232(7)	2.058(6)
Pt1-N1	2.178(6)	2.1751(16)	2.174(4)	2.188(5)
Pt1-N2	2.177(6)	2.1863(16)	2.196(5)	2.184(5)
Pt1-I3	2.7746(7)	2.7774(3)	2.7701(6)	2.785(5)
C2-Pt1-C1	88.3(4)	87.77(9)	87.4(2)	87.1(3)
C2-Pt1-C3	88.5(4)	89.57(9)	90.1(2)	85.7(3)
C1-Pt1-C3	85.8(4)	85.34(9)	84.5(2)	89.3(3)
C1-Pt1-N1	177.0(3)	176.81(8)	176.3(2)	177.6(2)
C2-Pt1-N1	90.9(3)	90.51(7)	89.9(2)	91.9(2)
C3-Pt1-N1	91.3(3)	91.96(8)	92.96(17)	88.5(2)
C1-Pt1-N2	91.8(3)	91.00(8)	91.9(2)	90.4(2)
C2-Pt1-N2	178.4(3)	178.51(7)	179.3(2)	176.5(2)
C3-Pt1-N2	89.9(3)	89.49(8)	90.02(17)	91.9(2)
C1-Pt1-I3	92.1(3)	92.88(7)	92.5(2)	89.0(2)
C2-Pt1-I3	92.1(3)	90.04(6)	90.02(19)	90.3(2)
C3-Pt1-I3	177.8(3)	178.20(7)	176.96(13)	175.7(2)
N1-Pt1-I3	90.83(15)	89.80(4)	90.08(12)	93.2(13)
N2-Pt1-I3	89.45(15)	90.87(4)	89.82(12)	92.06(13)
N1-Pt1-N2	88.9(2)	90.67(6)	90.72(16)	90.48(17)

2.2.4 ^1H NMR studies for the reaction of $[\text{PtMe}_3\text{I}]_4$ with $[\text{PtMe}_3\text{L}_2\text{I}]$ complexes (L = 4-MePy, 4-EtPy, 4-OMePy, 4-DMAP, 4- $^t\text{BuPy}$, 4-CNPy, 3-MePy, 3-EtPy, 3-OMePy, 3-CIPy)

Tetranuclear iodotrimethylplatinum(IV) reacts with mononuclear $[\text{PtMe}_3\text{L}_2\text{I}]$ (L= 3- and 4-substituted pyridines) complexes to form the corresponding dinuclear complexes of iodotrimethylplatinum(IV), $[\text{PtMe}_3\text{LI}]_2$. The ambient temperature (300 K) solution ^1H NMR spectrum for the reaction of an equimolar mixture of iodotrimethylplatinum(IV) and $[\text{PtMe}_3\text{L}_2\text{I}]$ at equilibrium exhibited well resolved signals. The ^1H NMR spectrum for the reaction of an equimolar mixture of $[\text{PtMe}_3(4\text{-OMePy})_2\text{I}]$ and iodotrimethylplatinum(IV) at equilibrium in CDCl_3 is shown in Figure 2.2.5, while the ^1H NMR spectrum for the reaction of $[\text{PtMe}_3(3\text{-CIPy})_2\text{I}]$ with $[\text{PtMe}_3\text{I}]_4$ in equimolar mixture at equilibrium is shown in Figure 2.2.6.



Scheme 2.2.2 The reaction of an equimolar mixture of iodotrimethylplatinum(IV) and mononuclear $[\text{PtMe}_3\text{L}_2\text{I}]$ (L = 4- and 3-substituted pyridines) complexes in chloroform showing the proton labelling.

The platinum-methyl regions of the spectra each comprised four sets of signals (one set due to the mononuclear $[\text{PtMe}_3\text{L}_2\text{I}]$, one to $[\text{PtMe}_3\text{I}]_4$ and two others corresponding to *cis* and *trans* dinuclear $[\text{PtMe}_3\text{LI}]_2$ complexes) with satellites due to ^{195}Pt -H scalar coupling. The mononuclear $[\text{PtMe}_3\text{L}_2\text{I}]$ shows two platinum-methyl signals in an intensity ratio of 2:1, assigned to the *trans* L (signal A) and *trans* I (signal B) platinum-methyl environments, respectively with same or different coupling constants (see Tables 2.2.2-2.2.3). The iodotrimethylplatinum(IV) shows only a single platinum-methyl resonance (signal C) at $\delta = 1.72$ ppm. The signals D and E correspond to *trans*- $[\text{PtMe}_3\text{LI}]_2$, while F and G were assigned to *cis*- $[\text{PtMe}_3\text{LI}]_2$.

The aromatic regions of the spectra each consist of signals for three complexes ($[\text{PtMe}_3\text{L}_2\text{I}]$, *cis* and *trans*- $[\text{PtMe}_3\text{LI}]_2$). For 4-substituted pyridine based systems, each of the three complexes comprised two signals for the ring protons while there are four signals for 3-substituted pyridines. Due to the shielding effect caused by the presence of aromatic ring current, the signal for the *trans* isomer appears at higher frequency than for the *cis* isomer. The highest frequency signals in each set of complexes displayed measurable ^{195}Pt -H scalar coupling (see Tables 2.2.2-2.2.3), which enabled an assignment to the hydrogen atoms adjacent to the coordinated nitrogens.

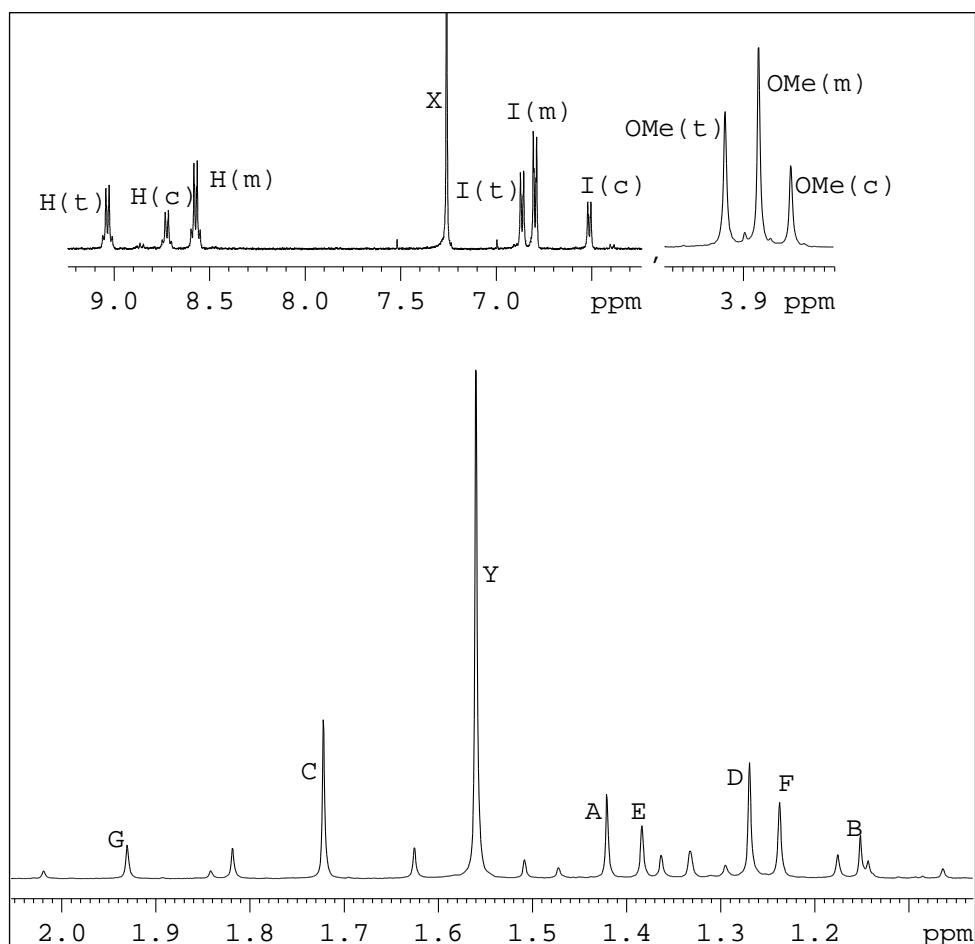


Figure 2.2.5 The 400 MHz ^1H NMR spectrum for the reaction of $[\text{PtMe}_3(4\text{-OMePy})_2\text{I}]$ with $[\text{PtMe}_3\text{I}]_4$ in equimolar mixture at equilibrium in CDCl_3 at 300 K. For labelling, see Scheme 2.2.2. (t) = *trans*- $[\text{PtMe}_3(4\text{-OMePy})\text{I}]_2$. (c) = *cis*- $[\text{PtMe}_3(4\text{-OMePy})\text{I}]_2$. (m) = $[\text{PtMe}_3(4\text{-OMePy})_2\text{I}]$. X is the solvent peak and Y is the peak for water present in CDCl_3 .

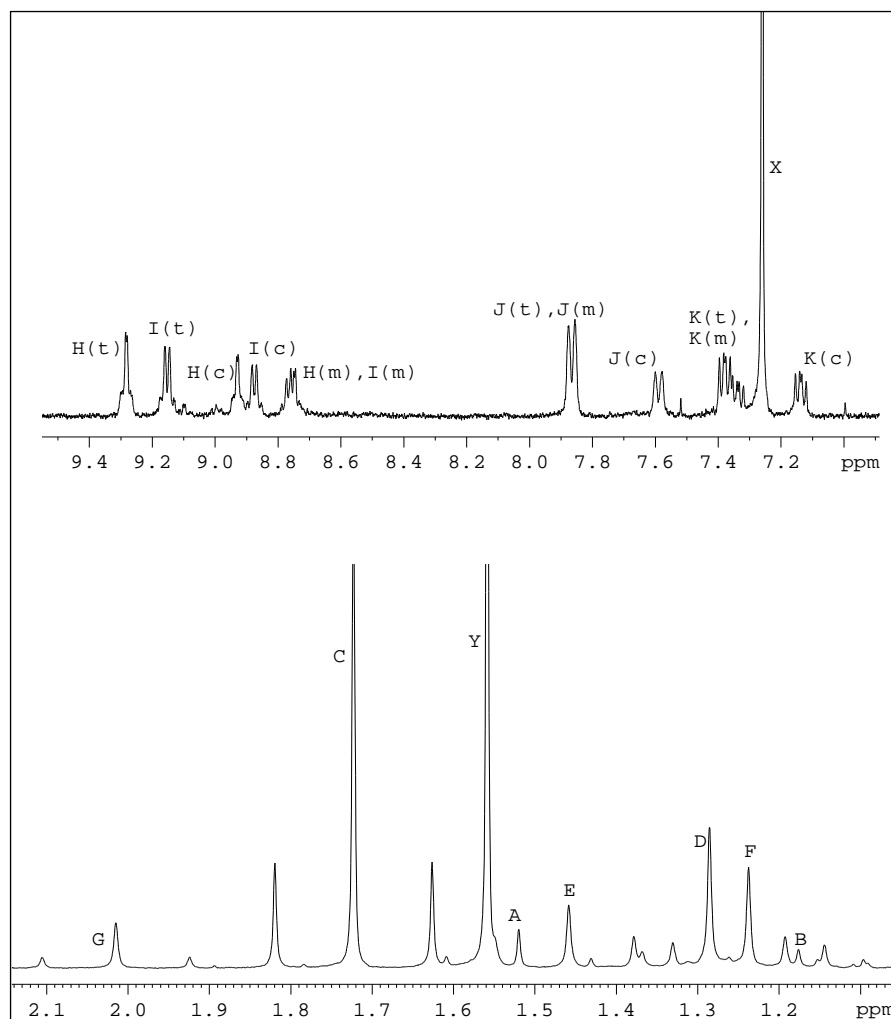
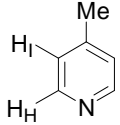
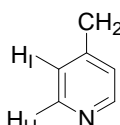
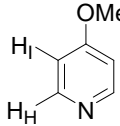
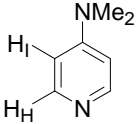
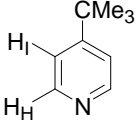
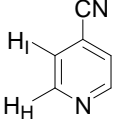


Figure 2.2.6 The 400 MHz ¹H NMR spectrum for the reaction of [PtMe₃(3-ClPy)₂I] with [PtMe₃I]₄ in equimolar mixture at equilibrium in CDCl₃ at 300 K. For labelling, see Scheme 2.2.2. (t) = *trans*-[PtMe₃(3-ClPy)I]₂. (c) = *cis*-[PtMe₃(3-ClPy)I]₂. (m) = [PtMe₃(3-ClPy)₂I]. X is the solvent peak and Y is the peak for water present in CDCl₃.

Table 2.2.2 ^1H NMR data^a for the reaction of $[\text{PtMe}_3\text{I}]_4$ with $[\text{PtMe}_3\text{L}_2\text{I}]$ at equilibrium at 300 K (L = 4-substituted pyridines) in CDCl_3

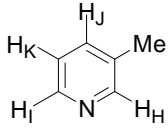
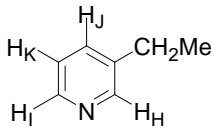
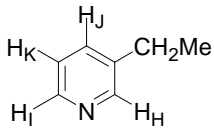
Ligand L of $[\text{PtMe}_3\text{L}_2\text{I}]$	Pt(IV) species present at equilibrium	$\delta(\text{Pt-Me})^{b, e}$	<i>Trans</i> ligand	$\delta(\text{ligand H})^{c, e}$	
 4-Methylpyridine (4-MePy)	$[\text{PtMe}_3(4\text{-MePy})_2\text{I}]$	A 1.45 (70.0) B 1.17 (70.0)	4-MePy I	H 8.61 (6.4) (19.0) ^d I 7.12 (6.0) Me 2.38	
	$[\text{PtMe}_3\text{I}]_4$	C 1.72 (77.3)	I	-	
	<i>trans</i> - $[\text{PtMe}_3(4\text{-MePy})\text{I}]_2$	D 1.27 (75.1) E 1.37 (71.1)	I 4-MePy	H 9.08 (6.5) (19.6) ^d I 7.19 (6.0) Me 2.41	
	<i>cis</i> - $[\text{PtMe}_3(4\text{-MePy})\text{I}]_2$	F 1.25 (75.1) G 1.97 (71.1)	I 4-MePy	H 8.76 (6.4) (19.2) ^d I 6.84 (5.8) Me 2.33	
	 4-Ethylpyridine (4-EtPy)	$[\text{PtMe}_3(4\text{-EtPy})_2\text{I}]$	A 1.45 (70.1) B 1.18 (70.2)	4-EtPy I	H 8.64 (6.4) (18.9) ^d I 7.15 (6.4) CH ₂ 2.68 Me 1.27
		$[\text{PtMe}_3\text{I}]_4$	C 1.72 (77.3)	I	-
<i>trans</i> - $[\text{PtMe}_3(4\text{-EtPy})\text{I}]_2$		D 1.28 (75.1) E 1.36 (71.0)	I 4-EtPy	H 9.11 (6.6) (19.8) ^d I 7.21 (6.3) CH ₂ 2.72 Me 1.30	
<i>cis</i> - $[\text{PtMe}_3(4\text{-EtPy})\text{I}]_2$		F 1.28 (75.1) G 1.99 (71.1)	I 4-EtPy	H 8.79 (6.5) (19.4) ^d I 6.88 (6.1) CH ₂ 2.62 Me 1.26	
 4-Methoxypyridine (4-OMePy)		$[\text{PtMe}_3(4\text{-OMePy})_2\text{I}]$	A 1.42 (70.0) B 1.15 (70.2)	4-OMePy I	H 8.58 (7.0) (19.0) ^d I 6.80 (7.0) OMe 3.89
		$[\text{PtMe}_3\text{I}]_4$	C 1.72 (77.3)	I	-
	<i>trans</i> - $[\text{PtMe}_3(4\text{-OMePy})\text{I}]_2$	D 1.27 (75.1) E 1.38 (71.0)	I 4-OMePy	H 9.04 (6.9) (19.7) ^d I 6.86 (7.0) OMe 3.92	
	<i>cis</i> - $[\text{PtMe}_3(4\text{-OMePy})\text{I}]_2$	F 1.24 (75.2) G 1.93 (71.0)	I 4-OMePy	H 8.73 (6.8) (19.5) ^d I 6.51 (6.9) OMe 3.85	

(Continued)

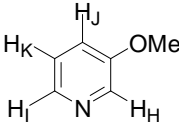
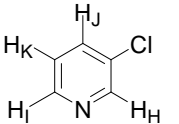
Ligand L of [PtMe ₃ L ₂ I]	Pt(IV) species present at equilibrium	$\delta(\text{Pt-Me})^{b, e}$	Trans ligand	$\delta(\text{ligand H})^{c, e}$	
 4-Dimethylaminopyridine (4-DMAP)	[PtMe ₃ (4-DMAP) ₂ I]	A 1.35 (69.3) B 1.14 (71.5)	4-DMAP I	H 8.29 (7.2) (19.6) ^d I 6.40 (7.2) NMe ₂ 3.02	
	[PtMe ₃ I] ₄	C 1.72 (77.3)	I	-	
	<i>trans</i> -[PtMe ₃ (4-DMAP)I] ₂	D 1.27 (75.6) E 1.39 (70.0)	I 4-DMAP	H 8.74 (7.1) (20.6) ^d I 6.49 (7.1) NMe ₂ 3.05	
	<i>cis</i> -[PtMe ₃ (4-DMAP)I] ₂	F 1.27 (75.6) G 1.90 (70.1)	I 4-DMAP	H 8.48 (7.0) (20.3) ^d I 6.20 (7.0) NMe ₂ 2.99	
	 4- ^t Butylpyridine (4- ^t BuPy)	[PtMe ₃ (4- ^t BuPy) ₂ I]	A 1.45 (69.9) B 1.19 (70.1)	4- ^t BuPy I	H 8.66 (6.5) (19.0) ^d I 7.30 (6.7) ^t Bu 1.33
		[PtMe ₃ I] ₄	C 1.72 (77.3)	I	-
<i>trans</i> -[PtMe ₃ (4- ^t BuPy)I] ₂		D 1.30 (75.1) E 1.35 (70.8)	I 4- ^t BuPy	H 9.12 (6.6) (19.8) ^d I 7.36 (6.6) ^t Bu 1.35	
<i>cis</i> -[PtMe ₃ (4- ^t BuPy)I] ₂		F 1.34 (75.1) G 2.01 (71.2)	I 4- ^t BuPy	H 8.82 (6.6) (19.4) ^d I 7.09 (6.4) ^t Bu 1.32	
 4-Cyanopyridine (4-CNPy)		[PtMe ₃ (4-CNPy) ₂ I]	A 1.53 (71.2) B 1.18 (67.3)	4-CNPy I	H 9.04 (6.4) (17.9) ^d I 7.64 (6.5)
		[PtMe ₃ I] ₄	C 1.72 (77.4)	I	-
	<i>trans</i> -[PtMe ₃ (4-CNPy)I] ₂	D 1.27 (73.9) E 1.41 (72.5)	I 4-CNPy	H 9.47 (6.4) (18.5) ^d I 7.67 (6.5)	
	<i>cis</i> -[PtMe ₃ (4-CNPy)I] ₂	F 1.25 G 2.04 (72.6)	I 4-CNPy	H 9.18 I 7.37	

^a Chemical shifts quoted in ppm are relative to an internal solvent peak (CDCl₃, $\delta = 7.26$ ppm). ^b ²J_{Pt-H}/Hz in parentheses. ^c ³J_{H-H}/Hz in parentheses. ^d ³J_{Pt-H}/Hz in parentheses. ^e labelling refers to Scheme 2.2.2. Not all scalar coupling resolved.

Table 2.2.3 ^1H NMR data^a for the reaction of $[\text{PtMe}_3\text{I}]_4$ with $[\text{PtMe}_3\text{L}_2\text{I}]$ at equilibrium at 300 K (L = 3-substituted pyridines) in CDCl_3

Ligand L of $[\text{PtMe}_3\text{L}_2\text{I}]$	Pt(IV) species present at equilibrium	$\delta(\text{Pt-Me})^{b, e}$	Trans ligand	$\delta(\text{ligand H})^{c, e}$
 3-Methylpyridine (3-MePy)	$[\text{PtMe}_3(3\text{-MePy})_2\text{I}]$	A 1.48 (70.0) B 1.18 (69.8)	3-MePy I	H 8.67 I 8.51 (5.7) (17.8) ^d J 7.64 K 7.20 (13.2) Me 2.35
	$[\text{PtMe}_3\text{I}]_4$	C 1.72 (77.3)	I	-
	<i>trans</i> - $[\text{PtMe}_3(3\text{-MePy})\text{I}]_2$	D 1.30 (75.1) E 1.40 (71.1)	I 3-MePy	H 9.16 I 9.01 (6.0) (19.4) ^d J 7.64 K 7.28 Me 2.44
 3-Ethylpyridine (3-EtPy)	$[\text{PtMe}_3(3\text{-EtPy})_2\text{I}]$	A 1.48 (70.0) B 1.19 (69.7)	3-EtPy I	H 8.64 I 8.56 (5.7) (17.2) ^d J 7.66 K 7.23 CH ₂ 2.65 Me 1.20
	$[\text{PtMe}_3\text{I}]_4$	C 1.72 (77.3)	I	-
	<i>trans</i> - $[\text{PtMe}_3(3\text{-EtPy})\text{I}]_2$	D 1.30 (75.0) E 1.39 (70.9)	I 3-EtPy	H 9.20 I 9.00 (6.4) (17.9) ^d J 7.66 K 7.30 CH ₂ 2.76 Me 1.32
 3-Ethylpyridine (3-EtPy)	<i>cis</i> - $[\text{PtMe}_3(3\text{-EtPy})\text{I}]_2$	F 1.28 (75.1) G 1.99 (71.1)	I 3-EtPy	H 8.78 I 8.75 J 7.43 (7.3) K 6.89 (13.3) CH ₂ 2.55 Me 1.19

(Continued)

Ligand L of [PtMe ₃ L ₂ I]	Pt(IV) species present at equilibrium	$\delta(\text{Pt-Me})^{b, e}$	Trans ligand	$\delta(\text{ligand H})^{c, e}$
 3-Methoxypyridine (3-OMePy)	[PtMe ₃ (3-OMePy) ₂ I]	A 1.49 (70.4) B 1.20 (69.7)	3-OMePy I	H 8.61 I 8.30 (6.1) (16.9) ^d J 7.33 K 7.24 OMe 3.84
	[PtMe ₃ I] ₄	C 1.72 (77.3)	I	-
	<i>trans</i> -[PtMe ₃ (3-OMePy)I] ₂	D 1.29 (74.8) E 1.42 (71.6)	I 3-OMePy	H 9.02 I 8.82 (6.3) (18.2) ^d J 7.29 K 7.22 OMe 3.94
	<i>cis</i> -[PtMe ₃ (3-OMePy)I] ₂	F 1.25 (75.0) G 1.98 (71.4)	I 3-OMePy	H 8.68 I 8.52 (6.1) (17.2) ^d J 7.06 K 6.94 (13.8) OMe 3.82
 3-Chloropyridine (3-ClPy)	[PtMe ₃ (3-ClPy) ₂ I]	A 1.52 (71.1) B 1.18 (68.3)	3-ClPy I	H 8.77 I 8.75 J 7.87 K 7.34
	[PtMe ₃ I] ₄	C 1.72 (77.3)	I	-
	<i>trans</i> -[PtMe ₃ (3-ClPy)I] ₂	D 1.29 (74.3) E 1.46 (72.2)	I 3-ClPy	H 9.28 I 9.15 (6.1) (16.8) ^d J 7.87 K 7.38
	<i>cis</i> -[PtMe ₃ (3-ClPy)I] ₂	F 1.24 (74.5) G 2.02 (72.3)	I 3-ClPy	H 8.93 I 8.87 (5.6) (17.3) ^d J 7.59 (8.4) K 7.14 (13.6)

^a Chemical shifts quoted in ppm are relative to an internal solvent peak (CDCl₃, $\delta = 7.26$ ppm). ^b ²J_{Pt-H}/Hz in parentheses. ^c ³J_{H-H}/Hz in parentheses. ^d ³J_{Pt-H}/Hz in parentheses. ^e labelling refers to Scheme 2.2.2. Not all scalar coupling resolved.

Table 2.2.4 Population ratios of different Pt(IV) species for the reaction of an equimolar mixture of $[\text{PtMe}_3\text{L}_2\text{I}]$ (L = 4-substituted pyridines) with iodotrimethylplatinum(IV) in CDCl_3 at equilibrium at 300 K

Ligand L	$[\text{PtMe}_3\text{LI}]_2 / [\text{PtMe}_3\text{L}_2\text{I}]$	<i>cis</i> - $[\text{PtMe}_3\text{LI}]_2$ (in %)	<i>trans</i> - $[\text{PtMe}_3\text{LI}]_2$ (in %)	<i>trans</i> - $[\text{PtMe}_3\text{LI}]_2 / \textit{cis}$ - $[\text{PtMe}_3\text{LI}]_2$
4-Cyanopyridine (4-CNPy)	4.7	7.7	74.7	9.70
4-Methoxypyridine (4-OMePy)	1.2	21.1	33.7	1.60
4-Methylpyridine (4-MePy)	1.11	15.3	37.2	2.43
4-Ethylpyridine (4-EtPy)	0.97	13.3	35.2	2.65
4- ¹ Butylpyridine (4- ¹ BuPy)	0.8	8.8	36.2	4.11
4-Dimethylaminopyridine (4-DMAP)	0.68	11.4	28.8	2.52

Table 2.2.5 Population ratios of different Pt(IV) species for the reaction of an equimolar mixture of $[\text{PtMe}_3\text{L}_2\text{I}]$ (L = 3-substituted pyridines) with iodotrimethylplatinum(IV) in CDCl_3 at equilibrium at 300 K

Ligand L	$[\text{PtMe}_3\text{LI}]_2 / [\text{PtMe}_3\text{L}_2\text{I}]$	<i>cis</i> - $[\text{PtMe}_3\text{LI}]_2$ (in %)	<i>trans</i> - $[\text{PtMe}_3\text{LI}]_2$ (in %)	<i>trans</i> - $[\text{PtMe}_3\text{LI}]_2 / \textit{cis}$ - $[\text{PtMe}_3\text{LI}]_2$
3-Methylpyridine (3-MePy)	1.37	18.9	38.9	2.06
3-Ethylpyridine (3-EtPy)	1.16	15.0	38.7	2.58
3-Methoxypyridine (3-OMePy)	1.34	24.3	33.0	1.36
3-Chloropyridine (3-ClPy)	3.15	32.8	43.1	1.31

The population ratios of the dinuclear $[\text{PtMe}_3\text{LI}]_2$ complexes to the mononuclear $[\text{PtMe}_3\text{L}_2\text{I}]$ complexes and the relative populations of *cis* and *trans*- $[\text{PtMe}_3\text{LI}]_2$ complexes for the reaction of an equimolar mixture of iodotrimethylplatinum(IV) and mononuclear $[\text{PtMe}_3\text{L}_2\text{I}]$ complexes in chloroform at equilibrium at 300 K in the case of L= 4-substituted pyridines are

reported in Table 2.2.4. It is clear that the electron density on the pyridine ring nitrogen which is influenced by the substituent attached to the pyridine ring plays a significant role in determining the population of both the mononuclear and dinuclear forms at equilibrium in iodotrimethylplatinum(IV) complexes of 4-substituted pyridines. For a strongly electron withdrawing pyridine such as 4-cyanopyridine, the dinuclear form is much more favourable than the mononuclear form. On the other hand, a strongly electron donating pyridine such as 4-dimethylaminopyridine (4-DMAP) favours the mononuclear form over the dinuclear form. This can be explained in terms of the stability of the mononuclear complexes associated with the Pt-N interaction in solution and would therefore be expected to be in accordance with the nucleophilicity of the pyridines, characterized by the electron density on the pyridine ring nitrogen. Cyano group (-CN), owing to its strong mesomeric effect (-M effect) and inductive effect (-I effect) considerably decreases the electron density on the pyridine nitrogen, thereby reducing the nucleophilicity of the heterocyclic nitrogen atom drastically. With the decrease in the nucleophilicity of the pyridine nitrogen, the Pt-N interaction in the mononuclear form is weakened, thus resulting in the destabilisation of the mononuclear form in solution. On the other hand, the strong mesomeric effect (+ M effect) of the NMe₂ group increases the electron density on the pyridine nitrogen significantly leading to a strong Pt-N interaction in the mononuclear complex. As a result of the strong Pt-N interaction, the mononuclear form [PtMe₃(4-DMAP)₂I] becomes highly stable in solution. The observed trend of population ratios of dinuclear to mononuclear form for 4-substituted pyridines is as follows: 4-CNPy >> 4-OMePy > 4-MePy > 4-EtPy > 4-^tBuPy > 4-DMAP (see Table 2.2.4). To explain the order of population ratio of the dinuclear to the mononuclear forms of trimethylplatinum(IV) complexes among the pyridine ligands (4-OMePy, 4-MePy, 4-EtPy and 4-^tBuPy), the steric and the electronic influences of the *p*-substituent of the pyridine ligands are taken into consideration. As the steric bulk of the *p*-substituent increases from Me to Et to ^tBu, the stability of the *cis* dinuclear form also decreases due to the increasing interaction of the pyridine ligands with the neighbouring pyridine ligands in the *cis* dinuclear form. The relative population of the *cis*-[PtMe₃LI]₂ for the pyridine ligands follows the order: 4-OMePy > 4-MePy > 4-EtPy > 4-^tBuPy (see Table 2.2.4). The higher stability of the *cis* dinuclear form in the case of 4-OMePy ligand than for 4-MePy ligand may be explained by the fact that the magnitude of repulsive steric interaction among the oxygen atoms in the *cis* dinuclear form in the case of 4-OMePy ligand is less than the steric interaction between the methyl groups in the case of 4-MePy ligand. The higher population of *trans* dinuclear form (where interaction between the pyridine ligands is absent) relative to the *cis* dinuclear form for all the 4-

substituted pyridines further proves the steric influences of the *p*-substituent in determining the population of both the mononuclear and dinuclear forms in solution. The formation of a very small amount of *cis* isomer relative to *trans* isomer in the case of 4-cyanopyridine ligand is most likely due to the weak stabilisation of the high dipole moment of the *cis* isomer by the rather apolar chloroform solvent.

The population ratios of the dinuclear to mononuclear pyridine complexes and the relative populations of *cis* and *trans*-[PtMe₃LI]₂ complexes in chloroform at equilibrium at 300 K for L= 3-substituted pyridines are reported in Table 2.2.5. Here the population of both the mononuclear and dinuclear trimethylplatinum(IV) complexes also depends on the substituent attached to the pyridine ring. The chlorine atom with its strong inductive effect and weak mesomeric effect considerably decreases the nucleophilicity of the pyridine nitrogen and thus favours the dinuclear form much more than the mononuclear form.

The population of the *cis* dinuclear form for 3-methylpyridine (3-MePy) is higher than for 4-methylpyridine (4-MePy). Similarly population of *cis* dinuclear form: 3-EtPy > 4-EtPy; 3-OMePy > 4-OMePy. This confirms that the repulsive steric interaction among the pyridine ligands in the *cis* dinuclear form is less in the case of 3-substituted pyridines as compared to the 4-substituted pyridines. On the other hand, the population ratio of dinuclear to mononuclear form at equilibrium for the 3-substituted pyridines is greater than for the 4-substituted pyridines [(population_{dimer}/population_{monomer}) : (i) 3-MePy > 4-MePy; (ii) 3-EtPy > 4-EtPy; (iii) 3- OMePy > 4-OMePy]. This is due to a decrease in both the nucleophilicity of the pyridine nitrogen and the steric influences of the substituent as we go from 4-substituted pyridines to 3-substituted pyridines.

2.2.5 Conclusion

Several mononuclear iodotrimethylplatinum(IV) complexes of 4- and 3-substituted pyridines, $[\text{PtMe}_3\text{L}_2\text{I}]$ were successfully synthesized and characterized by different techniques. The crystal structures of $[\text{PtMe}_3\text{L}_2\text{I}]$ (L = 4-MePy, 4-EtPy, 4-OMePy and 3-OMePy) confirmed the slightly distorted octahedral geometry in these iodotrimethylplatinum(IV) complexes of pyridines. All the synthesized mononuclear trimethylplatinum(IV) complexes of pyridines undergo reaction with iodotrimethylplatinum(IV) in equimolar ratio to form the iodide bridged dinuclear complexes, $[\text{PtMe}_3\text{LI}]_2$. These dinuclear complexes exist as a mixture of *cis* and *trans* isomers in chloroform. The equilibrium population of both the mononuclear and dinuclear iodotrimethylplatinum(IV) complexes depends to a large extent on both the electronic effect and the steric bulk of the pyridine substituent. Substituents with strong electron donating ability such as NMe_2 favour the mononuclear complexes over the dinuclear complexes. On the other hand, for strongly electron withdrawing substituents such as cyano and chlorine, the dinuclear complexes are more stable than the mononuclear complexes. The steric bulk of the substituent attached to the pyridine ring also plays a significant role. As the size of the pyridine substituent increases, the interaction of the pyridine ligand with the neighbouring pyridine ligand in the *cis* dinuclear form also increases. As a result, the stability of the *cis* dinuclear form decreases in solution. For all pyridine ligands, the *cis* dinuclear complexes are less stable than the *trans* form. However, the steric interaction among the pyridine ligands in the *cis* dinuclear form is smaller in the case of 3-substituted pyridines as compared to the 4-substituted pyridines.

2.3 Crystallographic Investigation of Dinuclear Iodotrimethylplatinum(IV) Complexes of Pyridines

2.3.1 Introduction

In coordination chemistry, the iodide ligand is considered as a versatile ligand because of its ability to bind the metal ion in monodentate fashion as well as in bridging fashion. In case of trimethylplatinum(IV) system, the extent of formation of octahedral geometry around Pt metal ion is so high that in absence of suitable ligand the binuclear or polynuclear species forms readily. Thus reaction of iodotrimethylplatinum(IV) with pyridine in equimolar ratio results in the formation of dinuclear complex $[\text{PtMe}_3(\text{py})\text{I}]_2$.^[38] Treatment of mononuclear pyridine complex, $[\text{PtMe}_3(\text{py})_2\text{I}]$ with one mole of dilute acid also gave the corresponding dinuclear complex $[\text{PtMe}_3(\text{py})\text{I}]_2$.^[38] It was shown in Chapter 2.2 that reaction of iodotrimethylplatinum with a series of mononuclear trimethylplatinum complexes of pyridines in equimolar ratio also results in the formation of a mixture of *cis* and *trans* dinuclear pyridine complexes. In order to establish the structure of these complexes, X-ray structural investigation of some dinuclear pyridine complexes was carried out. This chapter describes the structural characterization of five dinuclear pyridine complexes, *trans*- $[\text{PtMe}_3(\text{py})\text{I}]_2$, *cis*- $[\text{PtMe}_3\text{LI}]_2$ {L = 4-ethylpyridine (4-EtPy), 4-methoxypyridine (4-OMePy), 4-cyanopyridine (4-CNPy) and 3-chloropyridine (3-ClPy)}.

2.3.2 Crystal structures of *trans*- $[\text{PtMe}_3(\text{py})\text{I}]_2$, *cis*- $[\text{PtMe}_3\text{LI}]_2$ (L = 4-EtPy, 4-OMePy, 4-CNPy, 3-ClPy)

The yellow crystals of the dinuclear complexes, *trans*- $[\text{PtMe}_3(\text{py})\text{I}]_2$ and *cis*- $[\text{PtMe}_3\text{LI}]_2$ (L = 4-EtPy, 4-OMePy, 4-CNPy, 3-ClPy) were obtained by slow diffusion of n-hexane into an equilibrium mixture of equimolar iodotrimethylplatinum(IV) and corresponding mononuclear pyridine complexes in CDCl_3 . In each of the five complexes, two bridged iodine atoms hold two platinum atoms together. In *trans*- $[\text{PtMe}_3(\text{py})\text{I}]_2$, two pyridine ligands are positioned *trans* to each other, while in the other four dinuclear complexes, substituted pyridine ligands are *cis* to each other (see Figures 2.3.1-2.3.5). The X-ray diffraction parameters and crystallographic data of the complexes are reported in Tables 5.4.7-5.4.11.

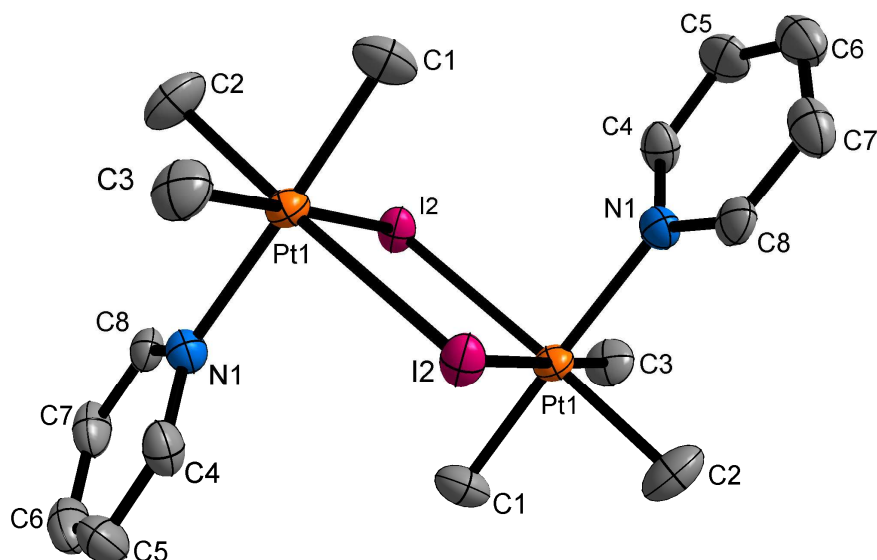


Figure 2.3.1 Molecular structure of *trans*-[PtMe₃(py)I]₂ showing the atom labelling scheme. Thermal ellipsoids are at the 50% probability level. Pt---Pt distance is 4.07 Å. Hydrogen atoms omitted for clarity.

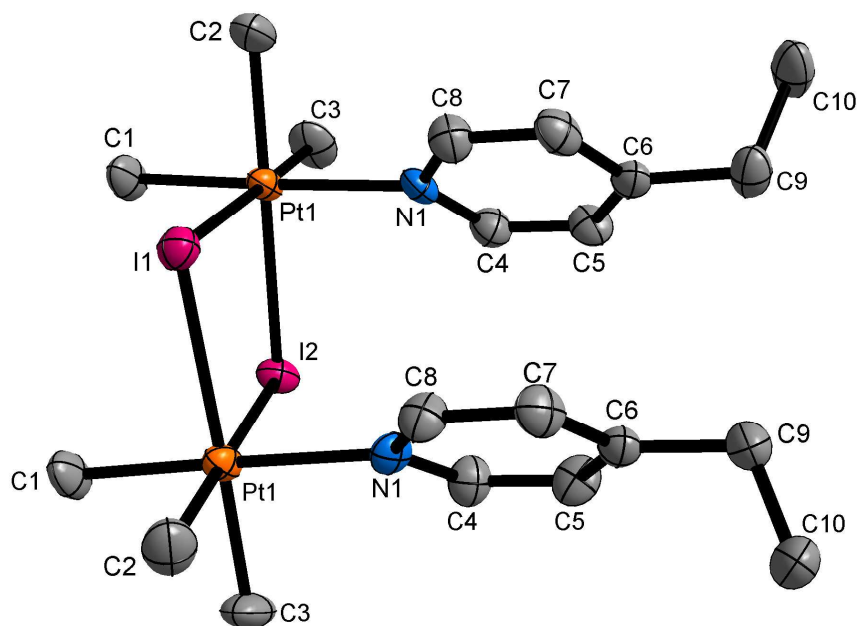


Figure 2.3.2 Molecular structure of *cis*-[PtMe₃(4-EtPy)I]₂ showing the atom labelling scheme. Thermal ellipsoids are at the 50% probability level. Pt---Pt distance is 4.05 Å. Hydrogen atoms omitted for clarity.

The complex *trans*-[PtMe₃(py)I]₂ crystallized in C2/c space group with monoclinic crystal system and possess an inversion centre at the centre of the four-membered Pt₂I₂ ring. The complexes, *cis*-[PtMe₃(4-OMePy)I]₂ and *cis*-[PtMe₃(4-CNPY)I]₂, both crystallize in monoclinic P2₁/n space group. On the other hand, *cis*-[PtMe₃(4-EtPy)I]₂ crystallized in orthorhombic Pnam space group and possess a mirror plane where two iodides lie on the

mirror plane. The complex cis -[PtMe₃(3-ClPy)I]₂ also crystallized in orthorhombic crystal system (though space group is different, P2₁2₁2₁). All the complexes contain four molecules in their unit cell. In case of cis -[PtMe₃(3-ClPy)I]₂, one molecule of [PtMe₃I]₄ also crystallized with it.

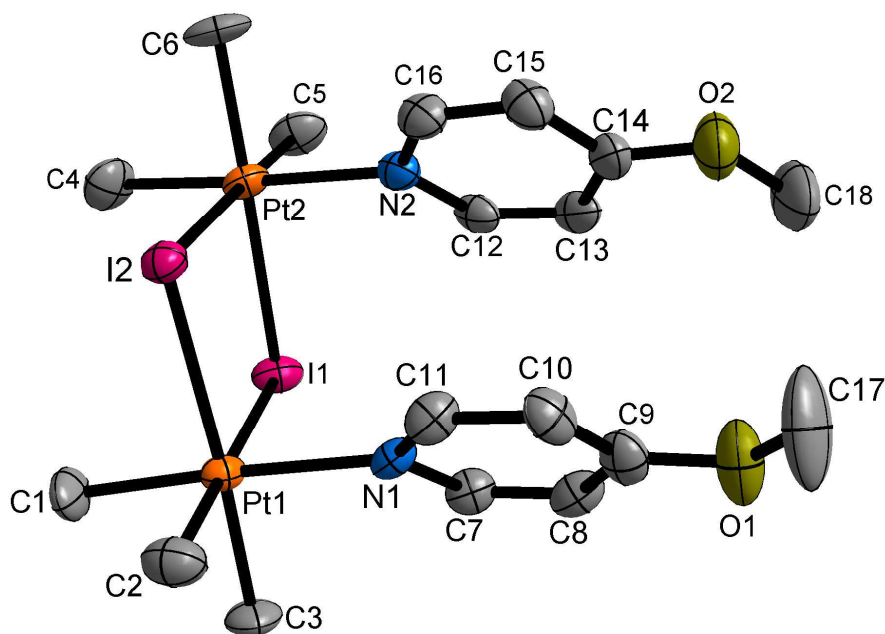


Figure 2.3.3 Molecular structure of cis -[PtMe₃(4-OMePy)I]₂ showing the atom labelling scheme. Thermal ellipsoids are at the 50% probability level. Pt---Pt distance is 4.06 Å. Hydrogen atoms omitted for clarity.

The important change at the Pt₂I₂ fragment caused by the change from pyridine to substituted pyridines is the slight shortening of the platinum-platinum non-bonded distance, from 4.07 Å in pyridine to 4.05 - 4.06 Å in 4-substituted pyridines to 4.03 Å in 3-chloropyridine analogue. This could be due to the change in *trans* geometry of the pyridine ligands in *trans*-[PtMe₃(py)I]₂ to *cis*-geometry of the substituted pyridine ligands in the dinuclear complexes. The Pt---Pt non-bonded distance in these pyridine complexes is much longer than the Pt---Pt distance in [(PtMe₃I)₂MeSeSeMe] (3.90 Å),^[64] [(PtMe₃Br)₂MeSeSeMe] (3.74 Å),^[65] [(PtMe₃Br)₂(dmas)₂] (3.79 Å) where dmas = (dimethylarsino)sulphide,^[66] Pt(DMG)₂ (3.23 Å) where DMG = dimethylglyoxime.^[67] This confirms that the Pt---Pt non-bonded distance depends on the nature of bridging ligand. Interestingly the changes of pyridine to substituted pyridines (both electron donating and electron withdrawing) do not produce any significant change in either the Pt-I, Pt-C or the Pt-N bond lengths (selected bond lengths and angles of the complexes are given in Tables 2.3.1-2.3.5). This also confirms that the Pt-N bond distances in the solid state structure of these complexes are not affected significantly by the

electronic effect of the pyridine substituent. The configuration about each platinum atom in each of the complexes is approximately octahedral, with interbond angles in the range of 85-95° and 177-179°.

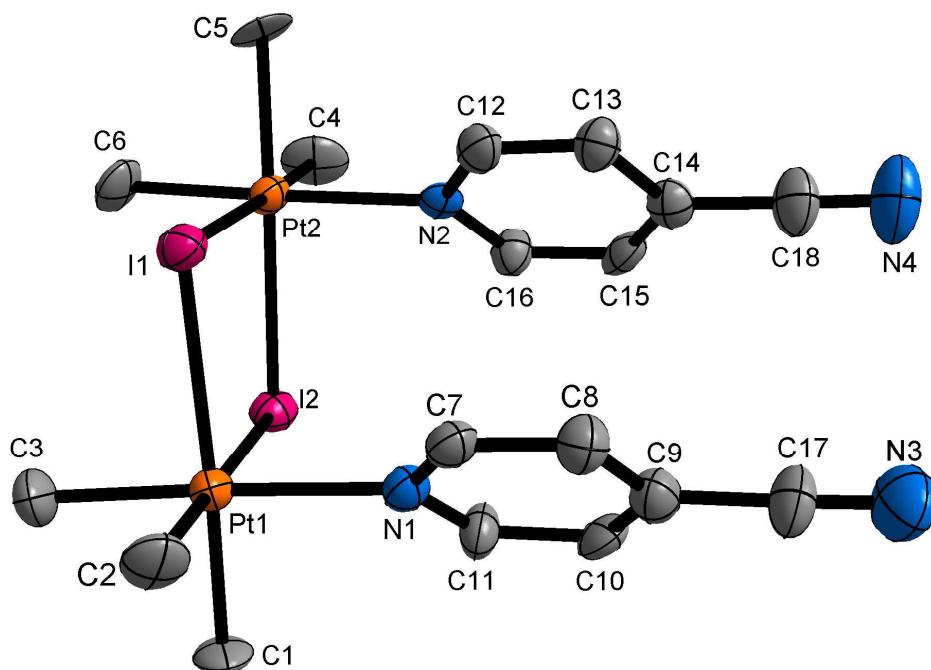


Figure 2.3.4 Molecular structure of *cis*-[PtMe₃(4-CNPy)I]₂ showing the atom labelling scheme. Thermal ellipsoids are at the 50% probability level. Pt---Pt distance is 4.06 Å. Hydrogen atoms omitted for clarity.

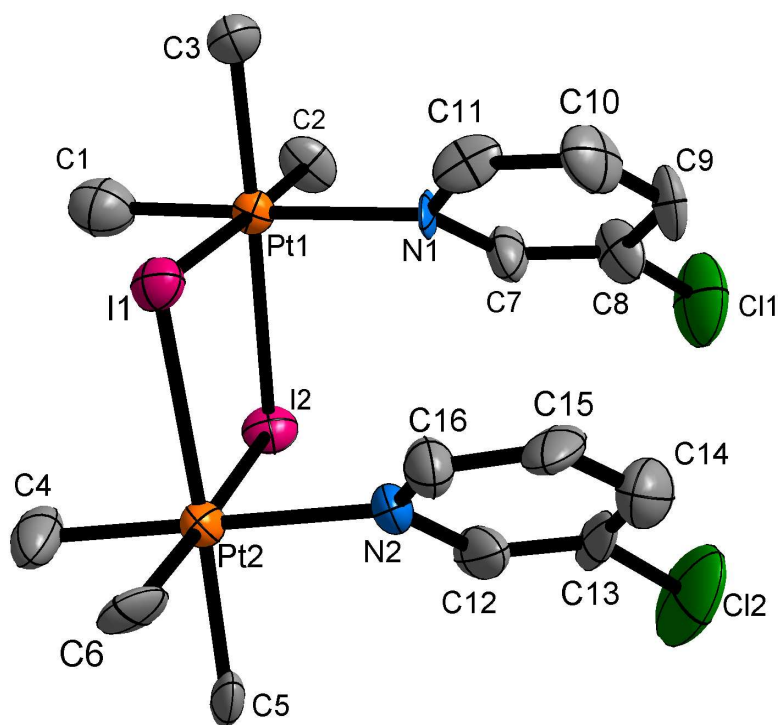


Figure 2.3.5 Molecular structure of *cis*-[PtMe₃(3-ClPy)I]₂ showing the atom labelling scheme. Thermal ellipsoids are at the 50% probability level. Pt---Pt distance is 4.03 Å. Hydrogen atoms omitted for clarity.

Table 2.3.1 Selected bond lengths [Å] and angles [°] for *trans*-[PtMe₃(py)I]₂

Pt1-C1	2.061(9)	Pt1-N1	2.174(6)
Pt1-C2	2.031(9)	Pt1-I2	2.811(6)
Pt1-C3	2.050(8)	Pt1-I2 ⁱ	2.800(7)
C2-Pt1-C3	85.7(4)	C2-Pt1-I2	93.7(3)
C2-Pt1-C1	87.0(5)	C3-Pt1-I2	178.4(3)
C3-Pt1-C1	89.4(4)	C1-Pt1-I2	92.0(3)
C2-Pt1-N1	91.6(4)	N1-Pt1-I2	89.17(17)
C3-Pt1-N1	89.4(3)	C2-Pt1-I2 ⁱ	177.2(4)
C1-Pt1-N1	178.2(3)	C3-Pt1-I2 ⁱ	93.6(3)
I2 ⁱ -Pt1-I2	87.15(2)	C1-Pt1-I2 ⁱ	90.3(3)
Pt1 ⁱ -I2-Pt1	92.85(2)	N1-Pt1-I2 ⁱ	91.14(17)

Symmetry transformations used to generate equivalent atoms:

(i) 0.5-x, 1.5-y, -z

Table 2.3.2 Selected bond lengths [Å] and angles [°] for *cis*-[PtMe₃(4-EtPy)I]₂

Pt1-C1	2.054(8)	Pt1-N1	2.188(6)
Pt1-C2	2.039(9)	Pt1-I2	2.8171(6)
Pt1-C3	2.059(9)	Pt1-I3	2.7793(6)
C2-Pt1-C3	85.3(5)	C2-Pt1-I2	178.1(3)
C2-Pt1-C1	88.1(4)	C3-Pt1-I2	93.1(3)
C3-Pt1-C1	88.7(4)	C1-Pt1-I2	90.8(3)
C2-Pt1-N1	90.3(3)	N1-Pt1-I2	90.81(17)
C3-Pt1-N1	90.7(3)	C2-Pt1-I1	94.7(3)
C1-Pt1-N1	178.3(3)	C3-Pt1-I1	178.5(3)
I3-Pt1-I1	86.828(18)	C1-Pt1-I1	89.9(3)
Pt1-I1-Pt1 ⁱ	91.98(3)	N1-Pt1-I1	90.75(18)
Pt1 ⁱ -I2-Pt1	93.61(3)		

Symmetry transformations used to generate equivalent atoms:

(i) x, y, -z+1/2

Table 2.3.3 Selected bond lengths [Å] and angles [°] for *cis*-[PtMe₃(4-OMePy)I]₂

Pt1-C1	2.054(8)	Pt2-C4	2.051(9)
Pt1-C2	2.053(8)	Pt2-C5	2.037(9)
Pt1-C3	2.044(7)	Pt2-C6	2.031(7)
Pt1-N1	2.186(7)	Pt2-N2	2.182(7)
Pt1-I1	2.7839(6)	Pt2-I1	2.8020(6)
Pt1-I2	2.8117(5)	Pt2-I2	2.7986(6)
C3-Pt1-C2	86.6(3)	Pt1-I1-Pt2	93.159(18)
C3-Pt1-C1	86.7(4)	Pt2-I2-Pt1	92.632(17)
C2-Pt1-C1	88.0(4)	I2-Pt2-I1	86.822(18)
C6-Pt2-C5	86.4(4)	I1-Pt1-I2	86.916(18)
C6-Pt2-C4	87.3(4)	C3-Pt1-I1	93.7(3)
C5-Pt2-C4	89.1(4)	C2-Pt1-I1	179.6(3)
C3-Pt1-N1	90.5(3)	C1-Pt1-I1	92.3(3)
C2-Pt1-N1	91.1(3)	C3-Pt1-I2	176.7(3)
C1-Pt1-N1	177.1(3)	C2-Pt1-I2	92.8(2)
C4-Pt2-N2	177.3(3)	C1-Pt1-I2	90.0(2)

C6-Pt2-N2	90.0(4)	C6-Pt2-I2	94.2(3)
C5-Pt2-N2	90.8(4)	C5-Pt2-I2	178.6(3)
N2-Pt2-I2	87.99(16)	C4-Pt2-I2	92.2(3)
N2-Pt2-I1	91.97(15)	C6-Pt2-I1	177.8(3)
N1-Pt1-I1	88.60(16)	C5-Pt2-I1	92.6(3)
N1-Pt1-I2	92.78(15)	C4-Pt2-I1	90.7(3)

Table 2.3.4 Selected bond lengths [\AA] and angles [$^\circ$] for *cis*-[PtMe₃(4-CNPy)I]₂

Pt1-C1	2.030(16)	Pt2-C4	2.024(15)
Pt1-C2	2.048(16)	Pt2-C5	2.015(15)
Pt1-C3	2.084(15)	Pt2-C6	2.030(15)
Pt1-N1	2.229(11)	Pt2-N2	2.210(10)
Pt1-I1	2.7902(11)	Pt2-I1	2.7984(10)
Pt1-I2	2.7968(11)	Pt2-I2	2.7966(11)
C1-Pt1-C2	89.5(8)	C5-Pt2-C4	87.7(7)
C1-Pt1-C3	86.3(7)	C5-Pt2-C6	88.5(7)
C2-Pt1-C3	88.6(7)	C4-Pt2-C6	87.1(8)
C1-Pt1-N1	91.6(6)	C5-Pt2-N2	89.8(5)
C2-Pt1-N1	90.7(6)	C4-Pt2-N2	92.6(6)
C3-Pt1-N1	177.8(6)	C6-Pt2-N2	178.4(6)
C1-Pt1-I2	90.8(6)	C5-Pt2-I1	91.2(4)
C2-Pt1-I2	179.7(6)	C4-Pt2-I1	177.7(6)
C3-Pt1-I2	91.6(5)	C6-Pt2-I1	90.8(5)
N1-Pt1-I2	89.1(3)	N2-Pt2-I1	89.4(3)
I1-Pt1-I2	86.82(3)	I2-Pt2-I1	86.66(3)
C5-Pt2-I2	177.8(4)	C1-Pt1-I1	175.6(6)
C4-Pt2-I2	94.4(6)	C2-Pt1-I1	93.0(6)
C6-Pt2-I2	91.0(6)	C3-Pt1-I1	90.1(5)
N2-Pt2-I2	90.6(3)	N1-Pt1-I1	92.0(3)
Pt1-I1-Pt2	93.07(3)	Pt2-I2-Pt1	92.97(3)

Table 2.3.5 Selected bond lengths [\AA] and angles [$^\circ$] for *cis*-[PtMe₃(3-ClPy)I]₂

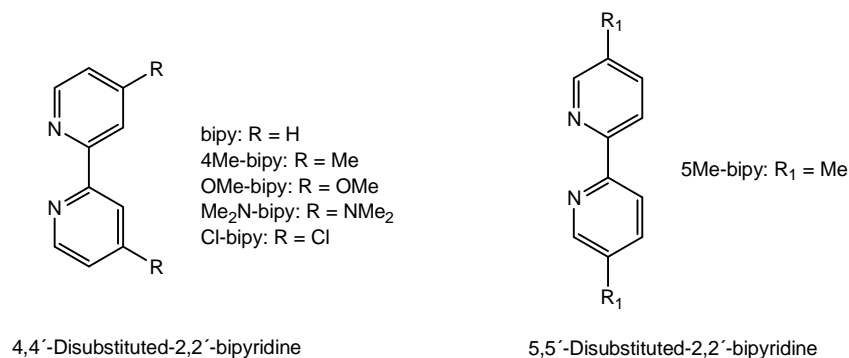
Pt1-C1	2.01(3)	Pt2-C4	2.02(2)
Pt1-C2	2.081(19)	Pt2-C5	2.15(2)
Pt1-C3	2.08(2)	Pt2-C6	2.09(2)
Pt1-N1	2.202(14)	Pt2-N2	2.208(15)
Pt1-I1	2.7766(15)	Pt2-I1	2.7827(15)
Pt1-I2	2.7923(15)	Pt2-I2	2.8006(16)
C1-Pt1-C3	87.4(10)	C4-Pt2-C6	87.3(11)
C1-Pt1-C2	88.8(10)	C4-Pt2-C5	86.6(9)
C3-Pt1-C2	86.8(9)	C6-Pt2-C5	87.2(8)
C1-Pt1-N1	178.9(10)	C4-Pt2-N2	179.6(9)
C3-Pt1-N1	91.6(8)	C6-Pt2-N2	92.5(8)
C2-Pt1-N1	90.7(8)	C5-Pt2-N2	93.6(7)
C1-Pt1-I1	89.5(8)	C4-Pt2-I1	90.8(7)
C3-Pt1-I1	92.2(7)	C6-Pt2-I1	92.5(6)
C2-Pt1-I1	178.0(6)	C5-Pt2-I1	177.4(6)
N1-Pt1-I1	91.0(5)	N2-Pt2-I1	88.9(4)
C1-Pt1-I2	90.6(8)	C4-Pt2-I2	90.2(9)
C3-Pt1-I2	178.0(6)	C6-Pt2-I2	177.5(6)
C2-Pt1-I2	93.6(6)	C5-Pt2-I2	93.1(6)
N1-Pt1-I2	90.4(4)	N2-Pt2-I2	90.0(5)
I1-Pt1-I2	87.44(4)	I1-Pt2-I2	87.15(4)

3 Iodotrimethylplatinum(IV) Complexes of 2,2'-Bipyridines

3.1 Introduction

2,2'-Bipyridine and its derivatives have received much attention due to their exceptional coordination chemistry. Unlike many other common ligands, such as cyclopentadienyls and phosphines which are prone to oxidation, they are extremely stable in aqueous media and atmospheric oxygen.^[68] The restricted rotation around the pyridyl-pyridyl bond during the complex formation results in an extremely stable species where nitrogen to metal σ -bond is further stabilised by the metal to ligand π -overlap. It was found that 2,2'-bipyridine complexes of transition metal such as ruthenium(II), osmium(II) or rhenium(I) possess interesting electrochemical and photochemical properties.^[69-76] The transition metal complexes of 2,2'-bipyridine and its derivatives are also used as building blocks in supramolecular assemblies,^[77] as electrochemical probes for DNA detection,^[71,78] as electron transfer mediators for glucose oxidase^[79] or as sensitizers in solar energy conversion.^[80-82]

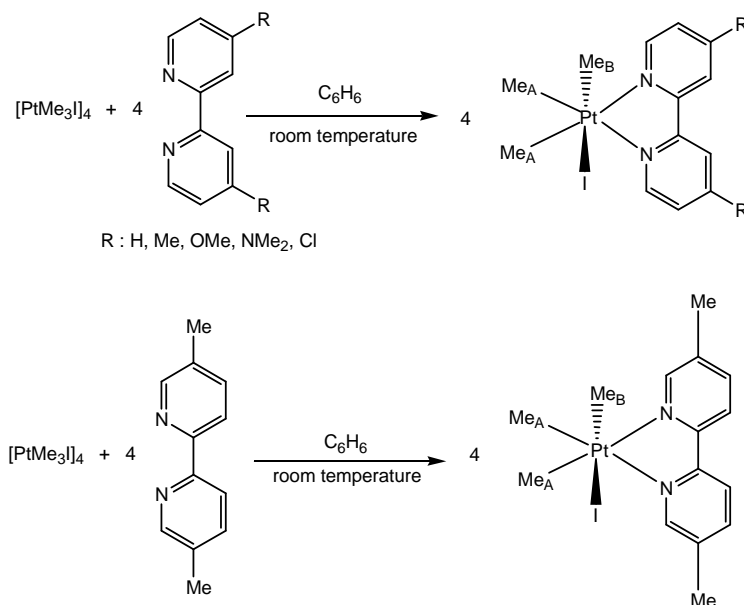
The focus of the present research lies on the exchange of pyridine ligands with 2,2'-bipyridine ligands in the trimethylplatinum(IV) system. Thus the syntheses and characterization of 2,2'-bipyridine complexes of trimethylplatinum(IV) become an essential step for this research. This chapter describes the syntheses and crystal structures of iodotrimethylplatinum(IV) complexes of six different 2,2'-bipyridines such as 2,2'-bipyridine (bipy), 4,4'-dimethyl-2,2'-bipyridine (4Me-bipy), 5,5'-dimethyl-2,2'-bipyridine (5Me-bipy), 4,4'-dimethoxy-2,2'-bipyridine (OMe-bipy), 4,4'-bis(dimethylamino)-2,2'-bipyridine (Me₂N-bipy), and 4,4'-dichloro-2,2'-bipyridine (Cl-bipy). The electronic effect of the substituent on both the solution and the solid state was examined and compared with the pyridine system.



Scheme 3.1 2,2'-Bipyridine and its derivatives.

3.2 Syntheses and characterization of the complexes

Mononuclear $[\text{PtMe}_3(\text{L-L})\text{I}]$ ($\text{L-L} = 2,2'$ -bipyridine and its derivatives) complexes were prepared by the treatment of iodotrimethylplatinum with 2,2'-bipyridines in equimolar ratio at room temperature in benzene (Scheme 3.2).



Scheme 3.2 Reaction of iodotrimethylplatinum(IV) with 2,2'-bipyridine and its derivatives in benzene.

Except $[\text{PtMe}_3(\text{Cl-bipy})\text{I}]$, which is a deep yellow to brown coloured complex, all the mononuclear complexes are pale yellow in colour. None of the complexes are light or air sensitive. The complexes are soluble in nitrobenzene, chloroform; however, the complexes are not soluble to the same extent and it was found that the solubility of $[\text{PtMe}_3(\text{Me}_2\text{N-bipy})\text{I}]$ is lowest among all the mononuclear complexes. Moreover, the solubility of these 2,2'-bipyridine complexes is much lower compared to that of the corresponding pyridine complexes in chloroform.

The synthesized complexes were characterized by ^1H NMR spectroscopy, IR spectroscopy, mass spectrometry and elemental analyses. Mass spectral analysis reflected the mononuclear nature of these complexes. For all the complexes, the highest m/z value corresponds to the loss of iodide, $[\text{M-I}]^+$. In addition, in all cases, the observed isotope patterns were consistent with those calculated for the formulated species. The infrared data are consistent with the PtMe_3 having *facial* octahedral coordination geometry.^[39] The analytical data for all the complexes are reported in Chapter 5.3.4.

3.2.1 ^1H NMR studies of the complexes

The ^1H NMR data for the synthesized mononuclear complexes are noted in Table 3.1 and the ^1H NMR spectrum of $[\text{PtMe}_3(\text{OMe-bipy})\text{I}]$ in CDCl_3 is illustrated in Figure 3.1. The platinum-methyl regions of the spectra each consist of two principal methyl-platinum resonances in the integral ratio of 2:1, each with satellites due to coupling between the methyl protons and the ^{195}Pt nuclei. The peak at the lower chemical shift (signal B) with relative integration 1 is due to the methyl group *trans* to iodide and the resonances at higher chemical shift (signal A) is due to the two methyl groups *trans* to the bipyridine ligand. The $^2J_{\text{Pt-H}}$ scalar coupling constants observed for the methyl groups *trans* to I were higher than for the methyl groups *trans* to 2,2'-bipyridines, indicating that the bipyridines exert a stronger *trans* influence than iodide.

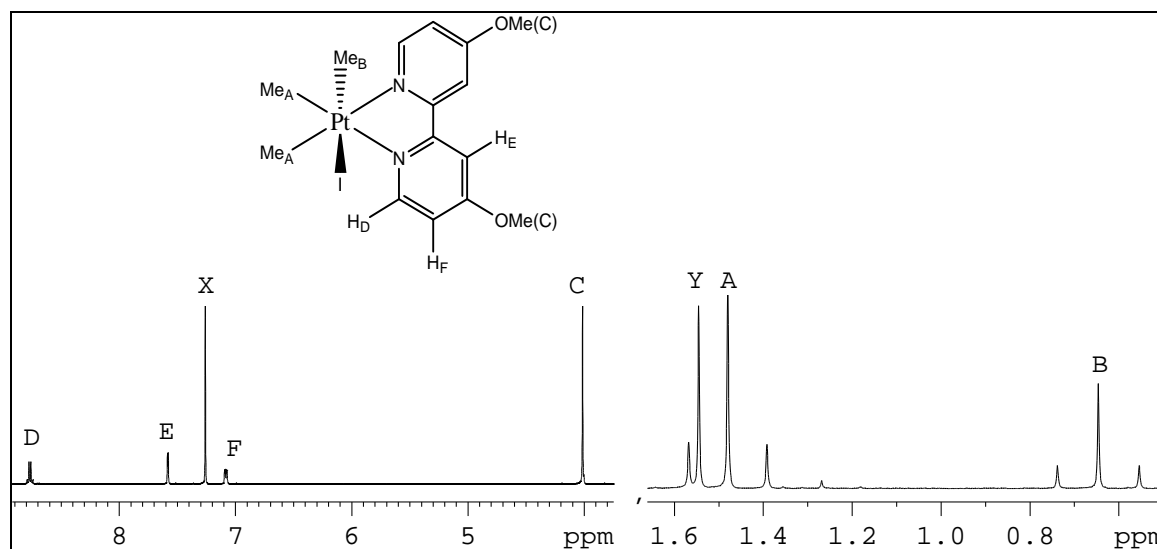
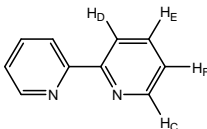
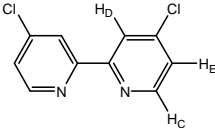
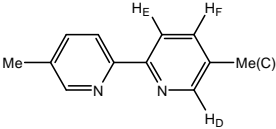
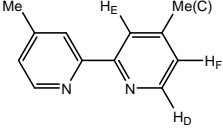
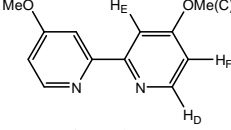
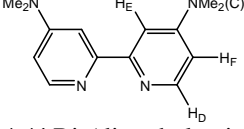


Figure 3.1 The 400 MHz ^1H NMR spectrum of $[\text{PtMe}_3(\text{OMe-bipy})\text{I}]$ in CDCl_3 at 300 K. For labelling, see inset. X is the solvent peak and Y is the peak for water present in CDCl_3 .

Furthermore, an examination of the $^2J_{\text{Pt-H}}$ scalar coupling constant for the methyl groups *trans* to bipyridine (signal A) in all the complexes, reveals a dependence on the chelate ligand, the trend in $^2J_{\text{Pt-H}}$ scalar coupling constant is $\text{Cl-bipy} > \text{bipy} \approx 5\text{Me-bipy} \approx 4\text{Me-bipy} \approx \text{OMe-bipy} > \text{Me}_2\text{N-bipy}$. This leads to the conclusion that the *trans* influence of the bipyridines is strongly influenced by the electronic effect of the substituent attached to it. Electron donating substituent increases the *trans* influence of the bipyridines while *trans* influence of the bipyridines decreases considerably when an electron withdrawing substituent is attached to it. For 2,2'-bipyridine complex, the aromatic region comprised four signals while it is three for

the disubstituted 2,2'-bipyridine complexes. The highest frequency signal in each of the complexes displayed measurable ^{195}Pt coupling by virtue of its proximity to the metal-coordinated nitrogen. The chelate ligand sub-spectra were assigned on the basis of their scalar coupling networks and by comparison with the ^1H NMR spectra of the free bipyridine ligand.

Table 3.1 ^1H NMR data^a for the $[\text{PtMe}_3(\text{L-L})\text{I}]$ ($\text{L-L} = 2,2'$ -bipyridine and its derivatives) complexes in CDCl_3 at 300 K

Complex (chelate ligand)	$\delta(\text{Pt-Me})^b$	<i>Trans</i> ligand	$\delta(\text{chelate H})^{c,e}$
 2,2'-Bipyridine (bipy)	A 1.56 (70.5) B 0.64 (73.1)	bipy I	C 9.02 (6.1) (17.8) ^d D 8.23 E 8.07 F 7.64
 4,4'-Dichloro-2,2'-bipyridine (Cl-bipy)	A 1.56 (71.2) B 0.62 (72.3)	Cl-bipy I	C 8.91 (6.0) (19.2) ^d D 8.18 E 7.66
 5,5'-Dimethyl-2,2'-bipyridine (5Me-bipy)	A 1.54 (70.4) B 0.62 (73.3)	5Me-bipy I	C 2.51 D 8.77 (1.1) (12.7) ^d E 8.04 F 7.81
 4,4'-Dimethyl-2,2'-bipyridine (4Me-bipy)	A 1.51 (70.3) B 0.63 (73.5)	4Me-bipy I	C 2.57 D 8.82 (5.8) (19.4) ^d E 8.01 F 7.42
 4,4'-Dimethoxy-2,2'-bipyridine(OMe-bipy)	A 1.48 (70.2) B 0.65 (73.7)	OMe-bipy I	C 4.02 D 8.77 (6.4) (19.8) ^d E 7.58 F 7.08
 4,4'-Bis(dimethylamino)-2,2'-bipyridine (Me ₂ N-bipy)	A 1.40 (69.6) B 0.68 (74.9)	Me ₂ N-bipy I	C 3.16 D 8.46 (6.6) (20.0) ^d E 7.14 F 6.68

^a Chemical shifts quoted in ppm are relative to an internal solvent peak (CDCl_3 , $\delta = 7.26$ ppm). ^b $^2J_{\text{Pt-H}}$ /Hz in parentheses. ^c $^3J_{\text{H-H}}$ /Hz in parentheses. ^d $^3J_{\text{Pt-H}}$ /Hz in parentheses. ^e Not all scalar coupling resolved.

3.3 X-ray crystallographic characterization of the complexes, [PtMe₃(L-L)I] (L-L = bipy, 4Me-bipy, 5Me-bipy, OMe-bipy and Me₂N-bipy)

Single crystals of [PtMe₃(OMe-bipy)I] were obtained by slow diffusion of n-hexane into its chloroform solution while the other four complexes were crystallized by mixing dilute benzene solution of iodotrimethylplatinum and corresponding 2,2'-bipyridine ligands in equimolar ratio. The crystal structure of all the complexes consists of a discrete monomeric unit in which the platinum atom is hexa-coordinated by the three methyl groups in a *facial* arrangement, a 2,2'-bipyridine ligand in a *bidentate* fashion and an iodine atom (Figures 3.2-3.6). Experimental X-ray diffraction parameters and crystal data are reported in Tables 5.4.12-5.4.16. The selected bond lengths and angles of [PtMe₃(bipy)I] are given in Table 3.2, while selected bond lengths and angles of other complexes are listed in Table 3.3.

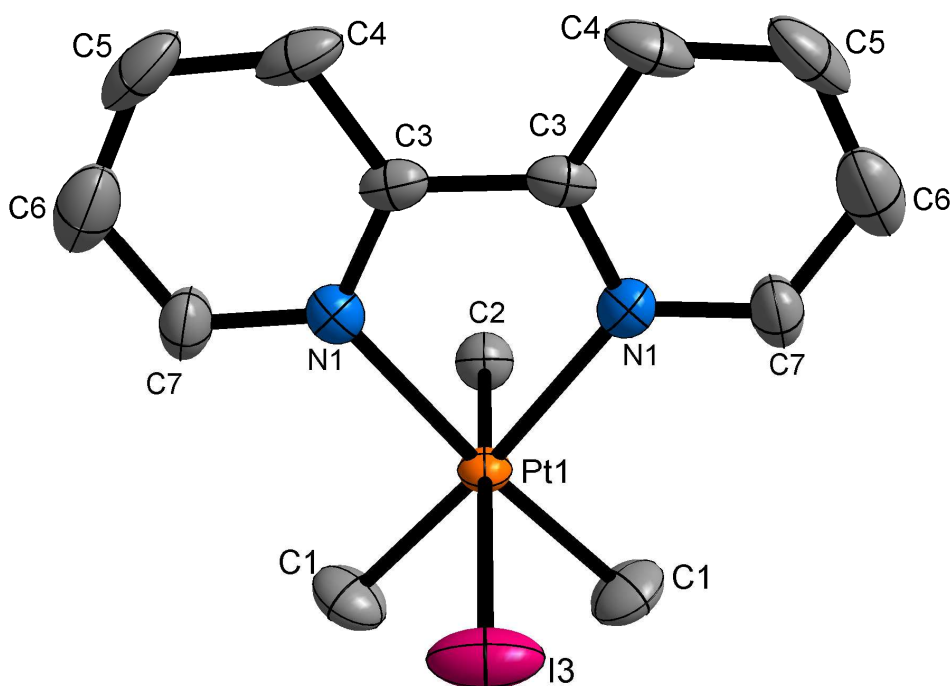


Figure 3.2 Molecular structure of [PtMe₃(bipy)I] showing the atom labelling scheme. Thermal ellipsoids are at the 50% probability level. Hydrogen atoms are omitted for clarity.

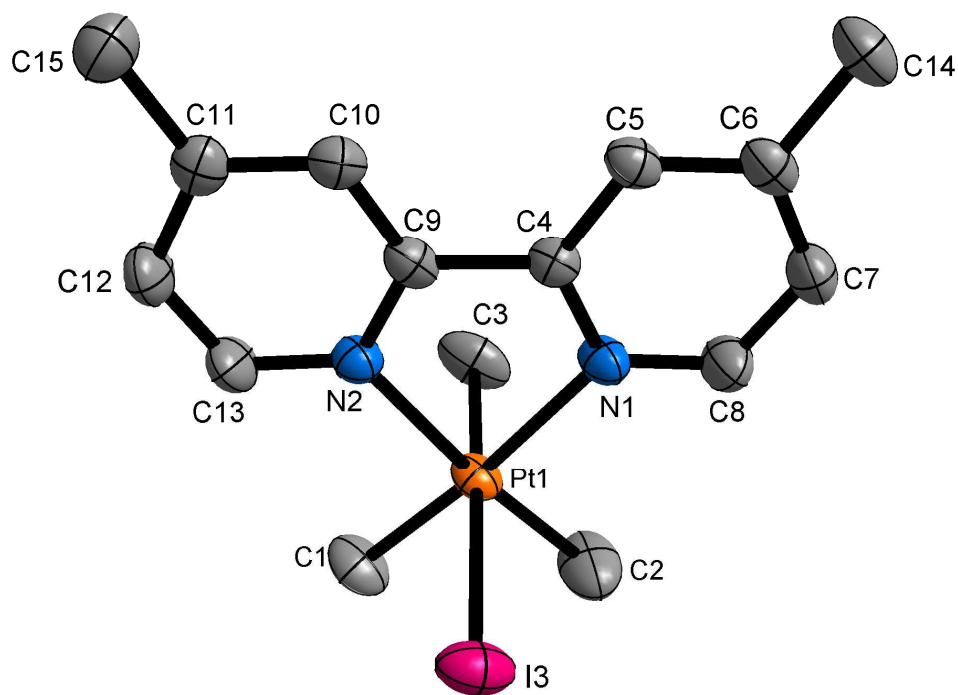


Figure 3.3 Molecular structure of [PtMe₃(4Me-bipy)I] showing the atom labelling scheme. Thermal ellipsoids are at the 50% probability level. Hydrogen atoms are omitted for clarity.

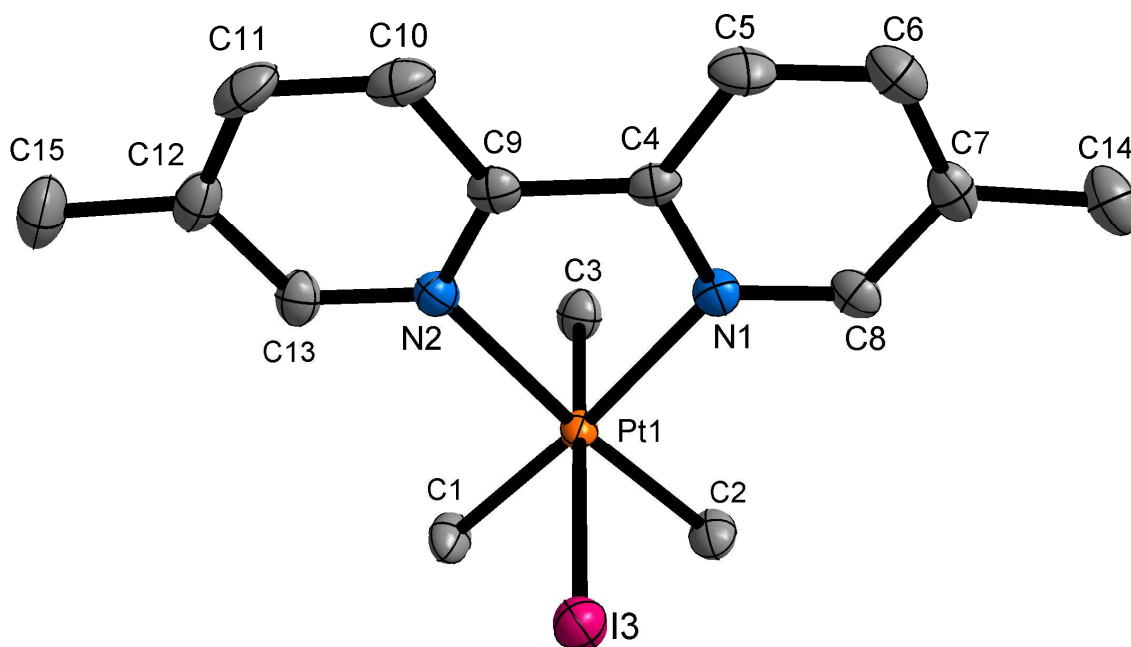


Figure 3.4 Molecular structure of [PtMe₃(5Me-bipy)I] showing the atom labelling scheme. Thermal ellipsoids are at the 50% probability level. Hydrogen atoms are omitted for clarity.

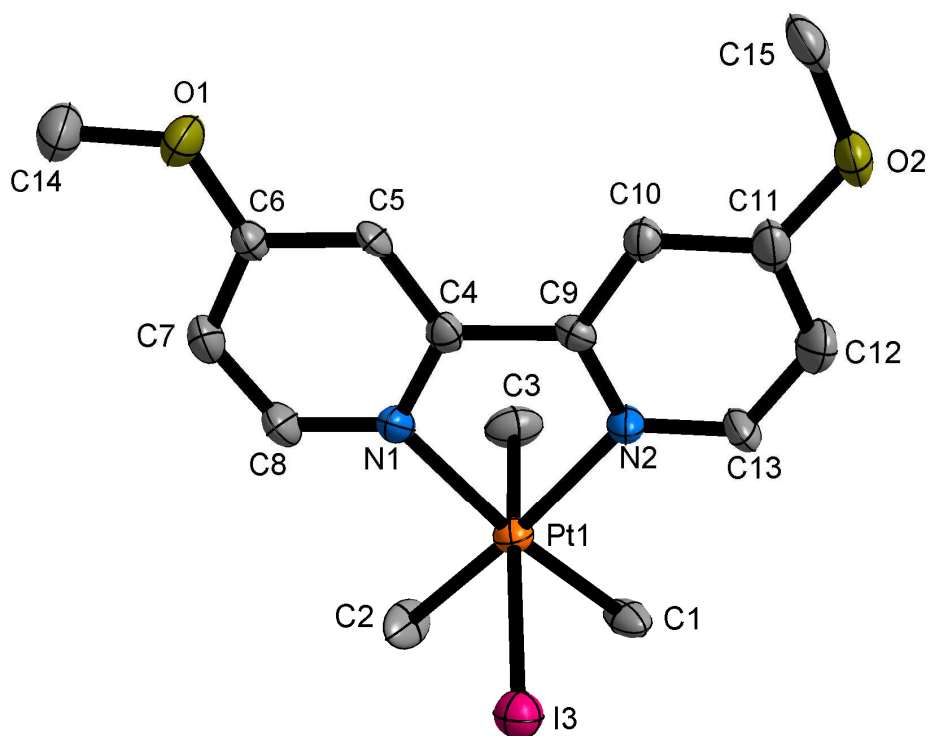


Figure 3.5 Molecular structure of [PtMe₃(OMe-bipy)I] showing the atom labelling scheme. Thermal ellipsoids are at the 50% probability level. Hydrogen atoms are omitted for clarity.

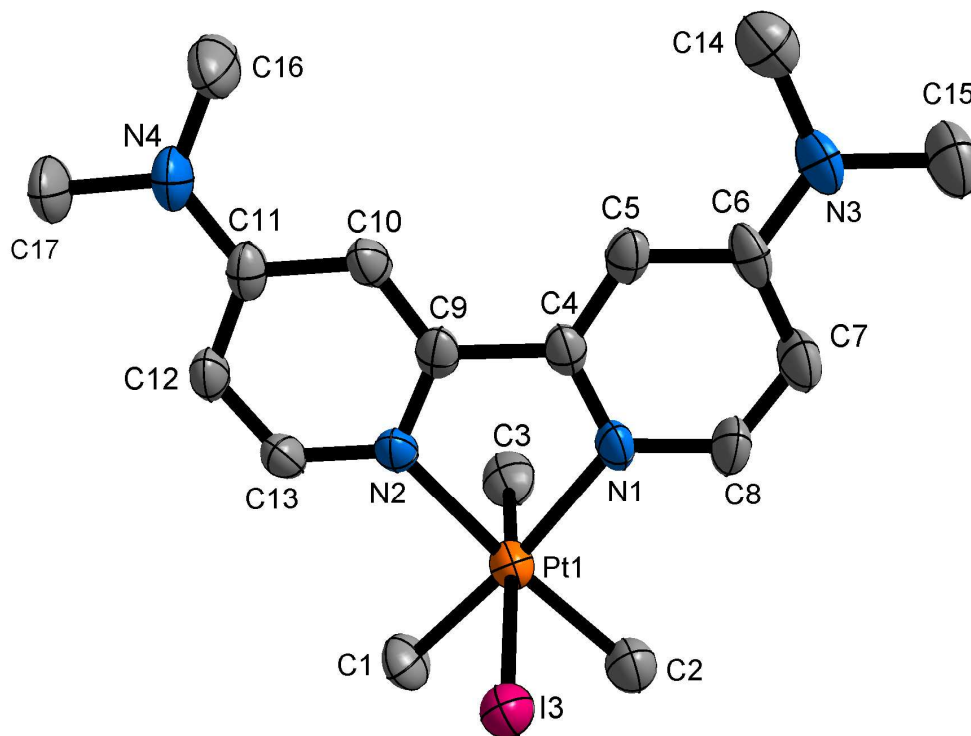


Figure 3.6 Molecular structure of [PtMe₃(Me₂N-bipy)I] showing the atom labelling scheme. Thermal ellipsoids are at the 30% probability level. Hydrogen atoms are omitted for clarity.

The complex $[\text{PtMe}_3(\text{Me}_2\text{N-bipy})\text{I}]$ has eight molecules in its unit cell while each of the other complexes contains four molecules in their unit cell. Figure 3.7 shows the unit cell structure of $[\text{PtMe}_3(\text{bipy})\text{I}]$. However, a benzene molecule also crystallized with the complex $[\text{PtMe}_3(4\text{Me-bipy})\text{I}]$ (see Figure 3.8).

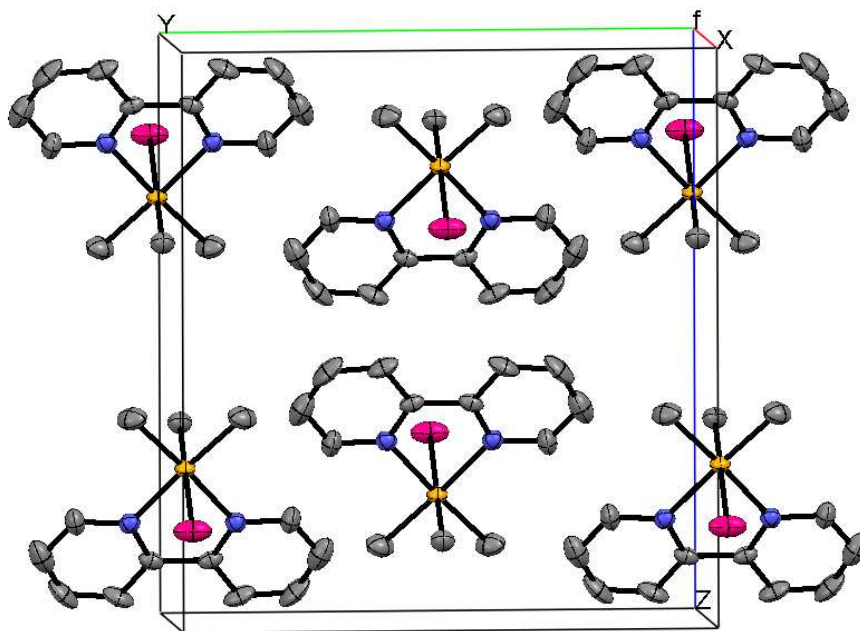


Figure 3.7 Unit cell structure of $[\text{PtMe}_3(\text{bipy})\text{I}]$. Thermal ellipsoids are at the 50% probability level. Hydrogen atoms are omitted for clarity.

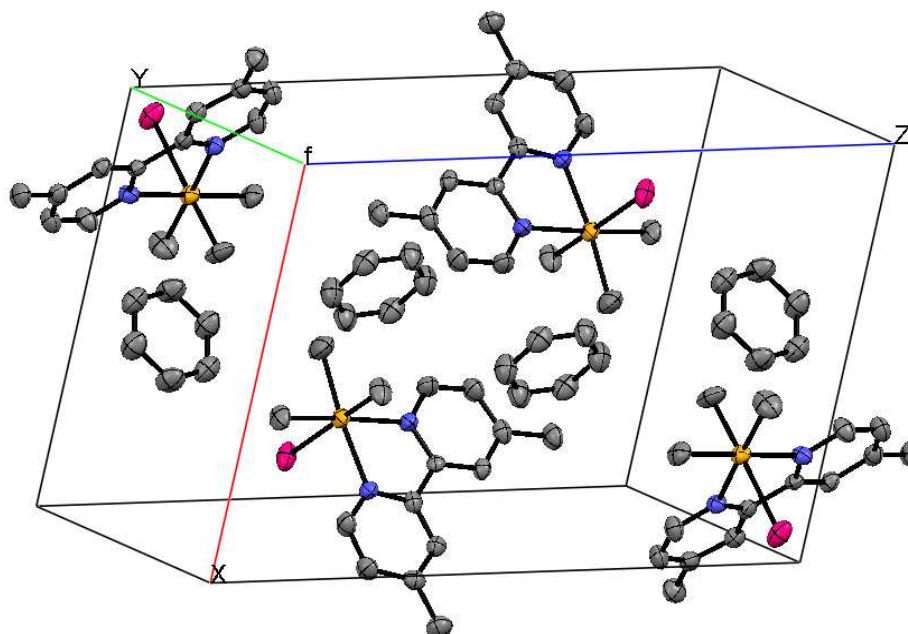


Figure 3.8 Unit cell structure of $[\text{PtMe}_3(4\text{Me-bipy})\text{I}]$ showing solvent benzene. Thermal ellipsoids are at the 50% probability level. Hydrogen atoms are omitted for clarity.

Each of the five complexes has distorted octahedral geometry around the platinum(IV) metal center. The N-Pt-N bite angle in all the complexes is almost the same (76.7° in $[\text{PtMe}_3(\text{bipy})\text{I}]$, 76.3° in $[\text{PtMe}_3(4\text{Me-bipy})\text{I}]$, 76.9° in $[\text{PtMe}_3(5\text{Me-bipy})\text{I}]$, 76.2° in $[\text{PtMe}_3(\text{OMe-bipy})\text{I}]$ and 76.1° in $[\text{PtMe}_3(\text{Me}_2\text{N-bipy})\text{I}]$). This bite angle is close to the value found in reported $[\text{PtMe}_3(\text{bipy})(\text{pydz})][\text{BF}_4]$ (75.3°),^[50] $[\text{PtMe}_3(\text{bipy})(\text{C}_3\text{H}_7\text{NS}_2)][\text{BF}_4]$ (76.2°),^[83] $[\text{PtMe}_3(\text{bipy})(\text{OCOMe})]\cdot\text{H}_2\text{O}$ (76.7°),^[84] and is somewhat larger than the bite angle found in $[\text{PtMe}_3(\text{abpy})\text{I}]$ (73.5°),^[85] $[\text{PtMe}_3(\text{abpy})\text{Br}]$ (73.7°).^[85] Also, the N-Pt-N bite angle is much smaller than that found in the mononuclear pyridine complexes of iodotrimethylplatinum(IV) reported in Chapter 2, confirming the dependence of bite angle on the rigidity of coordinating ligand.

The mean Pt-N bond distance (2.12 \AA) in $[\text{PtMe}_3(\text{bipy})\text{I}]$ is only slightly shorter than the mean Pt-N bond distance in the disubstituted bipyridine complexes (2.15 \AA in $[\text{PtMe}_3(4\text{Me-bipy})\text{I}]$, 2.15 \AA in $[\text{PtMe}_3(5\text{Me-bipy})\text{I}]$, 2.16 \AA in $[\text{PtMe}_3(\text{OMe-bipy})\text{I}]$ and 2.15 \AA in $[\text{PtMe}_3(\text{Me}_2\text{N-bipy})\text{I}]$). This also shows that the Pt-N bond distances in the bipyridine complexes are not influenced significantly by the electronic effect of the bipyridine substituent as observed in the case of pyridine substituent (shown in Chapter 2). However, the Pt-N bond distances in the bipyridine complexes are marginally shorter than the Pt-N bond distances in the corresponding pyridine complexes (shown in Chapter 2.1 and 2.2), reflecting the better π acceptor character of the bipyridines compared to the pyridines.

The Pt-I bond distance in all the bipyridine complexes is essentially identical ($2.77\text{-}2.79 \text{ \AA}$). Except $[\text{PtMe}_3(\text{Me}_2\text{N-bipy})\text{I}]$ where one of the two Pt- $C_{\text{trans } N}$ bonds is longer than the Pt- $C_{\text{trans } I}$ bond, in all the complexes the Pt- $C_{\text{trans } I}$ bond is longer than the Pt- $C_{\text{trans } N}$ bonds, but the difference is statistically insignificant.

Table 3.2 Selected bond lengths [\AA] and angles [$^\circ$] for $[\text{PtMe}_3(\text{bipy})\text{I}]$

Pt1-C1	2.018(7)	Pt1-I3	2.7679(7)
Pt1-C1 ⁱ	2.018(7)	Pt1-N1	2.121(5)
Pt1-C2	2.047(9)	Pt1-N1 ⁱ	2.121(5)
C1-Pt1-C2	89.0(3)	C1-Pt1-I3	91.1(2)
C1-Pt1-C1 ⁱ	85.4(5)	C2-Pt1-I3	179.9(3)
C1-Pt1-N1 ⁱ	98.9(3)	N1 ⁱ -Pt1-I3	91.40(13)
C2-Pt1-N1	88.5(2)	N1-Pt1-I3	91.40(13)
C1-Pt1-N1	175.0(3)	N1 ⁱ -Pt1-N1	76.7(3)

Symmetry transformations used to generate equivalent atoms:

(i) $x, -y, z$

Table 3.3 Selected bond lengths [\AA] and angles [$^\circ$] for $[\text{PtMe}_3(\text{L-L})\text{I}]$ (L-L = 4Me-bipy, 5Me-bipy, OMe-bipy, Me₂N-bipy) complexes

	$[\text{PtMe}_3(4\text{Me-bipy})\text{I}]$	$[\text{PtMe}_3(5\text{Me-bipy})\text{I}]$	$[\text{PtMe}_3(\text{OMe-bipy})\text{I}]$	$[\text{PtMe}_3(\text{Me}_2\text{N-bipy})\text{I}]$
Pt1-C1	2.030(5)	2.041(6)	2.036(7)	2.057(15)
Pt1-C2	2.038(6)	2.032(6)	2.056(8)	2.160(2)
Pt1-C3	2.052(5)	2.051(7)	2.070(8)	2.060(2)
Pt1-N1	2.152(4)	2.148(5)	2.155(6)	2.155(6)
Pt1-N2	2.145(4)	2.155(5)	2.161(7)	2.135(12)
Pt1-I3	2.7818(4)	2.7717(5)	2.7748(6)	2.7928(14)
C1-Pt1-C2	84.8(3)	85.8(2)	85.6(3)	85.9(8)
C2-Pt1-C3	87.7(3)	87.6(3)	88.1(4)	89.6(8)
C1-Pt1-C3	87.9(2)	87.6(3)	87.9(3)	85.5(7)
C1-Pt1-N1	174.8(2)	175.4(2)	173.2(3)	173.8(6)
C2-Pt1-N1	99.0(2)	98.6(2)	99.7(3)	99.7(6)
C3-Pt1-N1	88.7(2)	91.3(2)	88.0(3)	91.9(6)
C1-Pt1-N2	99.8(2)	98.7(2)	98.3(3)	98.2(6)
C2-Pt1-N2	174.5(2)	175.1(2)	175.6(3)	175.6(6)
C3-Pt1-N2	89.4(2)	90.5(2)	89.9(3)	89.0(6)
C1-Pt1-I3	91.55(17)	92.5(2)	89.7(2)	91.8(5)
C2-Pt1-I3	93.3(2)	92.3(2)	91.3(3)	90.9(6)
C3-Pt1-I3	178.8(2)	179.9(2)	177.6(2)	177.2(6)
N1-Pt1-I3	91.83(11)	88.66(13)	94.40(14)	90.8(3)
N2-Pt1-I3	89.71(11)	89.57(13)	90.94(17)	90.7(3)
N1-Pt1-N2	76.27(15)	76.86(18)	76.2(2)	76.1(5)

3.4 X-ray crystallographic characterization of [PtMe₃(Cl-bipy)I]

Deep yellow crystals of [PtMe₃(Cl-bipy)I] were obtained by mixing dilute benzene solution of iodotrimethylplatinum(IV) and 4,4'-dichloro-2,2'-bipyridine in equimolar ratio. The complex shows the expected *fac*-arrangement of the three methyl groups around the central platinum atom (Figure 3.9). The complex crystallizes in the P2₁/n space group with monoclinic crystal symmetry and contains four molecules in its unit cell. The experimental X-ray diffraction parameters and crystallographic data are given in Table 5.4.17, while selected bond lengths and angles are reported in Table 3.4.

The Pt-I distance (2.78 Å) is essentially similar to the value found for the Pt-I bond in the complexes [PtMe₃(L-L)I] (L-L = bipy, 4Me-bipy, 5Me-bipy, OMe-bipy and Me₂N-bipy). The Pt-C_{trans I} bond is marginally longer than the Pt-C_{trans N} bonds. The Pt-N bond distances (2.13 Å, 2.15 Å) are close to the values found for the other bipyridine complexes (shown in section 3.3) and smaller than the Pt-N bond distances found for the pyridine complexes. Deviations from the idealized octahedral geometry are substantial, mainly due to the small bite angle of bipyridyl [N1-Pt1-N2 77.0°], which opens up the N1-Pt1-C2 and N2-Pt1-C1 *cis* angles to 98.2° and 97.9° respectively, and narrows down the N1-Pt1-C1 and N2-Pt1-C2 *trans* angles to 174.6° and 174.8° respectively.

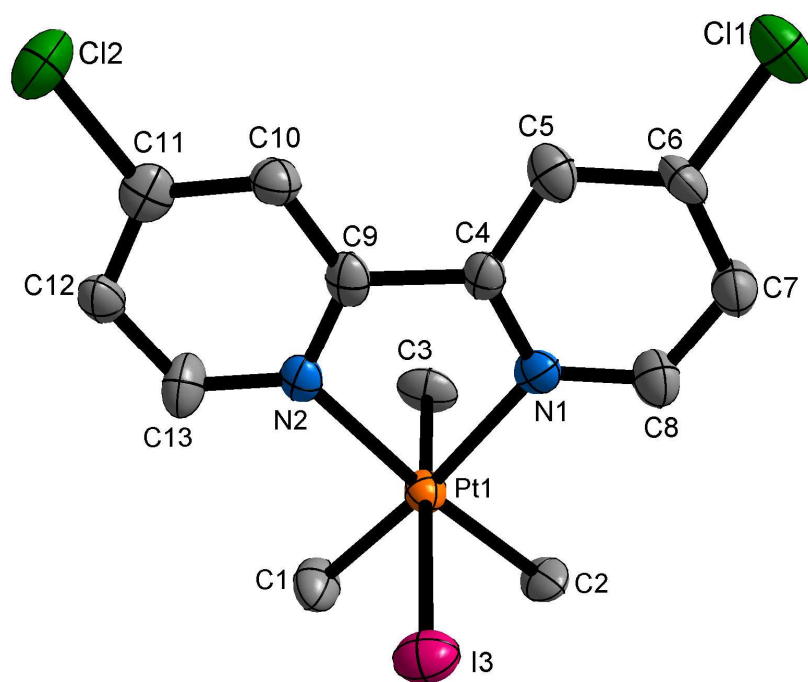
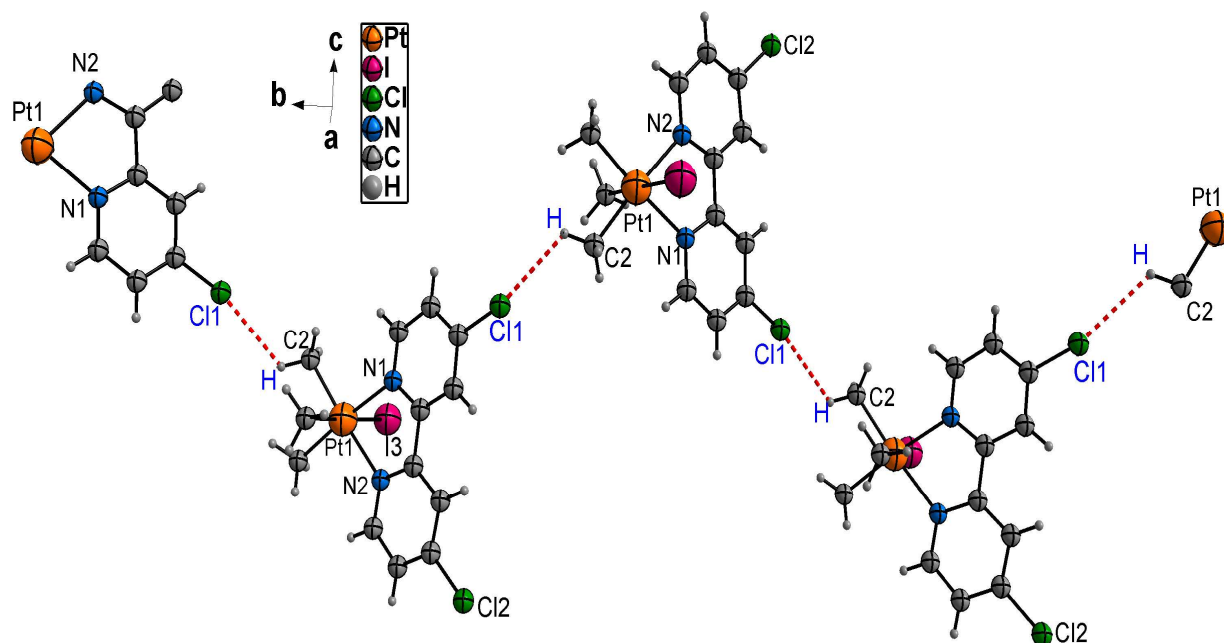


Figure 3.9 Molecular structure of [PtMe₃(Cl-bipy)I] showing the atom labelling scheme. Thermal ellipsoids are at the 50% probability level. Hydrogen atoms are omitted for clarity.

Table 3.4 Selected bond lengths [\AA] and angles [$^\circ$] for $[\text{PtMe}_3(\text{Cl-bipy})\text{I}]$

Pt1-C1	2.018(12)	Pt1-N1	2.128(10)
Pt1-C2	2.051(11)	Pt1-N2	2.150(9)
Pt1-C3	2.088(15)	Pt1-I3	2.7785(11)
C1-Pt1-C2	86.8(5)	N1-Pt1-N2	77.0(4)
C1-Pt1-C3	87.8(7)	C1-Pt1-I3	92.3(5)
C2-Pt1-C3	86.7(6)	C2-Pt1-I3	92.2(4)
C1-Pt1-N1	174.6(5)	C3-Pt1-I3	178.9(5)
C2-Pt1-N1	98.2(4)	N1-Pt1-I3	89.6(3)
C3-Pt1-N1	90.4(5)	N2-Pt1-I3	89.8(3)
C1-Pt1-N2	97.9(5)	C3-Pt1-N2	91.2(5)
C2-Pt1-N2	174.8(5)		

The crystal packing of $[\text{PtMe}_3(\text{Cl-bipy})\text{I}]$ also contains some additional features. Only one of the two chlorine atoms (labelled as Cl1) of $[\text{PtMe}_3(\text{Cl-bipy})\text{I}]$ interacts with the hydrogen atom (labelled as H, which is bonded to C2) (interaction is shown by red colour dotted bond) of another molecule of $[\text{PtMe}_3(\text{Cl-bipy})\text{I}]$ (see Figure 3.10) (the distance between them is 2.79 \AA which is less than the sum of the van der waals radii of H and Cl), thereby leading to the formation of an infinite chain of one dimensional *zig-zag* structure (Figure 3.11).

**Figure 3.10** A perspective view of $[\text{PtMe}_3(\text{Cl-bipy})\text{I}]$ showing the intermolecular interaction (red colour dotted bond) between the hydrogen atom (H) and chlorine atom (Cl1).

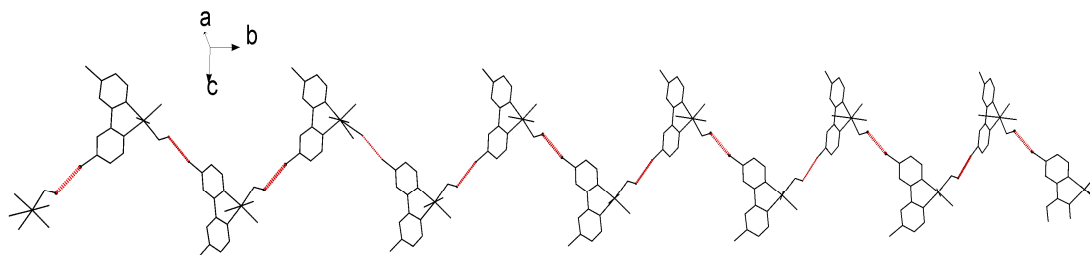


Figure 3.11 A perspective view of an infinite chain of one dimensional *zig-zag* structure of $[\text{PtMe}_3(\text{Cl-bipy})\text{I}]$.

π - π interaction^[86,87] plays an important role in controlling the packing or assembly of compounds. Although each 4,4'-dichloro-2,2'-bipyridine is parallel to an adjacent one, the position of each is shifted so that one is not directly above the other. The perpendicular distance between the two parallel rings is approximately 3.90 Å. This weak π - π interaction holds the *zig-zag* chains together, supporting a two-dimensional layer structure (Figure 3.12). Similar π - π interactions between interlocking chains are also observed in the crystal packing of adamantane derivatives of bipyridines.^[88,89]

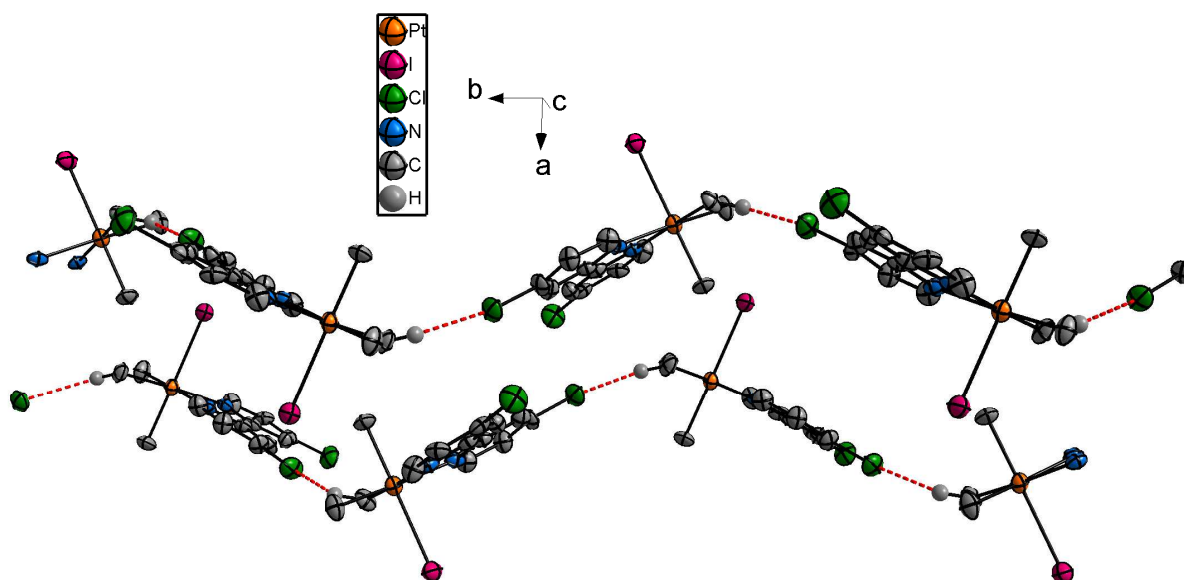


Figure 3.12 A perspective view of a two-dimensional framework structure of $[\text{PtMe}_3(\text{Cl-bipy})\text{I}]$.

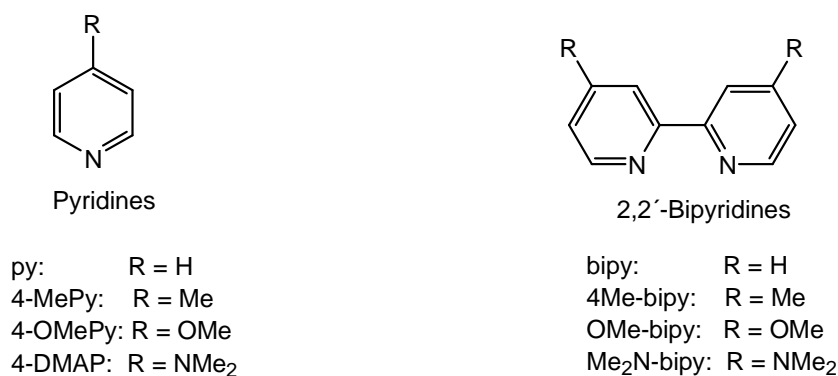
3.5 Conclusion

Reaction of iodotrimethylplatinum(IV) with 2,2'-bipyridines in equimolar ratio in benzene results in the formation of chelate complexes of bipyridines. The complexes were characterized by ^1H NMR, EI-MS, IR spectroscopy and elemental analyses. The $^2J_{\text{Pt-H}}$ coupling constant of these complexes confirms that the *trans* influence of the bipyridines is stronger than that of the iodide ligand and depends on the electronic nature of the substituent attached to the bipyridine ring. Electron donating substituents increase the *trans* influence of the bipyridines whereas electron withdrawing substituents reduce the extent of *trans* influence of the bipyridines. X-ray crystal structure analysis of the complexes reveals the *fac*-octahedral coordination of the PtMe_3 moiety and bidentate coordination of the aromatic ligand. The Pt-N bond distances are not affected significantly by the electronic effect of the bipyridine substituent. However, the Pt-N bonds for the bipyridine complexes are slightly shorter than for the corresponding pyridine complexes, indicating that the bipyridine ring is a better π -acceptor. The N-Pt-N bite angle for the bipyridine complexes is also much lower than that of the pyridines. The intermolecular non-covalent interaction between methyl hydrogen and chlorine atom in $[\text{PtMe}_3(\text{Cl-bipy})\text{I}]$ leads to the formation of *zig-zag* chains. In turn, these interlocking chains are linked through weak π - π interactions and thereby generate two-dimensional layer structure.

4 Ligand-Exchange Study on Iodotrimethylplatinum(IV) Complexes

4.1 Introduction

The presence of strongly electron donating methyl groups makes the ligand substitution reaction in methylplatinum(IV) complexes straightforward. The substitution reaction in these complexes can be electrophilic^[90] as well as nucleophilic.^[91,92] The reaction of a pyridine complex of iodotrimethylplatinum(IV) with 2,2'-bipyridine leads to the substitution of pyridine by 2,2'-bipyridine resulting in the formation of the chelate complex of 2,2'-bipyridine. Thus, with a view to exploring the chelate effect in the trimethylplatinum(IV) system, this chapter deals with the exchange of pyridine ligands by the 2,2'-bipyridine ligands in the complexes of iodotrimethylplatinum(IV). Different types of pyridines (py, 4-MePy, 4-OMePy and 4-DMAP) were substituted by the corresponding 2,2'-bipyridines (bipy, 4Me-bipy, OMe-bipy and Me₂N-bipy) (Scheme 4.1) in the iodotrimethylplatinum(IV) complexes to demonstrate the electronic effect of the substituent on the chelation reaction. The reactions were carried out in two solvents (CDCl₃, an apolar solvent and nitrobenzene-d₅, a polar solvent) to examine the solvent effect on the chelation reaction.



Scheme 4.1 Different pyridines and corresponding 2,2'-bipyridines used for the chelation reaction in trimethylplatinum(IV) system.

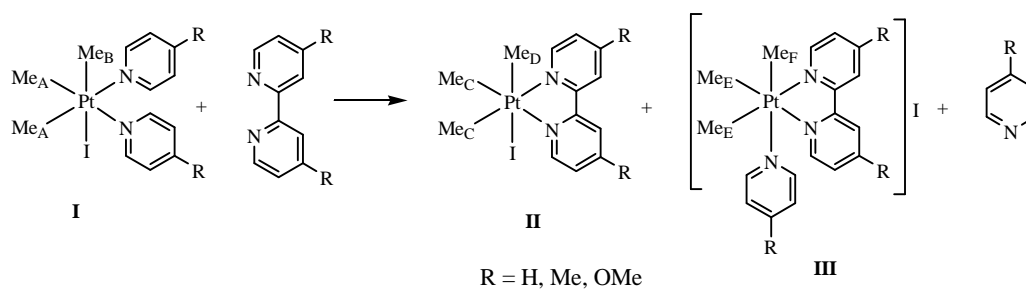
4.2 Result and Discussion

4.2.1 Syntheses and characterization of the complexes

The complexes $[\text{PtMe}_3\text{L}_2\text{I}]$ ($\text{L} = \text{py}, 4\text{-MePy}, 4\text{-OMePy}$) were synthesized by the treatment of tetranuclear iodotrimethylplatinum(IV) with pyridine ligands. Similarly, reaction of iodotrimethylplatinum(IV) with 2,2'-bipyridine and its derivatives results in the chelate complexes of 2,2'-bipyridines, $[\text{PtMe}_3(\text{L-L})\text{I}]$ ($\text{L-L} = \text{bipy}, 4\text{Me-bipy}, \text{OMe-bipy}$ and $\text{Me}_2\text{N-bipy}$). Full synthetic and analytical data of the complexes are reported in Section 5.3.3-5.3.4.

4.2.2 Reaction of $[\text{PtMe}_3\text{L}_2\text{I}]$ ($\text{L} = \text{py}, 4\text{-MePy}$ and 4-OMePy) complexes with corresponding 2,2'-bipyridines (bipy, 4Me-bipy and OMe-bipy)

Reaction of iodotrimethylplatinum(IV) complexes of pyridine (py) and its 4-substituted derivatives (4-MePy, 4-OMePy) with the corresponding 2,2'-bipyridines (bipy, 4Me-bipy and OMe-bipy) results in the formation of two chelate complexes of bipyridines along with the release of free pyridines (see Scheme 4.2). The reactions were followed by ^1H NMR spectroscopy. The ^1H NMR spectra of an equimolar mixture of pyridine complex and the corresponding 2,2'-bipyridine ligand at equilibrium at 300 K for each of the three substitution reactions show signals for the three trimethylplatinum(IV) complexes (**I**, **II** and **III**, as shown in Scheme 4.2), free pyridine ligand, and unreacted 2,2'-bipyridine ligand. Each of the trimethylplatinum(IV) complexes consists of two platinum-methyl resonances, due to $^{195}\text{Pt-H}$ scalar coupling, with an intensity ratio of 2:1. The ^1H NMR data for all three reactions in CDCl_3 and in nitrobenzene- d_5 are reported in Table 4.1. The ^1H NMR spectrum of an equimolar mixture of $[\text{PtMe}_3(\text{py})_2\text{I}]$ and bipy at equilibrium at 300 K in nitrobenzene- d_5 is shown in Figure 4.1, while ^1H NMR spectrum of an equimolar mixture of $[\text{PtMe}_3(4\text{-OMePy})_2\text{I}]$ and OMe-bipy in CDCl_3 at equilibrium at 300 K is illustrated in Figure 4.2.



Scheme 4.2 The substitution of pyridine ligands by the corresponding 2,2'-bipyridines in iodotrimethylplatinum complexes.

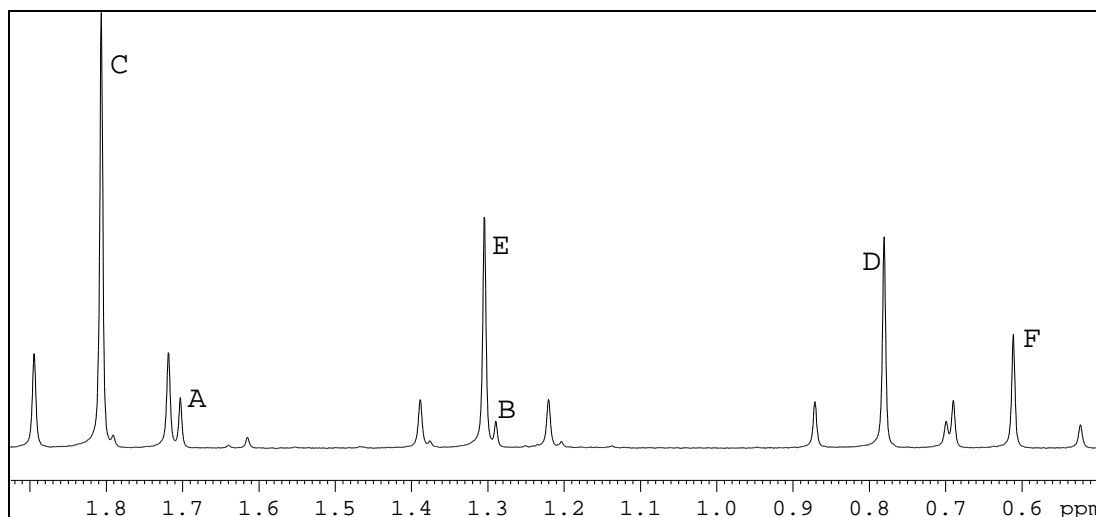


Figure 4.1 The platinum-methyl region in the ^1H NMR spectrum of an equimolar mixture of $[\text{PtMe}_3(\text{py})_2\text{I}]$ and bipy in nitrobenzene- d_5 at equilibrium at 300 K showing presence of three platinum(IV) complexes $[\text{PtMe}_3(\text{py})_2\text{I}]$ (I), $[\text{PtMe}_3(\text{bipy})\text{I}]$ (II) and $[\text{PtMe}_3(\text{bipy})(\text{py})\text{I}]$ (III). For labelling, see Scheme 4.2.

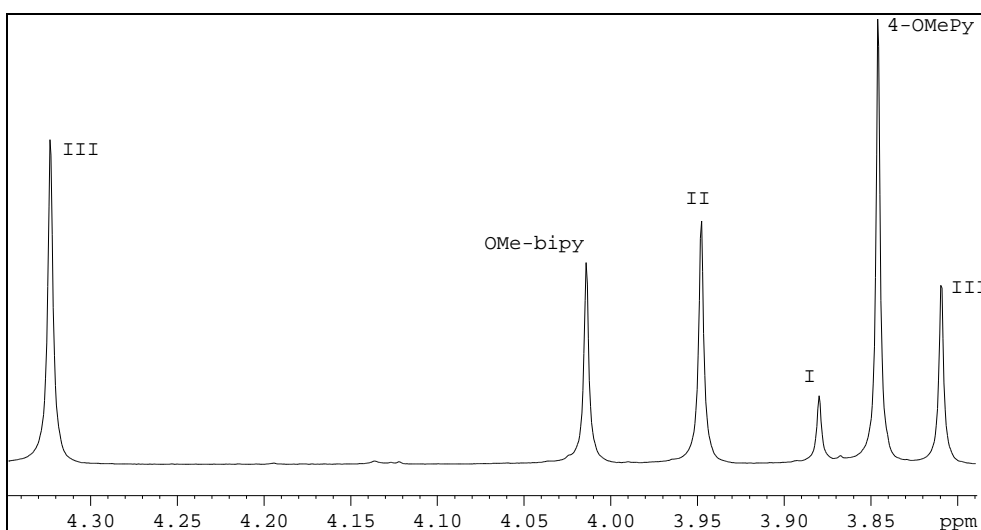
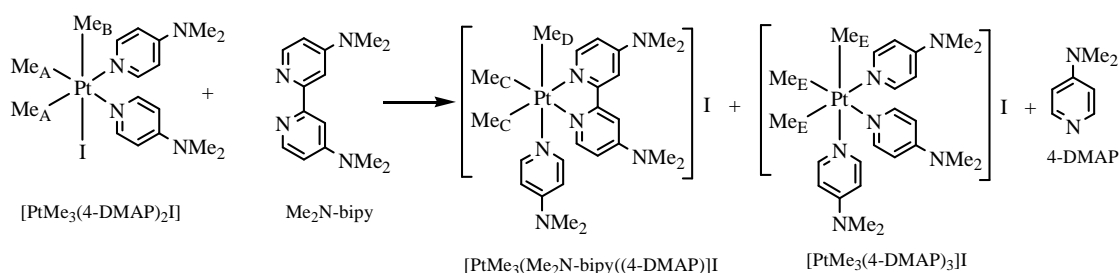


Figure 4.2 The methoxy region in the ^1H NMR spectrum of an equimolar mixture of $[\text{PtMe}_3(4\text{-OMePy})_2\text{I}]$ and OMe-bipy in CDCl_3 at equilibrium at 300 K. I = $[\text{PtMe}_3(4\text{-OMePy})_2\text{I}]$. II = $[\text{PtMe}_3(\text{OMe-bipy})\text{I}]$. III = $[\text{PtMe}_3(\text{OMe-bipy})(4\text{-OMePy})\text{I}]$. The signal at the left correspond to the methoxy group of OMe-bipy in complex III, while the signal at the utmost right correspond to the methoxy group of the 4-OMePy in complex III.

4.2.3 Reaction of $[\text{PtMe}_3(4\text{-DMAP})_2\text{I}]$ with $\text{Me}_2\text{N-bipy}$

Reaction of $[\text{PtMe}_3(4\text{-DMAP})_2\text{I}]$ with $\text{Me}_2\text{N-bipy}$ leads to the formation of exclusively one chelate complex, $[\text{PtMe}_3(\text{Me}_2\text{N-bipy})(4\text{-DMAP})\text{I}]$. A small amount of $[\text{PtMe}_3(4\text{-DMAP})_3\text{I}]$ is also formed in solution due to the reaction of $[\text{PtMe}_3(4\text{-DMAP})_2\text{I}]$ with the free 4-DMAP ligand, generated in solution because of the substitution process (see Scheme 4.3). The ^1H NMR data for the presence of different trimethylplatinum(IV) complexes for the reaction of an equimolar mixture of $[\text{PtMe}_3(4\text{-DMAP})_2\text{I}]$ and $\text{Me}_2\text{N-bipy}$ at equilibrium at 300 K in CDCl_3 and in nitrobenzene- d_5 is presented in Table 4.1.



Scheme 4.3 The substitution of 4-DMAP by $\text{Me}_2\text{N-bipy}$ in iodotrimethylplatinum(IV) complex.

Table 4.1 ^1H NMR data^a for the reaction of an equimolar mixture of $[\text{PtMe}_3\text{L}_2\text{I}]$ (L = pyridines) and corresponding 2,2'-bipyridines at equilibrium at 300 K in CDCl_3 and in nitrobenzene- d_5

Reaction	Pt(IV) species present in equilibrium	$\delta(\text{Pt-CH}_3)^{b,c}$ in CDCl_3	$\delta(\text{Pt-CH}_3)^{b,c}$ in nitrobenzene- d_5	Trans ligand
Equimolar mixture of $[\text{PtMe}_3(\text{py})_2\text{I}]$ and bipy	$[\text{PtMe}_3(\text{py})_2\text{I}]$	A 1.50 (70.3)	A 1.70 (70.4)	py
		B 1.20 (69.6)	B 1.29 (68.9)	I
	$[\text{PtMe}_3(\text{bipy})\text{I}]$	C 1.56 (70.5)	C 1.81 (70.5)	bipy
		D 0.64 (73.1)	D 0.78 (72.6)	I
	$[\text{PtMe}_3(\text{bipy})(\text{py})\text{I}]$	E 1.23 (67.1)	E 1.31 (67.2)	bipy
		F 0.57 (70.3)	F 0.61 (70.5)	py
Equimolar mixture of $[\text{PtMe}_3(4\text{-MePy})_2\text{I}]$ and 4Me-bipy	$[\text{PtMe}_3(4\text{-MePy})_2\text{I}]$	A 1.45 (70.0)	A 1.69 (70.1)	4-MePy
		B 1.17 (70.0)	B 1.28 (69.2)	I
	$[\text{PtMe}_3(4\text{Me-bipy})\text{I}]$	C 1.51 (70.3)	C 1.78 (70.3)	4Me-bipy
		D 0.63 (73.5)	D 0.81 (72.9)	I
	$[\text{PtMe}_3(4\text{Me-bipy})(4\text{-MePy})\text{I}]$	E 1.14 (66.9)	E 1.25 (67.2)	4Me-bipy
		F 0.52 (70.6)	F 0.61 (70.5)	4-MePy
Equimolar mixture of $[\text{PtMe}_3(4\text{-OMePy})_2\text{I}]$ and OMe-bipy	$[\text{PtMe}_3(4\text{-OMePy})_2\text{I}]$	A 1.42 (70.0)	A 1.69 (70.2)	4-OMePy
		B 1.15 (70.2)	B 1.29 (69.4)	I
	$[\text{PtMe}_3(\text{OMe-bipy})\text{I}]$	C 1.48 (70.2)	C 1.77 (70.5)	OMe-bipy
		D 0.65 (73.7)	D 0.86 (73.0)	I
	$[\text{PtMe}_3(\text{OMe-bipy})(4\text{-OMePy})\text{I}]$	E 1.09 (67.2)	E 1.23 (67.4)	OMe-bipy
		F 0.50 (70.4)	F 0.64 (70.5)	4-OMePy
Equimolar mixture of $[\text{PtMe}_3(4\text{-DMAP})_2\text{I}]$ and $\text{Me}_2\text{N-bipy}$	$[\text{PtMe}_3(4\text{-DMAP})_2\text{I}]$	A 1.35 (69.3)	Not present	4-DMAP
		B 1.14 (71.5)		I
	$[\text{PtMe}_3(\text{Me}_2\text{N-bipy})(4\text{-DMAP})\text{I}]$	C 0.94 (67.0)	C 1.13 (67.1)	$\text{Me}_2\text{N-bipy}$
		D 0.43 (70.3)	D 0.65 (70.0)	4-DMAP
	$[\text{PtMe}_3(4\text{-DMAP})_3\text{I}]$	E 0.92 (66.7)	E 1.04 (66.7)	4-DMAP

^a Chemical shifts quoted in ppm are relative to internal solvent peaks (in the case of CDCl_3 , $\delta = 7.26$ ppm; in the case of nitrobenzene- d_5 , $\delta = 8.11$ ppm). ^b $^2J_{\text{Pt-H}}$ /Hz in parentheses. ^c labelling refers to Schemes 4.2 and 4.3.

An analysis of Table 4.1 shows that changing the solvent from CDCl_3 to nitrobenzene- d_5 causes the platinum-methyl resonances to shift to higher frequency in the ^1H NMR spectrum. The difference in chemical shifts for the two platinum-methyl resonances is larger in the bipyridine complexes than in the pyridine complexes. Moreover, the difference in chemical shifts for the two platinum-methyl resonances is greater in the neutral chelate $[\text{PtMe}_3(\text{L-L})\text{I}]$ ($\text{L-L} = 2,2'$ -bipyridines) complexes than in the ionic chelate $[\text{PtMe}_3(\text{L-L})\text{L}]\text{I}$ ($\text{L-L} = 2,2'$ -bipyridines, $\text{L} =$ corresponding pyridines) complexes. The $^2J_{\text{Pt-H}}$ scalar coupling constants indicate that the *trans* influence of the 2,2'-bipyridines is stronger than the corresponding pyridines (*trans* influence: bipy > py, 4Me-bipy > 4-Mepy, OMe-bipy > 4-OMePy, $\text{Me}_2\text{N-bipy}$ > 4-DMAP). Also, the *trans* influence of the 2,2'-bipyridines is greater in the ionic chelate complexes than in the neutral chelate complexes. The results for the reaction of an equimolar mixture of $[\text{PtMe}_3\text{L}_2\text{I}]$ ($\text{L} =$ pyridines such as py, 4-MePy, 4-OMePy and 4-DMAP) and corresponding 2,2'-bipyridines at equilibrium in CDCl_3 and in nitrobenzene- d_5 are summarized in Table 4.2.

Table 4.2 The reaction of an equimolar mixture of $[\text{PtMe}_3\text{L}_2\text{I}]$ ($\text{L} =$ pyridines) and corresponding 2,2'-bipyridines (L-L) at equilibrium at 300 K in CDCl_3 and in nitrobenzene- d_5 *a, b*

Substitution of pyridine ligands by 2,2'-bipyridines	In CDCl_3		In nitrobenzene- d_5	
	Chelate complex /Non-chelate complex	Ionic chelate /Neutral chelate	Chelate complex /Non-chelate complex	Ionic chelate /Neutral chelate
py by bipy	15.67	0.20	13.29	0.52
4-MePy by 4Me-bipy	11.5	0.64	6.14	1.17
4-OMePy by OMe-bipy	8.09	1.54	5.25	2.23
4-DMAP by $\text{Me}_2\text{N-bipy}$	19.0	Only ionic chelate present	15.67	Only ionic chelate present

^a Chelate complex is the mixture of ionic chelate $[\text{PtMe}_3(\text{L-L})\text{L}]\text{I}$ and neutral chelate $[\text{PtMe}_3(\text{L-L})\text{I}]$. Non chelate complex is $[\text{PtMe}_3\text{L}_2\text{I}]$. ($\text{L} =$ pyridines such as py, 4-MePy and 4-OMePy; $\text{L-L} =$ corresponding bipyridines such as bipy, 4Me-bipy and OMe-bipy).

^bIn the case of the substitution of 4-DMAP by $\text{Me}_2\text{N-bipy}$, only the ionic chelate $[\text{PtMe}_3(\text{Me}_2\text{N-bipy})(4\text{-DMAP})\text{I}]$ is present in solution in both the solvents. In CDCl_3 , the non-chelate complex is the mixture of $[\text{PtMe}_3(4\text{-DMAP})_2\text{I}]$ and $[\text{PtMe}_3(4\text{-DMAP})_3\text{I}]$, while in nitrobenzene- d_5 , the non-chelate complex is $[\text{PtMe}_3(4\text{-DMAP})_3\text{I}]$.

Table 4.2 shows that the equilibrium for all the four substitution reactions in both the solvents (CDCl_3 and nitrobenzene- d_5) strongly favour the formation of chelate 2,2'-bipyridine complexes which are more stable than the corresponding non-chelate pyridine complexes. The formation of the chelate complexes at equilibrium for each of the four substitution reactions depends on the electronic effect of the substituent as well as on the nature of the solvent. As the electron donating property of the substituent increases from H to NMe_2 in the order $\text{H} < \text{Me} < \text{OMe} < \text{NMe}_2$, the population ratio of the ionic chelate $[\text{PtMe}_3(\text{L-L})\text{L}]\text{I}$ to the neutral chelate $[\text{PtMe}_3(\text{L-L})\text{I}]$ ($\text{L} = \text{pyridines}$, $\text{L-L} = \text{corresponding bipyridines}$) also increases in the same order in both the solvents. This can be rationalised in terms of the stability of the ionic chelates in solution. As the electron donating ability of the substituent increases, the electron density in both the pyridine and bipyridine ring N also increases. The resulting increase in the electron density on the aromatic ring N also causes an increase in the extent of Pt-N interaction which accounts for the increased stability of the ionic chelates in solution, and in the case of NMe_2 substituent, the stability of the ionic chelate is so high (because of the extremely strong Pt-N interaction) that exclusively the ionic chelate $[\text{PtMe}_3(\text{Me}_2\text{N-bipy})(4\text{-DMAP})]\text{I}$ is formed in solution. The strength of the chelate effect for the different substituents in both the solvents is in the order: $\text{NMe}_2 > \text{H} > \text{Me} > \text{OMe}$. To explain the above order of chelation among the substituents (H, Me, and OMe), the stability of the reactant complexes in solution is also taken into consideration. As the electron donating ability of the substituent increases from H to Me to OMe, the stability of the reactant non-chelate pyridine complexes also increases (from H to Me to OMe) due to the increasing Pt-N interaction in the reactant complexes, thereby leading to a decrease in the strength of the chelate effect. For H, Me and OMe substituents, the population ratio of the ionic chelate to the neutral chelate is more in nitrobenzene- d_5 than in CDCl_3 . This is supported by the fact that the ionic complexes are more stable in polar solvent (nitrobenzene- d_5) than in apolar solvent (CDCl_3). The strength of chelation for a particular substituent is greater in CDCl_3 than in nitrobenzene- d_5 . This is most likely due to the lower solvent stabilization of the reactant complexes in CDCl_3 than in nitrobenzene- d_5 .

4.3 Conclusion

The reaction of iodotrimethylplatinum(IV) complexes of pyridines, $[\text{PtMe}_3\text{L}_2\text{I}]$ ($\text{L} = \text{py}, 4\text{-MePy}, 4\text{-OMePy}, 4\text{-DMAP}$) with the corresponding 2,2'-bipyridines (bipy, 4Me-bipy, OMe-bipy, $\text{Me}_2\text{N-bipy}$) lead to the substitution of the pyridine ligands by the bipyridines, resulting in the formation of neutral $[\text{PtMe}_3(\text{L-L})\text{I}]$ and ionic $[\text{PtMe}_3(\text{L-L})\text{L}]\text{I}$ ($\text{L-L} = 2,2'\text{-bipyridines}$, $\text{L} = \text{corresponding pyridines}$) chelate complexes along with the release of pyridines. The equilibrium for all the substitution reactions strongly favours the formation of chelate complexes. The formation of chelate complexes in solution at equilibrium depends on the electronic effect of the substituents as well as on the nature of the solvent. Increasing electron donating ability of the substituent leads to an increase in the stability of the ionic chelate in solution. The tendency for the chelation is very high for strong electron donating substituents such as NMe_2 ; however, for H and moderately electron donating substituents such as Me and OMe, increasing electron donating ability decreases the strength of the chelate effect. The stability of ionic chelate is more in nitrobenzene- d_5 (polar solvent) than in CDCl_3 (apolar solvent); however, the strength of chelation is greater in CDCl_3 than in nitrobenzene- d_5 .

5 Experimental Section

5.1 Characterization Methods

5.1.1 ^1H NMR Spectroscopy

^1H NMR spectra were recorded on a Bruker Avance II 400 MHz spectrometer, operating at 400 MHz. Chemical shifts are relative to an internal solvent peak (for CDCl_3 stabilized with Ag-foil, $\delta = 7.26$ ppm; for DMSO-d_6 , $\delta = 2.50$ ppm; for D_2O , $\delta = 4.79$ ppm; for nitrobenzene- d_5 , $\delta = 8.11$ ppm).

^1H DOSY NMR spectra were recorded on a Bruker Avance III 600 MHz spectrometer, equipped with a 5 mm broadband BBO Z-gradient probe (maximum gradient strength 53.5 G/cm), operating at 600 MHz. All diffusion experiments were performed with a convection suppressing Double STE pulse sequence in pseudo-two dimensional mode and processed with Bruker TOPSPIN software package (Version 2.0). The temperature was set and controlled at 298 K with airflow of 5351 h^{-1} . For each experiment, 16 dummy scans and 24 scans were used, with a relaxation delay of 2 s and a diffusion delay of 100 ms. The shape of the gradients was sinusoidal, with a length of 1 m, and the strength was varied in 32 increments (2-95%) in a linear ramp.

5.1.2 IR Spectroscopy

Infrared spectra were recorded as pressed KBr discs on an IFS 48 spectrometer, equipped with a KBr beam splitter, operating in the region 4000-400 cm^{-1} .

5.1.3 Elemental Analysis

Elemental analyses were performed on a Thermo Electron Flash EA 1112 series.

5.1.4 EI-Mass Spectroscopy

EI-mass spectra were acquired on a Finnigan MAT 95 (EI: 70 eV) mass spectrometer.

5.2 Materials and Working Conditions

The following compounds were commercially available:

- Pyridine (py), 4-dimethylaminopyridine (4-DMAP), 4-cyanopyridine (4-CNPy), 2,2'-bipyridine (bipy), nitrobenzene-d₅ from Aldrich
- Potassium hexachloroplatinate, 4-methylpyridine (4-MePy), 4-ethylpyridine (4-EtPy), 4-methoxypyridine (4-OMePy), 4-^tbutylpyridine (4-^tBuPy), 3-bromopyridine (3-BrPy), 3-methoxypyridine (3-OMePy), 4,4'-dimethoxy-2,2'-bipyridine (OMe-bipy) from Acros Organics
- 3-Methylpyridine (3-MePy), 3-ethylpyridine (3-EtPy), 3-chloropyridine (3-ClPy), 4,4'-dimethyl-2,2'-bipyridine (4Me-bipy), 5,5'-dimethyl-2,2'-bipyridine (5Me-bipy) from Alfa Aesar
- 30% Hydrogen peroxide (H₂O₂) from Merck
- CDCl₃, DMSO-d₆, D₂O from Euriso-top
- Magnesium turning, sodium metal, molecular sieve (3 Å), potassium bromide (KBr), sodium hydroxide (NaOH), calcium chloride (CaCl₂), calcium hydride (CaH₂), anhydrous calcium sulfate (CaSO₄), anhydrous magnesium sulfate (MgSO₄), glacial acetic acid (CH₃COOH), oleum-sulfuric acid, fuming nitric acid from the chemical storage of the Institute of Inorganic and Analytical Chemistry, Justus-Liebig-University of Giessen
- Acetyl chloride (CH₃COCl), methyl iodide (CH₃I) and phosphorous trichloride (PCl₃) from the chemical storage of the Institute of Organic Chemistry, Justus-Liebig-University of Giessen
- The solvents acetone, benzene, chloroform, dichloromethane (DCM), diethyl ether, n-hexane, n-pentane, methanol, ethanol from the chemical storage of the Institute of Inorganic and Analytical Chemistry, Justus-Liebig-University of Giessen
- N,N-Dimethylformamide from the chemical storage of the Institute of Organic Chemistry, Justus-Liebig-University of Giessen

All the chemicals were of reagent grade. Solvents for the air-sensitive reactions were redistilled under argon. The ligands 4,4'-bis(dimethylamino)-2,2'-bipyridine (Me₂N-bipy), 4,4'-dichloro-2,2'-bipyridine (Cl-bipy) and the complex [PtMe₃I]₄ were synthesized under inert conditions using standard Schlenk techniques. The rest of the complexes were prepared under ambient conditions.

5.3 Syntheses

5.3.1 Synthesis of Iodotrimethylplatinum(IV)

The complex iodotrimethylplatinum(IV) was prepared by the method of Baldwin *et al.*^[28]

The Grignard reagent, CH_3MgI , was prepared by dropping 10.0 mL (22.8 g, 160 mmol) of methyl iodide in 40 mL of dry diethyl ether onto flame-dried magnesium turnings (2.20 g, 90.4 mmol) under argon. The resulting black suspension was then stirred until the last pieces of magnesium were dissolved and subsequently filtered through a sintered-glass disk (medium porosity) directly into a dropping funnel mounted atop a flask which contained 4.00 g (8.24 mmol) of finely powdered potassium hexachloroplatinate (K_2PtCl_6) in 20 mL of diethyl ether and 80 mL of benzene. The reaction mixture was allowed to warm gradually up to room temperature after the addition and left to stir under argon. Within 4 h, the mixture faded from yellow to white. After stirring the mixture overnight, the white salts were allowed to settle. The supernatant was then filtered through a medium sintered-glass disk under argon. The clear, nearly colourless filtrate was cooled to 0 °C and 10 mL of ice-cold acetone was slowly added dropwise to the stirring filtrate. As the acetone was added a vigorous reaction took place, which turned the mixture yellow and then orange. A two-phase mixture resulted with a yellow layer at the top and an orange layer below. After opening the flask to the air, 50 mL of ice-cold water was added to the stirring mixture. The mixture was acidified with 60 mL of 10% HCl which dissolves the solid and gives an orange-yellow organic layer over a pinkish orange aqueous layer with a small amount of orange solid at the interphase. The orange solid was filtered and the layers were separated. The aqueous layer was extracted with 3 30-mL portions of benzene. The extracts were combined with the organic layer and dried by filtration through a cone of anhydrous CaSO_4 . The clear, yellow-orange solution then evaporated to dryness, and the resulting yellow solid dissolved in 40 mL of CHCl_3 . This solution was evaporated to about 15 mL, 15 mL of acetone was added, and the mixture was cooled in ice. The yellow crystals formed were collected and air-dried. Yield: 2.3 g (76%).

^1H NMR (CDCl_3 ; ppm): $\delta = 1.72$ (s, 9H, PtCH_3 , $^2\text{J}_{\text{Pt-H}}$: 77.3 Hz).

5.3.2 Syntheses of 4,4'-disubstituted-2,2'-bipyridine ligands

5.3.2.1 Synthesis of 4,4'-bis(dimethylamino)-2,2'-bipyridine (Me₂N-bipy)

The ligand Me₂N-bipy was synthesized by the following steps:

Step 1 Synthesis of 2,2'-bipyridine N,N'-dioxide (bipy N-Oxide)^[93]

A 30 mL solution of 30% hydrogen peroxide was added to 2,2'-bipyridine (10.0 g, 64 mmol) in 50 mL of glacial acetic acid at a rate that maintained the temperature between 70 °C and 80 °C. The mixture was stirred at 75 °C for an additional 8 h. The solution was then cooled to room temperature, and a large amount (750 mL) of acetone was added to precipitate the product as a white solid, which was collected by filtration and air-dried. Yield: 11.3 g (60 mmol, 94% yield).

¹H NMR (D₂O; ppm): δ = 7.76 (m, 4H), 7.85 (m, 2H), 8.47 (m, 2H).

Step 2 Synthesis of 4,4'-dinitro-2,2'-bipyridine N,N'-dioxide (O₂N-bipy N-Oxide)^[93]

A solution of bipy N-Oxide (9.0 g, 47.8 mmol) in 26 mL of oleum-sulfuric acid was cooled to 0 °C. Fuming nitric acid (20 mL) was carefully added, and the mixture was stirred at 100 °C for 8 h. The solution was then cooled to 0 °C and very cautiously poured onto ice water (200 g). The resultant yellow product was filtered off and washed with water until neutral. Yield: 9.6 g (34.5 mmol, 72%).

¹H NMR (DMSO-d₆; ppm): δ = 8.38 (dd, 2H), 8.60 (d, 2H), 8.70 (d, 2H).

Step 3 Synthesis of 4,4'-dichloro-2,2'-bipyridine N,N'-dioxide (Cl-bipy N-Oxide)^[94]

A suspension of 1 g of O₂N-bipy N-Oxide (3.59 mmol) in 50 mL of acetyl chloride was refluxed under argon for 3 h. The solid product was filtered off, washed with 50 mL of diethyl ether, and dried under vacuum. Yield: 700 mg of pale yellow powder (2.72 mmol, 76%).

¹H NMR (CDCl₃; ppm): δ = 7.35 (dd, 2H), 7.72 (d, 2H), 8.25 (d, 2H).

Step 4 Synthesis of 4,4'-bis(dimethylamino)-2,2'-bipyridine (Me₂N-bipy)^[93]

A suspension of 1 g of Cl-bipy N-Oxide (3.89 mmol) in 150 mL DMF was refluxed under argon for 48 h. The solvent was evaporated nearly completely, and the crude product was dissolved in 100 mL of chloroform. Phosphorous trichloride (8.5 mL, 97.4 mmol) was added dropwise to the cooled solution at 0 °C. The reaction mixture was then refluxed for 3 h and then poured onto 250 mL of ice water. The chloroform layer was washed with 3 × 50 mL of water and the combined aqueous extracts were concentrated under vacuum to 75 mL and made alkaline with saturated aqueous sodium hydroxide. The resulting precipitate was recrystallized twice from water/methanol (1.5 v/v) to give 150 mg of the beige product Me₂N-bipy (0.62 mmol, 16%).

¹H NMR (DMSO-d₆; ppm): δ = 3.02 [s, 12H, N(CH₃)₂], 6.63 (dd, 2H), 7.66 (d, 2H), 8.20 (d, 2H).

5.3.2.2 Synthesis of 4,4'-dichloro-2,2'-bipyridine (Cl-bipy)^[94]

A suspension of 1 g of O₂N-bipy N-Oxide (3.59 mmol) in 50 mL of acetyl chloride was refluxed under argon for 3 h. The reaction mixture was cooled to 0 °C, and 8.8 mL of phosphorous trichloride (100 mmol) was added. The suspension was refluxed under argon for another 3 h. After cooling to room temperature, the reaction mixture was poured into 150 mL of ice water and made alkaline with saturated sodium hydroxide solution. The resulting precipitate was filtered off and dissolved in 100 mL of dichloromethane. The solution was dried over MgSO₄, and the solvent was removed in vacuum. The crude product was purified by column chromatography, using 1% methanol in dichloromethane as eluent. Recrystallization from ethanol/water (1.5 v/v) yielded 490 mg of white product (2.18 mmol, 61%).

¹H NMR (DMSO-d₆; ppm): δ = 7.66 (dd, 2H), 8.36 (d, 2H), 8.68 (d, 2H).

5.3.3 Syntheses of mononuclear iodotrimethylplatinum(IV) complexes of pyridines

5.3.3.1 Synthesis of [PtMe₃(py)₂I]

The complex [PtMe₃(py)₂I] was synthesized by a slight modification of the route reported.^[37] An excess of pyridine (0.2 mL, 2.48 mmol) was added to a stirred benzene solution (10 mL) of iodotrimethylplatinum (200 mg, 0.54 mmol). The reaction mixture was stirred at room temperature for 30 minutes. The benzene solution was then concentrated to about 2-3 mL and an excess of n-hexane (25 mL) added. The resultant white solid was isolated, washed with n-hexane and dried in *vacuo*. Yield: 252 mg (0.48 mmol, 88%).

¹H NMR (CDCl₃; ppm): $\delta = 1.20$ [s, 3H, PtCH₃ (*trans* to I), ²J_{Pt-H}: 69.6 Hz], 1.50 [s, 6H, PtCH₃ (*trans* to N), ²J_{Pt-H}: 70.3 Hz], 7.35 (t, 2H, ³J_{H-H}: 13.9 Hz), 7.85 (t, 4H, ³J_{H-H}: 15.3 Hz), 8.80 (d, 4H, ³J_{H-H}: 4.9 Hz, ³J_{Pt-H}: 17.3 Hz).

¹H NMR (nitrobenzene-d₅; ppm): $\delta = 1.29$ [s, 3H, PtCH₃ (*trans* to I), ²J_{Pt-H}: 68.9 Hz], 1.70 [s, 6H, PtCH₃ (*trans* to N), ²J_{Pt-H}: 70.4 Hz], 7.37 (t, 2H, ³J_{H-H}: 13.5 Hz), 7.88 (t, 4H, ³J_{H-H}: 15.2 Hz), 8.93 (d, 4H, ³J_{H-H}: 5.5 Hz, ³J_{Pt-H}: 18.0 Hz).

Elemental analysis: C₁₃H₁₉IN₂Pt (525.29 g.mol⁻¹)

Calculated (in %): C: 29.72, H: 3.65, N: 5.33

Experimental (in %): C: 29.72, H: 3.57, N: 5.13

IR (KBr, cm⁻¹): 2959, 2898, 2818 (methyl C-H); 571, 558 (Pt-C)

5.3.3.2 Synthesis of [PtMe₃(4-MePy)₂I]

To a chloroform solution (10 mL) of iodotrimethylplatinum (150 mg, 0.41 mmol), an excess of 4-methylpyridine (0.15 mL, 1.54 mmol) was added and the reactants were stirred at room temperature for 30 minutes. After stirring, the solution was concentrated and 30 mL n-pentane added to precipitate the product as a pale yellow solid. The solid was filtered off, washed with n-pentane and air-dried. Yield: 185 mg (0.33 mmol, 82%).

¹H NMR (CDCl₃; ppm): $\delta = 1.17$ [s, 3H, PtCH₃ (*trans* to I), ²J_{Pt-H}: 70.0 Hz], 1.45 [s, 6H, PtCH₃ (*trans* to N), ²J_{Pt-H}: 70.0 Hz], 2.38 (s, 6H, CH₃), 7.12 (d, 4H, ³J_{H-H}: 6.0 Hz), 8.61 (d, 4H, ³J_{H-H}: 6.4 Hz, ³J_{Pt-H}: 19.0 Hz).

^1H NMR (nitrobenzene- d_5 ; ppm): $\delta = 1.28$ [s, 3H, PtCH₃ (*trans* to I), $^2J_{\text{Pt-H}}$: 69.2 Hz], 1.69 [s, 6H, PtCH₃ (*trans* to N), $^2J_{\text{Pt-H}}$: 70.1 Hz], 2.28 (s, 6H, CH₃), 7.12 (d, 4H, $^3J_{\text{H-H}}$: 5.9 Hz), 8.73 (d, 4H, $^3J_{\text{H-H}}$: 6.4 Hz, $^3J_{\text{H-Pt}}$: 19.1 Hz).

Elemental analysis: C₁₅H₂₃IN₂Pt (553.34 g.mol⁻¹)

Calculated (in %): C: 32.56, H: 4.19, N: 5.06

Experimental (in %): C: 32.40, H: 4.10, N: 4.70

IR (KBr, cm⁻¹): 2951, 2893, 2813 (methyl C-H); 556, 543 (Pt-C)

5.3.3.3 Synthesis of [PtMe₃(3-MePy)₂I]

An amount of 150 mg of iodotrimethylplatinum(IV) (0.41 mmol) was dissolved in chloroform (10 mL) and 0.15 mL of 3-methylpyridine (1.54 mmol) was added to the solution. The reactants were stirred at room temperature for 30 minutes. After stirring, the solution was concentrated and an excess n-pentane (30 mL) added. The resultant pale yellow solid was isolated, washed with n-pentane and air-dried. Yield: 194 mg (0.35 mmol, 86%).

^1H NMR (CDCl₃; ppm): $\delta = 1.18$ [s, 3H, PtCH₃ (*trans* to I), $^2J_{\text{Pt-H}}$: 69.8 Hz], 1.48 [s, 6H, PtCH₃ (*trans* to N), $^2J_{\text{Pt-H}}$: 70.0 Hz], 2.35 (s, 6H, CH₃), 7.20 (dd, 2H, $^3J_{\text{H-H}}$: 13.2 Hz), 7.64 (d, 2H), 8.51 (d, 2H, $^3J_{\text{H-H}}$: 5.7 Hz, $^3J_{\text{Pt-H}}$: 17.8 Hz), 8.67 (s, br, 2H).

Elemental analysis: C₁₅H₂₃IN₂Pt (553.34 g.mol⁻¹)

Calculated (in %): C: 32.56, H: 4.19, N: 5.06

Experimental (in %): C: 32.43, H: 4.10, N: 4.82

IR (KBr, cm⁻¹): 2960, 2899, 2818 (methyl C-H); 571, 556 (Pt-C)

5.3.3.4 Synthesis of [PtMe₃(4-EtPy)₂I]

To a chloroform solution (10 mL) of iodotrimethylplatinum(IV) (150 mg, 0.41 mmol), an excess of 4-ethylpyridine (0.15 mL, 1.32 mmol) was added and the solution stirred for 30 minutes. After stirring, the solution was concentrated to about 2-3 mL and a large excess of n-pentane (20 mL) added to precipitate the complex [PtMe₃(4-EtPy)₂I] as a pale yellow product. The product was filtered, washed several times with n-pentane and air-dried. Yield: 200 mg (0.34 mmol, 84%).

^1H NMR (CDCl_3 ; ppm): $\delta = 1.18$ [s, 3H, PtCH₃ (*trans* to I), $^2J_{\text{Pt-H}}$: 70.2 Hz], 1.45 [s, 6H, PtCH₃ (*trans* to N), $^2J_{\text{Pt-H}}$: 70.1 Hz], 1.27 (t, 6H, CH₃), 2.68 (q, 4H, CH₂), 7.15 (d, 4H, $^3J_{\text{H-H}}$: 6.4 Hz), 8.64 (d, 4H, $^3J_{\text{H-H}}$: 6.4 Hz, $^3J_{\text{Pt-H}}$: 18.9 Hz).

Elemental analysis: C₁₇H₂₇IN₂Pt (581.40 g.mol⁻¹)

Calculated (in %): C: 35.12, H: 4.68, N: 4.82

Experimental (in %): C: 35.14, H: 4.41, N: 4.56

IR (KBr, cm⁻¹): 2964, 2897, 2815 (methyl C-H); 578, 554 (Pt-C)

5.3.3.5 Synthesis of [PtMe₃(3-EtPy)₂I]

0.15 mL of 3-ethylpyridine (1.32 mmol) was added to a stirred solution of iodotrimethylplatinum(IV) (150 mg, 0.41 mmol) in 10 mL of chloroform. The reaction mixture was stirred for an additional 45 minutes. After stirring, the solution was concentrated and 30 mL of n-pentane added. The resultant pale yellow precipitate was filtered off, washed with n-pentane and air-dried. Yield: 162 mg (0.28 mmol, 68%).

^1H NMR (CDCl_3 ; ppm): $\delta = 1.19$ [s, 3H, PtCH₃ (*trans* to I), $^2J_{\text{Pt-H}}$: 69.7 Hz], 1.48 [s, 6H, PtCH₃ (*trans* to N), $^2J_{\text{Pt-H}}$: 70.0 Hz], 1.20 (t, 6H, CH₃), 2.65 (q, 4H, CH₂), 7.23 (dd, 2H), 7.66 (d, 2H), 8.56 (d, 2H, $^3J_{\text{H-H}}$: 5.7 Hz, $^3J_{\text{Pt-H}}$: 17.2 Hz), 8.64 (d, 2H).

Elemental analysis: C₁₇H₂₇IN₂Pt (581.40 g.mol⁻¹)

Calculated (in %): C: 35.12, H: 4.68, N: 4.82

Experimental (in %): C: 35.03, H: 4.52, N: 4.62

IR (KBr, cm⁻¹): 2965, 2894, 2813 (methyl C-H); 578, 560 (Pt-C)

5.3.3.6 Synthesis of [PtMe₃(4-OMePy)₂I]

An amount of 150 mg of iodotrimethylplatinum(IV) (0.41 mmol) was dissolved in chloroform (10 mL) and 0.15 mL of 4-methoxypyridine (1.48 mmol) added to the stirred solution. The reactants were stirred at room temperature for 45 minutes. After stirring, the solution was concentrated to 2-3 mL and an excess of n-pentane (25 mL) added. The resultant pale yellow solid was isolated, washed with n-pentane and air-dried. Yield: 222 mg (0.38 mmol, 93%).

^1H NMR (CDCl_3 ; ppm): $\delta = 1.15$ [s, 3H, PtCH_3 (*trans* to I), $^2J_{\text{Pt-H}}$: 70.2 Hz], 1.42 [s, 6H, PtCH_3 (*trans* to N), $^2J_{\text{Pt-H}}$: 70.0 Hz], 3.89 (s, 6H, OCH_3), 6.80 (d, 4H, $^3J_{\text{H-H}}$: 7.0 Hz), 8.58 (d, 4H, $^3J_{\text{H-H}}$: 7.0 Hz, $^3J_{\text{Pt-H}}$: 19.0 Hz).

^1H NMR (nitrobenzene- d_5 ; ppm): $\delta = 1.29$ [s, 3H, PtCH_3 (*trans* to I), $^2J_{\text{Pt-H}}$: 69.4 Hz], 1.69 [s, 6H, PtCH_3 (*trans* to N), $^2J_{\text{Pt-H}}$: 70.2 Hz], 3.81 (s, 6H, OCH_3), 6.79 (d, 4H, $^3J_{\text{H-H}}$: 6.9 Hz), 8.70 (d, 4H, $^3J_{\text{H-H}}$: 6.8 Hz, $^3J_{\text{H-Pt}}$: 19.1 Hz).

Elemental analysis: $\text{C}_{15}\text{H}_{23}\text{IN}_2\text{O}_2\text{Pt}$ (585.34 $\text{g}\cdot\text{mol}^{-1}$)

Calculated (in %): C: 30.78, H: 3.96, N: 4.79

Experimental (in %): C: 30.82, H: 3.97, N: 4.60

IR (KBr, cm^{-1}): 2961, 2894, 2815 (methyl C-H); 569, 540 (Pt-C)

5.3.3.7 Synthesis of $[\text{PtMe}_3(3\text{-OMePy})_2\text{I}]$

To a chloroform solution (10 mL) of iodotrimethylplatinum(IV) (150 mg, 0.41 mmol), an excess of 3-methoxypyridine (0.15 mL, 1.48 mmol) was added and the solution stirred for 45 minutes. The solution was then concentrated and 25 mL *n*-pentane added to precipitate the complex $[\text{PtMe}_3(3\text{-OMePy})_2\text{I}]$ as a pale yellow solid. The solid was filtered, washed with *n*-pentane and air-dried. Yield: 203 mg (0.35 mmol, 85%).

^1H NMR (CDCl_3 ; ppm): $\delta = 1.20$ [s, 3H, PtCH_3 (*trans* to I), $^2J_{\text{Pt-H}}$: 69.7 Hz], 1.49 [s, 6H, PtCH_3 (*trans* to N), $^2J_{\text{Pt-H}}$: 70.4 Hz], 3.84 (s, 6H, OCH_3), 7.24 (dd, 2H), 7.33 (d, 2H), 8.30 (d, 2H, $^3J_{\text{H-H}}$: 6.1 Hz, $^3J_{\text{Pt-H}}$: 16.9 Hz), 8.61 (d, 2H).

Elemental analysis: $\text{C}_{15}\text{H}_{23}\text{IN}_2\text{O}_2\text{Pt}$ (585.34 $\text{g}\cdot\text{mol}^{-1}$)

Calculated (in %): C: 30.78, H: 3.96, N: 4.79

Experimental (in %): C: 30.59, H: 3.86, N: 4.50

IR (KBr, cm^{-1}): 2960, 2899, 2817 (methyl C-H); 564 (Pt-C)

5.3.3.8 Synthesis of [PtMe₃(4-DMAP)₂I]

The complex iodotrimethylplatinum(IV) (150 mg, 0.41 mmol) and 4-dimethylaminopyridine (100 mg, 0.82 mmol) were stirred in chloroform (10 mL) for 30 minutes. The resulting solution was then concentrated and 30 mL n-pentane added. The pale yellow solid which formed was isolated, washed with n-pentane and air-dried. Yield: 210 mg (0.34 mmol, 84%).

¹H NMR (CDCl₃; ppm): δ = 1.14 [s, 3H, PtCH₃ (*trans* to I), ²J_{Pt-H}: 71.5 Hz], 1.35 [s, 6H, PtCH₃ (*trans* to N), ²J_{Pt-H}: 69.3 Hz], 3.02 [s, 12H, N(CH₃)₂], 6.40 (d, 4H, ³J_{H-H}: 7.2 Hz), 8.29 (d, 4H, ³J_{H-H}: 7.2 Hz, ³J_{Pt-H}: 19.6 Hz).

¹H NMR (nitrobenzene-d₅; ppm): δ = 1.33 [s, 3H, PtCH₃ (*trans* to I), ²J_{Pt-H}: 70.6 Hz], 1.70 [s, 6H, PtCH₃ (*trans* to N), ²J_{Pt-H}: 69.3 Hz], 2.89 [s, 12H, N(CH₃)₂], 6.28 (d, 4H, ³J_{H-H}: 7.0 Hz), 8.38 (d, 4H, ³J_{H-H}: 6.9 Hz, ³J_{H-Pt}: 19.4 Hz).

Elemental analysis: C₁₇H₂₉IN₄Pt (611.43 g.mol⁻¹)

Calculated (in %): C: 33.39, H: 4.78, N: 9.16

Experimental (in %): C: 33.55, H: 4.49, N: 8.96

IR (KBr, cm⁻¹): 2950, 2894, 2811 (methyl C-H); 572, 529 (Pt-C)

5.3.3.9 Synthesis of [PtMe₃(4-^tBuPy)₂I]

0.16 mL of 4-^tbutylpyridine (1.09 mmol) was added to a stirred chloroform solution (15 mL) of iodotrimethylplatinum(IV) (150 mg, 0.41 mmol). The reaction mixture was stirred for 45 minutes. After stirring, the chloroform solution was concentrated and an excess of n-pentane (30 mL) added to precipitate the white solid. The solid was separated, washed with n-pentane and dried in *vacuo*. Yield: 205 mg (0.32 mmol, 79%).

¹H NMR (CDCl₃; ppm): δ = 1.19 [s, 3H, PtCH₃ (*trans* to I), ²J_{Pt-H}: 70.1 Hz], 1.45 [s, 6H, PtCH₃ (*trans* to N), ²J_{Pt-H}: 69.9 Hz], 1.33 [s, 18H, C(CH₃)₃], 7.30 (d, 4H, ³J_{H-H}: 6.7 Hz), 8.66 (d, 4H, ³J_{H-H}: 6.5 Hz, ³J_{Pt-H}: 19.0 Hz).

Elemental analysis: C₂₁H₃₅IN₂Pt (637.5 g.mol⁻¹)

Calculated (in %): C: 39.56, H: 5.53, N: 4.39

Experimental (in %): C: 39.31, H: 5.37, N: 4.28

IR (KBr, cm⁻¹): 2963, 2897, 2816 (methyl C-H); 571, 544 (Pt-C)

5.3.3.10 Synthesis of [PtMe₃(4-CNPy)₂I]

250 mg of 4-cyanopyridine (2.40 mmol) and iodotrimethylplatinum(IV) (150 mg, 0.41 mmol) were dissolved in chloroform (10 mL) and stirred for 35 minutes. The solution was then concentrated and excess n-pentane (30 mL) added. The yellow solid which formed was isolated, washed with n-pentane and air-dried. Yield: 204 mg (0.35 mmol, 87%).

¹H NMR (CDCl₃; ppm): δ = 1.18 [s, 3H, PtCH₃ (*trans* to I), ²J_{Pt-H}: 67.3 Hz], 1.53 [s, 6H, PtCH₃ (*trans* to N), ²J_{Pt-H}: 71.2 Hz], 7.64 (d, 4H, ³J_{Pt-H}: 6.5 Hz), 9.04 [d, 4H, ³J_{H-H}: 6.4 Hz, ³J_{Pt-H}: 17.9 Hz].

Elemental analysis: C₁₅H₁₇IN₄Pt (575.30 g.mol⁻¹)

Calculated (in %): C: 31.32, H: 2.98, N: 9.74

Experimental (in %): C: 31.25, H: 2.88, N: 9.55

IR (KBr, cm⁻¹): 2962, 2899, 2816 (methyl C-H); 563 (Pt-C)

5.3.3.11 Synthesis of [PtMe₃(3-BrPy)₂I]

An excess of 3-bromopyridine (0.2 mL, 2.08 mmol) was added to a solution of iodotrimethylplatinum(IV) (150 mg, 0.41 mmol) in chloroform (10 mL). The reactants were stirred for 45 minutes, after which the volume of the solution was reduced to 3-4 mL. Addition of n-pentane (30 mL) produced a pale yellow product, which was filtered, washed with n-pentane and air-dried. Yield: 250 mg (0.37 mmol, 90%).

¹H NMR (CDCl₃; ppm): δ = 1.17 [s, 3H, PtCH₃ (*trans* to I), ²J_{Pt-H}: 68.3 Hz], 1.51 [s, 6H, PtCH₃ (*trans* to N), ²J_{Pt-H}: 71.1 Hz], 7.28 (dd, 2H), 8.01 (d, 2H), 8.79 (d, 2H), 8.83 (d, 2H).

Elemental analysis: C₁₃H₁₇Br₂IN₂Pt (683.08 g.mol⁻¹)

Calculated (in %): C: 22.86, H: 2.51, N: 4.10

Experimental (in %): C: 22.59, H: 2.45, N: 3.90

IR (KBr, cm⁻¹): 2959, 2893, 2815 (methyl C-H); 575, 554 (Pt-C)

5.3.3.12 Synthesis of [PtMe₃(3-ClPy)₂I]

To a chloroform solution (10 mL) of iodotrimethylplatinum(IV) (150 mg, 0.41 mmol), an excess of 3-chloropyridine (0.2 mL, 2.10 mmol) was added and the resulting solution was stirred for 45 minutes. After stirring, the solution was concentrated to 3-4 mL and large excess of n-pentane (35 mL) was added to precipitate the complex as a pale yellow product. The product was filtered, washed several times with n-pentane and air-dried. Yield: 223 mg (0.375 mmol, 92%).

¹H NMR (CDCl₃; ppm): δ = 1.18 [s, 3H, PtCH₃ (*trans* to I), ²J_{Pt-H}: 68.3 Hz], 1.52 [s, 6H, PtCH₃ (*trans* to N), ²J_{Pt-H}: 71.1 Hz], 7.34 (dd, 2H), 7.87 (d, 2H), 8.75 (d, 2H), 8.77 (d, 2H).

Elemental analysis: C₁₃H₁₇Cl₂IN₂Pt (594.18 g.mol⁻¹)

Calculated (in %): C: 26.28, H: 2.88, N: 4.71

Experimental (in %): C: 25.96, H: 2.72, N: 4.52

IR (KBr, cm⁻¹): 2962, 2899, 2815 (methyl C-H); 572, 554 (Pt-C).

5.3.4 Syntheses of iodotrimethylplatinum(IV) complexes of 2,2'-bipyridines

5.3.4.1 Synthesis of [PtMe₃(bipy)I]

The complex [PtMe₃(bipy)I] was synthesized according to the method of Clegg *et al.*^[39] A benzene solution (6 mL) of iodotrimethylplatinum(IV) (200 mg, 0.54 mmol) was mixed with a benzene solution (6 mL) of 2,2'-bipyridine (85 mg, 0.54 mmol). The solution was filtered immediately, and the filtrate allowed to stand. The pale yellow crystals that formed were filtered, washed with n-hexane and air-dried. Yield: 255 mg (0.49 mmol, 89%).

¹H NMR (CDCl₃; ppm): δ = 0.64 [s, 3H, PtCH₃ (*trans* to I), ²J_{Pt-H}: 73.1 Hz], 1.56 [s, 6H, PtCH₃ (*trans* to N), ²J_{Pt-H}: 70.5 Hz], 7.64 (m, 2H), 8.07 (m, 2H), 8.23 (d, 2H), 9.02 (d, 2H, ³J_{H-H}: 6.1 Hz, ³J_{Pt-H}: 17.8 Hz).

¹H NMR (nitrobenzene-d₅; ppm): δ = 0.78 [s, 3H, PtCH₃ (*trans* to I), ²J_{Pt-H}: 72.6 Hz], 1.81 [s, 6H, PtCH₃ (*trans* to N), ²J_{Pt-H}: 70.5 Hz], 7.67 (m, 2H), 8.08 (m, 2H), 8.33 (d, 2H), 9.08 (d, 2H, ³J_{H-H}: 6.4 Hz, ³J_{Pt-H}: 18.5 Hz).

Elemental analysis: $C_{13}H_{17}IN_2Pt$ (523.28 g.mol⁻¹)

Calculated (in %): C: 29.84, H: 3.27, N: 5.35

Experimental (in %): C: 30.05, H: 3.46, N: 5.42

IR (KBr, cm⁻¹): 2957, 2892, 2811 (methyl C-H); 573, 557 (Pt-C)

EI-MS: m/z 395 [M-I]⁺

5.3.4.2 Synthesis of [PtMe₃(4Me-bipy)I]

Iodotrimethylplatinum(IV) (200 mg, 0.54 mmol) was dissolved in benzene (15 mL) and 4,4'-dimethyl-2,2'-bipyridine (100 mg, 0.54 mmol) added to the stirred solution. The reactants were stirred for another 1.5 h. The resulting pale yellow solid was filtered off, washed with n-hexane and dried under vacuum. Yield: 258 mg (0.47 mmol, 86%).

¹H NMR (CDCl₃; ppm): δ = 0.63 [s, 3H, PtCH₃ (*trans* to I), ²J_{Pt-H}: 73.5 Hz], 1.51 [s, 6H, PtCH₃ (*trans* to N), ²J_{Pt-H}: 70.3 Hz], 2.57 (s, 6H, CH₃), 7.42 (d, 2H), 8.01 (s, br, 2H), 8.82 (d, 2H, ³J_{H-H}: 5.8 Hz, ³J_{Pt-H}: 19.4 Hz).

¹H NMR (nitrobenzene-d₅; ppm): δ = 0.81 [s, 3H, PtCH₃ (*trans* to I), ²J_{Pt-H}: 72.9 Hz], 1.78 [s, 6H, PtCH₃ (*trans* to N), ²J_{Pt-H}: 70.3 Hz], 2.52 (s, 6H, CH₃), 7.42 (d, 2H), 8.05 (s, br, 2H), 8.87 (d, 2H, ³J_{H-H}: 5.6 Hz, ³J_{Pt-H}: 19.6 Hz).

Elemental analysis: $C_{15}H_{21}IN_2Pt$ (551.33 g.mol⁻¹)

Calculated (in %): C: 32.68, H: 3.84, N: 5.08

Experimental (in %): C: 32.46, H: 3.97, N: 4.98

IR (KBr, cm⁻¹): 2952, 2890, 2809 (methyl C-H); 556, 521 (Pt-C)

EI-MS: m/z 423 [M-I]⁺

5.3.4.3 Synthesis of [PtMe₃(5Me-bipy)I]

An amount of 100 mg of 5,5'-dimethyl-2,2'-bipyridine (0.54 mmol) was added to a stirred solution of iodotrimethylplatinum(IV) (200 mg, 0.54 mmol) in benzene (14 mL) for 1.5 h. The resulting pale yellow solid was filtered off, washed with n-hexane and dried in vacuum. Yield: 270 mg (0.49 mmol, 90%).

^1H NMR (CDCl_3 ; ppm): $\delta = 0.62$ [s, 3H, PtCH_3 (*trans* to I), $^2J_{\text{Pt-H}}$: 73.3 Hz], 1.54 [s, 6H, PtCH_3 (*trans* to N), $^2J_{\text{Pt-H}}$: 70.4 Hz], 2.51 (s, 6H, CH_3), 7.81 (d, 2H), 8.04 (s, 2H), 8.77 (d, 2H, $^3J_{\text{H-H}}$: 1.1 Hz, $^3J_{\text{Pt-H}}$: 12.7 Hz).

^1H NMR (nitrobenzene- d_5 ; ppm): δ 0.82 [s, 3H, PtCH_3 (*trans* to I), $^2J_{\text{Pt-H}}$: 72.7 Hz], 1.83 [s, 6H, PtCH_3 (*trans* to N), $^2J_{\text{Pt-H}}$: 70.3 Hz], 2.35 (s, 6H, CH_3), 7.80 (d, 2H), 8.13 (2H), 8.93 (s, br, 2H).

Elemental analysis: $\text{C}_{15}\text{H}_{21}\text{IN}_2\text{Pt}$ (551.33 $\text{g}\cdot\text{mol}^{-1}$)

Calculated (in %): C: 32.68, H: 3.84, N: 5.08

Experimental (in %): C: 32.49, H: 3.92, N: 4.89

IR (KBr, cm^{-1}): 2963, 2897, 2812 (methyl C-H); 558, 537 (Pt-C)

EI-MS: m/z 423 $[\text{M-I}]^+$

5.3.4.4 Synthesis of $[\text{PtMe}_3(\text{OMe-bipy})\text{I}]$

To a benzene solution (10 mL) of iodotrimethylplatinum(IV) (200 mg, 0.54 mmol), the ligand 4,4'-dimethoxy-2,2'-bipyridine (120 mg, 0.56 mmol) was added and the solution was stirred at room temperature for 2 h. The pale yellow solid formed was then filtered off, washed with benzene and dried under vacuum. Yield: 267 mg (0.46 mmol, 84%).

^1H NMR (CDCl_3 ; ppm): $\delta = 0.65$ [s, 3H, PtCH_3 (*trans* to I), $^2J_{\text{Pt-H}}$: 73.7 Hz], 1.48 [s, 6H, PtCH_3 (*trans* to N), $^2J_{\text{Pt-H}}$: 70.2 Hz], 4.02 (s, 6H, OCH_3), 7.08 (dd, 2H), 7.58 (d, 2H), 8.77 (d, 2H, $^3J_{\text{H-H}}$: 6.4 Hz, $^3J_{\text{Pt-H}}$: 19.8 Hz).

^1H NMR (nitrobenzene- d_5 ; ppm): δ 0.86 [s, 3H, PtCH_3 (*trans* to I), $^2J_{\text{Pt-H}}$: 73.0 Hz], 1.77 [s, 6H, PtCH_3 (*trans* to N), $^2J_{\text{Pt-H}}$: 70.5 Hz], 3.96 (s, 6H, OCH_3), 7.09 (d, 2H), 7.61 (d, 2H), 8.83 (d, 2H, $^3J_{\text{H-H}}$: 6.4 Hz, $^3J_{\text{Pt-H}}$: 19.9 Hz).

Elemental analysis: $\text{C}_{15}\text{H}_{21}\text{IN}_2\text{O}_2\text{Pt}$ (583.33 $\text{g}\cdot\text{mol}^{-1}$)

Calculated (in %): C: 30.89, H: 3.63, N: 4.80

Experimental (in %): C: 30.78, H: 3.76, N: 4.72

IR (KBr, cm^{-1}): 2945, 2892, 2811 (methyl C-H); 575, 522 (Pt-C)

EI-MS: m/z 455 $[\text{M-I}]^+$

5.3.4.5 Synthesis of [PtMe₃(Me₂N-bipy)I]

132 mg of 4,4'-bis(dimethylamino)-2,2'-bipyridine (0.55 mmol) was added to a stirred solution of iodotrimethylplatinum (200 mg, 0.54 mmol) in benzene (15 mL) and the reactants were stirred at room temperature for 1 h, after which the resultant pale yellow solid was isolated, washed in benzene and dried in vacuum. Yield: 286 mg (0.47 mmol, 87%).

¹H NMR (CDCl₃; ppm): δ = 0.68 [s, 3H, PtCH₃ (*trans* to I), ²J_{Pt-H}: 74.9 Hz], 1.40 [s, 6H, PtCH₃ (*trans* to N), ²J_{Pt-H}: 69.6 Hz], 3.16 [s, 12H, N(CH₃)₂], 6.68 (dd, 2H), 7.14 (d, 2H), 8.46 (d, 2H, ³J_{H-H}: 6.6 Hz, ³J_{Pt-H}: 20.0 Hz).

¹H NMR (nitrobenzene-d₅; ppm): δ = 0.97 [s, 3H, PtCH₃ (*trans* to I), ²J_{Pt-H}: 74.2 Hz], 1.76 [s, 6H, PtCH₃ (*trans* to N), ²J_{Pt-H}: 69.5 Hz], 3.04 [s, 12H, N(CH₃)₂], 6.58 (dd, 2H), 7.16 (d, 2H), 8.50 (d, 2H, ³J_{H-H}: 6.6 Hz, ³J_{Pt-H}: 20.0 Hz).

Elemental analysis: C₁₇H₂₇IN₄Pt (609.42 g.mol⁻¹)

Calculated (in %): C: 33.51, H: 4.47, N: 9.19

Experimental (in %): C: 33.66, H: 4.29, N: 8.96

IR (KBr, cm⁻¹): 2941, 2890, 2811 (methyl C-H); 562 (Pt-C)

EI-MS: m/z 481 [M-I]⁺

5.3.4.6 Synthesis of [PMe₃(Cl-bipy)I]

To a benzene solution (10 mL) of iodotrimethylplatinum (200 mg, 0.54 mmol), 4,4'-dichloro-2,2'-bipyridine (125 mg, 0.56 mmol) in benzene (6 mL) was added and stirred for 2 h. The yellow solid which formed was isolated, washed with n-hexane and dried in vacuum. Yield: 297 mg (0.50 mmol, 92%).

¹H NMR (CDCl₃; ppm): δ = 0.62 [s, 3H, PtCH₃ (*trans* to I), ²J_{Pt-H}: 72.3 Hz], 1.56 [s, 6H, PtCH₃ (*trans* to N), ²J_{Pt-H}: 71.2 Hz], 7.66 (dd, 2H), 8.18 (d, 2H), 8.91 (d, 2H, ³J_{H-H}: 6.0 Hz, ³J_{Pt-H}: 19.2 Hz).

^1H NMR (nitrobenzene- d_5 ; ppm): δ 0.83 [s, 3H, PtCH₃ (*trans* to I), $^2J_{\text{Pt-H}}$: 72.1 Hz], 1.80 [s, 6H, PtCH₃ (*trans* to N), $^2J_{\text{Pt-H}}$: 71.3 Hz], 7.66 (2H), 8.25 (d, 2H), 9.00 (d, 2H, $^3J_{\text{H-H}}$: 6.0 Hz, $^3J_{\text{Pt-H}}$: 13.5 Hz).

Elemental analysis: C₁₃H₁₅Cl₂IN₂Pt (592.16 g.mol⁻¹)

Calculated (in %): C: 26.37, H: 2.55, N: 4.73

Experimental (in %): C: 26.55, H: 2.46, N: 4.42

IR (KBr, cm⁻¹): 2952, 2891, 2808 (methyl C-H); 562, 533 (Pt-C)

EI-MS: m/z 462 [M-I]⁺

5.4 Crystallography

The single crystal X-ray diffraction studies for the platinum(IV) complexes were performed with the following equipment:

- A STOE IPDS diffractometer equipped with a low temperature system (Karlsruher Glastechnisches Werk), a graphite monochromator and IP detector system. MoK α radiation ($\lambda = 0.71069 \text{ \AA}$) was used. The frames were integrated with the *STOE* software package.^[95] Multi-scan absorption corrections were applied.^[96]
- A smart CCD Bruker-AXS diffractometer equipped with a graphite monochromator and a CCD detector. MoK α radiation ($\lambda = 0.71073 \text{ \AA}$) was used. Cell refinement and data reduction were carried out with the *SAINT* software.^[97] The collected reflections were corrected for absorption effects using multi-scan *SADABS* programme.^[98]

The structures were solved using the programme *SHELXS-97*^[99] and refined by full-matrix least squares on F^2 with *SHELXL-97* programme.^[99] All the non-hydrogen atoms were refined with anisotropic thermal parameters. Hydrogen atoms were introduced in proper positions with isotropic thermal parameters using the 'riding model'. *Mercury*^[100] and *DIAMOND*^[101] programmes were used for structure drawing.

Table 5.4.1 Crystal data and structure refinement for [PtMe₃(4-DMAP)₂I]

Empirical formula	C ₁₇ H ₂₉ IN ₄ Pt	
Formula weight	611.43	
Temperature	133(2) K	
Wavelength	0.71073 Å	
Diffractometer type	SMART CCD Bruker AXS	
Crystal size	0.35 x 0.13 x 0.11 mm ³	
Crystal colour and shape	yellow, needle	
Crystal system	Monoclinic	
Space group	P2 ₁ /n	
Unit cell dimensions	a = 7.7058(13) Å	α = 90°
	b = 15.118(3) Å	β = 97.363(3)°
	c = 17.171(3) Å	γ = 90°
Volume	1983.8(6) Å ³	
Z	4	
Density (calculated)	2.047 Mg/m ³	
Absorption coefficient	8.634 mm ⁻¹	
F(000)	1160	
Theta range for data collection	1.80 to 30.55°	
Index ranges	-11 ≤ h ≤ 10, -21 ≤ k ≤ 20, -16 ≤ l ≤ 24	
Reflections collected	32045	
Independent reflections	6040 [R(int) = 0.0212]	
Completeness to theta = 30.55°	0.993	
Absorption correction	multi-scan	
Max. and min. transmission	0.746 and 0.403	
Refinement method	Full-matrix least-squares on F ²	
Data / restraints / parameters	6040 / 0 / 215	
Goodness-of-fit on F ²	1.052	
Final R indices [I > 2σ(I)]	R1 = 0.0170, wR2 = 0.0395	
R indices (all data)	R1 = 0.0207, wR2 = 0.0408	
Largest diff. peak and hole	1.985 and -0.470 e.Å ⁻³	

Table 5.4.2 Crystal data and structure refinement for [PtMe₃(3-BrPy)₂I]

Empirical formula	C ₁₃ H ₁₇ Br ₂ IN ₂ Pt	
Formula weight	683.08	
Temperature	193(2) K	
Wavelength	0.71073 Å	
Diffractometer type	STOE IPDS	
Crystal size	0.21 x 0.10 x 0.08 mm ³	
Crystal colour and shape	yellow, needle	
Crystal system	Monoclinic	
Space group	P2 ₁ /n	
Unit cell dimensions	a = 10.3932(14) Å	α = 90°
	b = 14.1705(14) Å	β = 104.290(16)°
	c = 12.1056(17) Å	γ = 90°
Volume	1727.7(4) Å ³	
Z	4	
Density (calculated)	2.626 Mg/m ³	
Absorption coefficient	14.523 mm ⁻¹	
F(000)	1240	
Theta range for data collection	2.48 to 28.14°	
Index ranges	-13 ≤ h ≤ 13, -18 ≤ k ≤ 17, -15 ≤ l ≤ 16	
Reflections collected	15116	
Independent reflections	4158 [R(int) = 0.0826]	
Completeness to theta = 28.14°	0.983	
Absorption correction	multi-scan	
Max. and min. transmission	0.3329 and 0.1295	
Refinement method	Full-matrix least-squares on F ²	
Data / restraints / parameters	4158 / 0 / 176	
Goodness-of-fit on F ²	0.914	
Final R indices [I > 2σ(I)]	R1 = 0.0485, wR2 = 0.1153	
R indices (all data)	R1 = 0.0724, wR2 = 0.1255	
Largest diff. peak and hole	3.274 and -2.592 e.Å ⁻³	

Table 5.4.3 Crystal data and structure refinement for [PtMe₃(4-MePy)₂I]

Empirical formula	C ₁₅ H ₂₃ IN ₂ Pt	
Formula weight	553.34	
Temperature	193(2) K	
Wavelength	0.71073 Å	
Diffractometer type	STOE IPDS	
Crystal size	0.16 x 0.16 x 0.16 mm ³	
Crystal colour and shape	yellow, cube	
Crystal system	Monoclinic	
Space group	P2 ₁ /n	
Unit cell dimensions	a = 11.2077(15) Å	α = 90°
	b = 12.9162(13) Å	β = 98.822(16)°
	c = 12.2592(16) Å	γ = 90°
Volume	1753.7(4) Å ³	
Z	4	
Density (calculated)	2.096 Mg/m ³	
Absorption coefficient	9.752 mm ⁻¹	
F(000)	1032	
Theta range for data collection	3.11 to 28.08°	
Index ranges	-14 ≤ h ≤ 14, -17 ≤ k ≤ 17, -16 ≤ l ≤ 16	
Reflections collected	15855	
Independent reflections	3952 [R(int) = 0.0612]	
Completeness to theta = 28.08°	0.924	
Absorption correction	multi-scan	
Max. and min. transmission	0.2310 and 0.1861	
Refinement method	Full-matrix least-squares on F ²	
Data / restraints / parameters	3952 / 0 / 178	
Goodness-of-fit on F ²	0.939	
Final R indices [I > 2σ(I)]	R1 = 0.0360, wR2 = 0.0814	
R indices (all data)	R1 = 0.0582, wR2 = 0.0881	
Largest diff. peak and hole	1.981 and -2.500 e.Å ⁻³	

Table 5.4.4 Crystal data and structure refinement for [PtMe₃(4-EtPy)₂I]

Empirical formula	C ₁₇ H ₂₇ IN ₂ Pt	
Formula weight	581.40	
Temperature	133(2) K	
Wavelength	0.71073 Å	
Diffractometer type	SMART CCD Bruker AXS	
Crystal size	0.41 x 0.21 x 0.18 mm ³	
Crystal colour and shape	yellow, prism	
Crystal system	Monoclinic	
Space group	P2 ₁ /c	
Unit cell dimensions	a = 12.0156(17) Å	α = 90°
	b = 12.0304(17) Å	β = 102.370(3)°
	c = 13.4566(19) Å	γ = 90°
Volume	1900.0(5) Å ³	
Z	4	
Density (calculated)	2.032 Mg/m ³	
Absorption coefficient	9.007 mm ⁻¹	
F(000)	1096	
Theta range for data collection	1.74 to 30.58°	
Index ranges	-17 ≤ h ≤ 15, -17 ≤ k ≤ 16, -19 ≤ l ≤ 19	
Reflections collected	30876	
Independent reflections	5837 [R(int) = 0.0201]	
Completeness to theta = 30.58°	0.999	
Absorption correction	multi-scan	
Max. and min. transmission	0.433 and 0.238	
Refinement method	Full-matrix least-squares on F ²	
Data / restraints / parameters	5837 / 0 / 195	
Goodness-of-fit on F ²	1.102	
Final R indices [I > 2σ(I)]	R1 = 0.0150, wR2 = 0.0358	
R indices (all data)	R1 = 0.0187, wR2 = 0.0373	
Largest diff. peak and hole	0.552 and -1.457 e.Å ⁻³	

Table 5.4.5 Crystal data and structure refinement for [PtMe₃(4-OMePy)₂I]

Empirical formula	C ₁₅ H ₂₃ IN ₂ O ₂ Pt	
Formula weight	585.34	
Temperature	133(2) K	
Wavelength	0.71073 Å	
Diffractometer type	SMART CCD Bruker AXS	
Crystal size	0.28 x 0.12 x 0.04 mm ³	
Crystal colour and shape	yellow, needle	
Crystal system	Orthorhombic	
Space group	Pbca	
Unit cell dimensions	a = 17.304(3) Å	α = 90°
	b = 8.2179(14) Å	β = 90°
	c = 25.158(4) Å	γ = 90°
Volume	3577.4(11) Å ³	
Z	8	
Density (calculated)	2.174 Mg/m ³	
Absorption coefficient	9.576 mm ⁻¹	
F(000)	2192	
Theta range for data collection	2.00 to 30.57°	
Index ranges	-24 ≤ h ≤ 24, -11 ≤ k ≤ 9, -35 ≤ l ≤ 35	
Reflections collected	52384	
Independent reflections	5485 [R(int) = 0.0439]	
Completeness to theta = 30.57°	0.999	
Absorption correction	multi-scan	
Max. and min. transmission	0.746 and 0.416	
Refinement method	Full-matrix least-squares on F ²	
Data / restraints / parameters	5485 / 0 / 195	
Goodness-of-fit on F ²	1.130	
Final R indices [I > 2σ(I)]	R1 = 0.0352, wR2 = 0.0825	
R indices (all data)	R1 = 0.0439, wR2 = 0.0862	
Largest diff. peak and hole	2.927 and -1.818 e.Å ⁻³	

Table 5.4.6 Crystal data and structure refinement for [PtMe₃(3-OMePy)₂I]

Empirical formula	C ₁₅ H ₂₃ IN ₂ O ₂ Pt	
Formula weight	585.34	
Temperature	193(2) K	
Wavelength	0.71073 Å	
Diffractometer type	STOE IPDS	
Crystal size	0.53 x 0.11 x 0.08 mm ³	
Crystal colour and shape	yellow, needle	
Crystal system	Monoclinic	
Space group	P2 ₁ /a	
Unit cell dimensions	a = 14.7578(15) Å	α = 90°
	b = 7.6872(9) Å	β = 113.803(11)°
	c = 17.2104(18) Å	γ = 90°
Volume	1786.4(3) Å ³	
Z	4	
Density (calculated)	2.176 Mg/m ³	
Absorption coefficient	9.588 mm ⁻¹	
F(000)	1096	
Theta range for data collection	2.76 to 28.10°	
Index ranges	-19 ≤ h ≤ 19, -10 ≤ k ≤ 10, -22 ≤ l ≤ 22	
Reflections collected	15226	
Independent reflections	4317 [R(int) = 0.0586]	
Completeness to theta = 28.10°	0.992	
Absorption correction	multi-scan	
Max. and min. transmission	0.5049 and 0.1635	
Refinement method	Full-matrix least-squares on F ²	
Data / restraints / parameters	4317 / 0 / 196	
Goodness-of-fit on F ²	0.986	
Final R indices [I > 2σ(I)]	R1 = 0.0320, wR2 = 0.0920	
R indices (all data)	R1 = 0.0389, wR2 = 0.0952	
Largest diff. peak and hole	2.755 and -1.636 e.Å ⁻³	

Table 5.4.7 Crystal data and structure refinement for *trans*-[PtMe₃(py)I]₂

Empirical formula	C ₁₆ H ₂₈ I ₂ N ₂ Pt ₂	
Formula weight	892.38	
Temperature	193(2) K	
Wavelength	0.71073 Å	
Diffractometer type	STOE IPDS	
Crystal size	0.48 x 0.40 x 0.16 mm ³	
Crystal colour and shape	yellow, prism	
Crystal system	Monoclinic	
Space group	C2/c	
Unit cell dimensions	a = 17.433(2) Å	α = 90°
	b = 10.0346(9) Å	β = 118.295(15)°
	c = 13.7500(19) Å	γ = 90°
Volume	2118.0(5) Å ³	
Z	4	
Density (calculated)	2.799 Mg/m ³	
Absorption coefficient	16.110 mm ⁻¹	
F(000)	1600	
Theta range for data collection	3.60 to 28.12°	
Index ranges	-21 ≤ h ≤ 23, -13 ≤ k ≤ 12, -18 ≤ l ≤ 18	
Reflections collected	9143	
Independent reflections	2536 [R(int) = 0.0686]	
Completeness to theta = 28.12°	0.975	
Absorption correction	multi-scan	
Max. and min. transmission	0.1160 and 0.0285	
Refinement method	Full-matrix least-squares on F ²	
Data / restraints / parameters	2536 / 0 / 104	
Goodness-of-fit on F ²	1.044	
Final R indices [I > 2σ(I)]	R1 = 0.0437, wR2 = 0.1068	
R indices (all data)	R1 = 0.0479, wR2 = 0.1092	
Largest diff. peak and hole	3.055 and -3.466 e.Å ⁻³	

Table 5.4.8 Crystal data and structure refinement for *cis*-[PtMe₃(4-EtPy)I]₂

Empirical formula	C ₂₀ H ₃₆ I ₂ N ₂ Pt ₂	
Formula weight	948.49	
Temperature	193(2) K	
Wavelength	0.71073 Å	
Diffractometer type	STOE IPDS	
Crystal size	0.34 x 0.32 x 0.16 mm ³	
Crystal colour and shape	yellow, plate	
Crystal system	Orthorhombic	
Space group	Pnam	
Unit cell dimensions	a = 10.7003(10) Å	α = 90°
	b = 12.7871(9) Å	β = 90°
	c = 18.4091(17) Å	γ = 90°
Volume	2518.8(4) Å ³	
Z	4	
Density (calculated)	2.501 Mg/m ³	
Absorption coefficient	13.554 mm ⁻¹	
F(000)	1728	
Theta range for data collection	3.33 to 27.03°	
Index ranges	-13 ≤ h ≤ 13, -15 ≤ k ≤ 15, -23 ≤ l ≤ 23	
Reflections collected	19833	
Independent reflections	2719 [R(int) = 0.0679]	
Completeness to theta = 27.03°	0.953	
Absorption correction	multi-scan	
Max. and min. transmission	0.1480 and 0.0562	
Refinement method	Full-matrix least-squares on F ²	
Data / restraints / parameters	2719 / 0 / 126	
Goodness-of-fit on F ²	1.102	
Final R indices [I > 2σ(I)]	R1 = 0.0485, wR2 = 0.1262	
R indices (all data)	R1 = 0.0535, wR2 = 0.1328	
Largest diff. peak and hole	2.890 and -4.746 e.Å ⁻³	

Table 5.4.9 Crystal data and structure refinement for *cis*-[PtMe₃(4-OMePy)I]₂

Empirical formula	C ₁₈ H ₃₂ I ₂ N ₂ O ₂ Pt ₂	
Formula weight	952.44	
Temperature	193(2) K	
Wavelength	0.71073 Å	
Diffractometer type	STOE IPDS	
Crystal size	0.24 x 0.23 x 0.18 mm ³	
Crystal colour and shape	yellow, plate	
Crystal system	Monoclinic	
Space group	P2 ₁ /n	
Unit cell dimensions	a = 10.4070(9) Å	α = 90°
	b = 11.7649(6) Å	β = 98.377(10)°
	c = 20.7823(17) Å	γ = 90°
Volume	2517.4(3) Å ³	
Z	4	
Density (calculated)	2.513 Mg/m ³	
Absorption coefficient	13.568 mm ⁻¹	
F(000)	1728	
Theta range for data collection	2.34 to 25.97°	
Index ranges	-12 ≤ h ≤ 12, -14 ≤ k ≤ 13, -25 ≤ l ≤ 25	
Reflections collected	18359	
Independent reflections	4928 [R(int) = 0.0548]	
Completeness to theta = 25.97°	0.995	
Absorption correction	multi-scan	
Max. and min. transmission	0.1115 and 0.0529	
Refinement method	Full-matrix least-squares on F ²	
Data / restraints / parameters	4928 / 0 / 245	
Goodness-of-fit on F ²	0.925	
Final R indices [I > 2σ(I)]	R1 = 0.0287, wR2 = 0.0728	
R indices (all data)	R1 = 0.0402, wR2 = 0.0761	
Largest diff. peak and hole	1.091 and -1.363 e.Å ⁻³	

Table 5.4.10 Crystal data and structure refinement for *cis*-[PtMe₃(4-CNPy)I]₂

Empirical formula	C ₁₈ H ₂₆ I ₂ N ₄ Pt ₂	
Formula weight	942.41	
Temperature	193(2) K	
Wavelength	0.71073 Å	
Diffractometer type	STOE IPDS	
Crystal size	0.76 x 0.16 x 0.16 mm ³	
Crystal colour and shape	yellow, needle	
Crystal system	Monoclinic	
Space group	P2 ₁ /n	
Unit cell dimensions	a = 22.7305(14) Å	α = 90°
	b = 12.1314(9) Å	β = 98.978(7)°
	c = 8.8971(5) Å	γ = 90°
Volume	2423.3(3) Å ³	
Z	4	
Density (calculated)	2.583 Mg/m ³	
Absorption coefficient	14.090 mm ⁻¹	
F(000)	1696	
Theta range for data collection	2.35 to 26.01°	
Index ranges	-27 ≤ h ≤ 27, -14 ≤ k ≤ 14, -10 ≤ l ≤ 10	
Reflections collected	17266	
Independent reflections	4585 [R(int) = 0.0813]	
Completeness to theta = 26.01°	0.964	
Absorption correction	multi-scan	
Max. and min. transmission	0.1348 and 0.0423	
Refinement method	Full-matrix least-squares on F ²	
Data / restraints / parameters	4585 / 0 / 242	
Goodness-of-fit on F ²	1.000	
Final R indices [I > 2σ(I)]	R1 = 0.0720, wR2 = 0.1799	
R indices (all data)	R1 = 0.0800, wR2 = 0.1857	
Largest diff. peak and hole	6.440 and -5.116 e.Å ⁻³	

Table 5.4.11 Crystal data and structure refinement for *cis*-[PtMe₃(3-ClPy)I]₂·[PtMe₃I]₄

Empirical formula	C ₂₈ H ₆₂ Cl ₂ I ₆ N ₂ Pt ₆	
Formula weight	2429.64	
Temperature	193(2) K	
Wavelength	0.71073 Å	
Diffractometer type	STOE IPDS	
Crystal size	0.08 x 0.06 x 0.02 mm ³	
Crystal colour and shape	yellow, needle	
Crystal system	Orthorhombic	
Space group	P2 ₁ 2 ₁ 2 ₁	
Unit cell dimensions	a = 9.8450(5) Å	α = 90°
	b = 15.0987(9) Å	β = 90°
	c = 33.7665(18) Å	γ = 90°
Volume	5019.3(5) Å ³	
Z	4	
Density (calculated)	3.215 Mg/m ³	
Absorption coefficient	20.476 mm ⁻¹	
F(000)	4256	
Theta range for data collection	1.81 to 23.29°	
Index ranges	-10 ≤ h ≤ 10, -16 ≤ k ≤ 16, -37 ≤ l ≤ 37	
Reflections collected	27403	
Independent reflections	7201 [R(int) = 0.0770]	
Completeness to theta = 23.29°	0.998	
Absorption correction	multi-scan	
Max. and min. transmission	0.3108 and 0.1554	
Refinement method	Full-matrix least-squares on F ²	
Data / restraints / parameters	7201 / 0 / 416	
Goodness-of-fit on F ²	0.955	
Final R indices [I > 2σ(I)]	R1 = 0.0362, wR2 = 0.0894	
R indices (all data)	R1 = 0.0431, wR2 = 0.0913	
Largest diff. peak and hole	2.092 and -1.282 e.Å ⁻³	

Table 5.4.12 Crystal data and structure refinement for [PtMe₃(bipy)I]

Empirical formula	C ₁₃ H ₁₇ IN ₂ Pt	
Formula weight	523.28	
Temperature	193(2) K	
Wavelength	0.71073 Å	
Diffractometer type	STOE IPDS	
Crystal size	0.16 x 0.16 x 0.14 mm ³	
Crystal colour and shape	yellow, cube	
Crystal system	Monoclinic	
Space group	I2/m	
Unit cell dimensions	a = 7.7977(9) Å	α = 90°
	b = 13.2724(14) Å	β = 90.639(14)°
	c = 14.4543(17) Å	γ = 90°
Volume	1495.8(3) Å ³	
Z	4	
Density (calculated)	2.324 Mg/m ³	
Absorption coefficient	11.426 mm ⁻¹	
F(000)	960	
Theta range for data collection	2.98 to 28.16°	
Index ranges	-10 ≤ h ≤ 10, -17 ≤ k ≤ 17, -19 ≤ l ≤ 19	
Reflections collected	6662	
Independent reflections	1877 [R(int) = 0.0596]	
Completeness to theta = 28.16°	0.98	
Absorption correction	multi-scan	
Max. and min. transmission	0.2198 and 0.1248	
Refinement method	Full-matrix least-squares on F ²	
Data / restraints / parameters	1877 / 0 / 85	
Goodness-of-fit on F ²	1.038	
Final R indices [I > 2σ(I)]	R1 = 0.0306, wR2 = 0.0838	
R indices (all data)	R1 = 0.0347, wR2 = 0.0856	
Largest diff. peak and hole	1.591 and -1.609 e.Å ⁻³	

Table 5.4.13 Crystal data and structure refinement for [PtMe₃(4Me-bipy)I]. 0.5 C₆H₆

Empirical formula	C ₁₈ H ₂₄ IN ₂ Pt	
Formula weight	590.38	
Temperature	193(2) K	
Wavelength	0.71073 Å	
Diffractometer type	STOE IPDS	
Crystal size	0.33 x 0.30 x 0.29 mm ³	
Crystal colour and shape	yellow, cube	
Crystal system	Monoclinic	
Space group	P2 ₁ /c	
Unit cell dimensions	a = 11.8248(12) Å	α = 90°
	b = 8.3843(7) Å	β = 96.794(12)°
	c = 19.403(2) Å	γ = 90°
Volume	1910.2(3) Å ³	
Z	4	
Density (calculated)	2.053 Mg/m ³	
Absorption coefficient	8.961 mm ⁻¹	
F(000)	1108	
Theta range for data collection	3.22 to 27.05°	
Index ranges	-14 ≤ h ≤ 14, -10 ≤ k ≤ 10, -24 ≤ l ≤ 24	
Reflections collected	15096	
Independent reflections	4076 [R(int) = 0.0492]	
Completeness to theta = 27.05°	0.969	
Absorption correction	multi-scan	
Max. and min. transmission	0.1084 and 0.0451	
Refinement method	Full-matrix least-squares on F ²	
Data / restraints / parameters	4076 / 0 / 205	
Goodness-of-fit on F ²	1.052	
Final R indices [I > 2σ(I)]	R1 = 0.0313, wR2 = 0.0769	
R indices (all data)	R1 = 0.0359, wR2 = 0.0803	
Largest diff. peak and hole	1.218 and -2.185 e.Å ⁻³	

Table 5.4.14 Crystal data and structure refinement for [PtMe₃(5Me-bipy)I]

Empirical formula	C ₁₅ H ₂₁ IN ₂ Pt	
Formula weight	551.33	
Temperature	193(2) K	
Wavelength	0.71073 Å	
Diffractometer type	STOE IPDS	
Crystal size	0.27 x 0.24 x 0.07 mm ³	
Crystal colour and shape	yellow, prism	
Crystal system	Monoclinic	
Space group	P2 ₁ /a	
Unit cell dimensions	a = 9.0193(10) Å	α = 90°
	b = 12.3325(14) Å	β = 105.756(11)°
	c = 15.1944(14) Å	γ = 90°
Volume	1626.6(3) Å ³	
Z	4	
Density (calculated)	2.251 Mg/m ³	
Absorption coefficient	10.514 mm ⁻¹	
F(000)	1024	
Theta range for data collection	3.24 to 28.10°	
Index ranges	-11 ≤ h ≤ 11, -16 ≤ k ≤ 16, -19 ≤ l ≤ 19	
Reflections collected	14169	
Independent reflections	3914 [R(int) = 0.0588]	
Completeness to theta = 28.10°	0.989	
Absorption correction	multi-scan	
Max. and min. transmission	0.4910 and 0.2303	
Refinement method	Full-matrix least-squares on F ²	
Data / restraints / parameters	3914 / 0 / 178	
Goodness-of-fit on F ²	0.966	
Final R indices [I > 2σ(I)]	R1 = 0.0295, wR2 = 0.0716	
R indices (all data)	R1 = 0.0405, wR2 = 0.0742	
Largest diff. peak and hole	2.220 and -0.877 e.Å ⁻³	

Table 5.4.15 Crystal data and structure refinement for [PtMe₃(OMe-bipy)I]

Empirical formula	C ₁₅ H ₂₁ IN ₂ O ₂ Pt	
Formula weight	583.33	
Temperature	193(2) K	
Wavelength	0.71073 Å	
Diffractometer type	STOE IPDS	
Crystal size	0.27 x 0.25 x 0.22 mm ³	
Crystal colour and shape	yellow, plate	
Crystal system	Monoclinic	
Space group	P2 ₁ /n	
Unit cell dimensions	a = 11.1515(11) Å	α = 90°
	b = 11.6097(15) Å	β = 103.077(12)°
	c = 13.6162(14) Å	γ = 90°
Volume	1717.1(3) Å ³	
Z	4	
Density (calculated)	2.256 Mg/m ³	
Absorption coefficient	9.975 mm ⁻¹	
F(000)	1088	
Theta range for data collection	2.68 to 28.15°	
Index ranges	-14 ≤ h ≤ 13, -15 ≤ k ≤ 15, -18 ≤ l ≤ 17	
Reflections collected	15369	
Independent reflections	4053 [R(int) = 0.0679]	
Completeness to theta = 28.15°	0.964	
Absorption correction	multi-scan	
Max. and min. transmission	0.1409 and 0.0792	
Refinement method	Full-matrix least-squares on F ²	
Data / restraints / parameters	4053 / 0 / 196	
Goodness-of-fit on F ²	0.858	
Final R indices [I > 2σ(I)]	R1 = 0.0416, wR2 = 0.1108	
R indices (all data)	R1 = 0.0502, wR2 = 0.1169	
Largest diff. peak and hole	2.285 and -3.396 e.Å ⁻³	

Table 5.4.16 Crystal data and structure refinement for [PtMe₃(Me₂N-bipy)I]

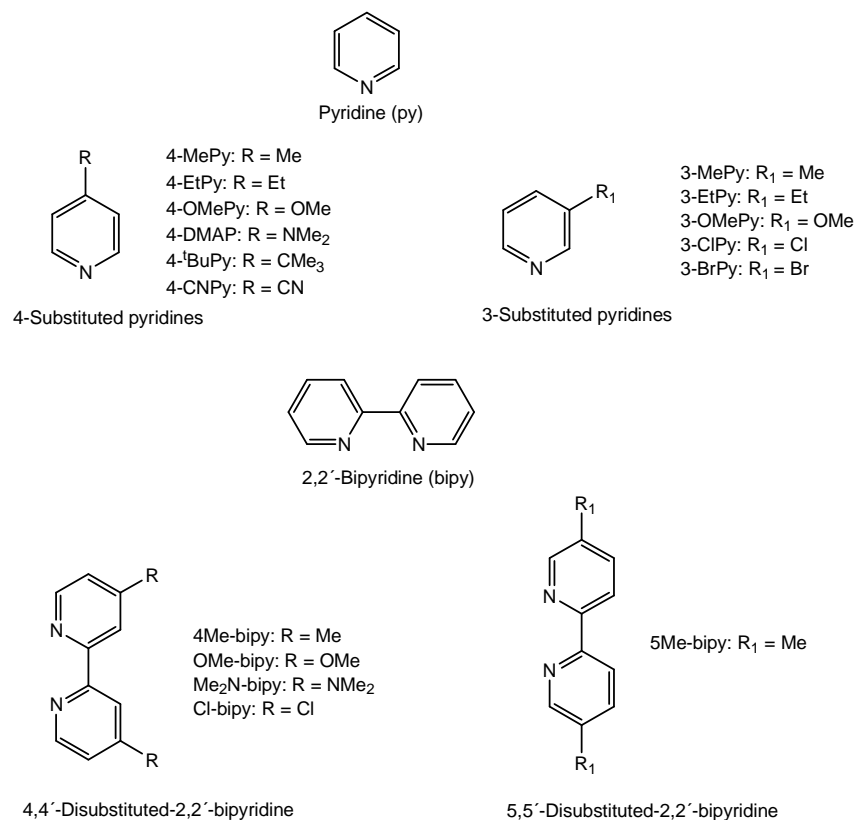
Empirical formula	C ₁₇ H ₂₇ IN ₄ Pt	
Formula weight	609.42	
Temperature	193(2) K	
Wavelength	0.71073 Å	
Diffractometer type	STOE IPDS	
Crystal colour and shape	yellow, plate	
Crystal size	0.58 x 0.24 x 0.16 mm ³	
Crystal system	Orthorhombic	
Space group	Pcan	
Unit cell dimensions	a = 13.7054(11) Å	α = 90°
	b = 17.6237(14) Å	β = 90°
	c = 18.1731(16) Å	γ = 90°
Volume	4389.5(6) Å ³	
Z	8	
Density (calculated)	1.844 Mg/m ³	
Absorption coefficient	7.804 mm ⁻¹	
F(000)	2303	
Theta range for data collection	2.19 to 25.96°	
Index ranges	-16 ≤ h ≤ 16, -14 ≤ k ≤ 21, -22 ≤ l ≤ 22	
Reflections collected	21595	
Independent reflections	4236 [R(int) = 0.0967]	
Completeness to theta = 25.96°	0.984	
Absorption correction	multi-scan	
Max. and min. transmission	0.3003 and 0.2449	
Refinement method	Full-matrix least-squares on F ²	
Data / restraints / parameters	4236 / 0 / 216	
Goodness-of-fit on F ²	0.927	
Final R indices [I > 2σ(I)]	R1 = 0.0606, wR2 = 0.1461	
R indices (all data)	R1 = 0.1299, wR2 = 0.1694	
Largest diff. peak and hole	1.962 and -0.981 e.Å ⁻³	

Table 5.4.17 Crystal data and structure refinement for [PtMe₃(Cl-bipy)I]

Empirical formula	C ₁₃ H ₁₅ Cl ₂ IN ₂ Pt	
Formula weight	592.16	
Temperature	193(2) K	
Wavelength	0.71073 Å	
Diffractometer type	STOE IPDS	
Crystal size	0.84 x 0.48 x 0.24 mm ³	
Crystal colour and shape	yellow, prism	
Crystal system	Monoclinic	
Space group	P2 ₁ /n	
Unit cell dimensions	a = 7.8468(7) Å	α = 90°
	b = 18.2385(17) Å	β = 98.854(12)°
	c = 11.4267(12) Å	γ = 90°
Volume	1615.8(3) Å ³	
Z	4	
Density (calculated)	2.434 Mg/m ³	
Absorption coefficient	10.913 mm ⁻¹	
F(000)	1088	
Theta range for data collection	2.85 to 26.93°	
Index ranges	-9 ≤ h ≤ 8, -23 ≤ k ≤ 23, -14 ≤ l ≤ 14	
Reflections collected	12733	
Independent reflections	3268 [R(int) = 0.0621]	
Completeness to theta = 26.93°	0.931	
Absorption correction	multi-scan	
Max. and min. transmission	0.1048 and 0.0145	
Refinement method	Full-matrix least-squares on F ²	
Data / restraints / parameters	3268 / 0 / 176	
Goodness-of-fit on F ²	1.968	
Final R indices [I > 2σ(I)]	R1 = 0.0881, wR2 = 0.2229	
R indices (all data)	R1 = 0.0911, wR2 = 0.2286	
Largest diff. peak and hole	5.215 and -13.392 e.Å ⁻³	

6 Summary

In this doctoral thesis, iodotrimethylplatinum(IV) complexes of different pyridine and 2,2'-bipyridine ligands are investigated. Scheme 6.1 shows the pyridine and 2,2'-bipyridine ligands used in this thesis.



Scheme 6.1 The pyridine and 2,2'-bipyridine ligands used in this doctoral work.

Iodotrimethylplatinum(IV) complexes of pyridine and its mono-substituted derivatives are demonstrated in Chapter 2. The crystal structures of both the mononuclear [PtMe₃L₂I] (L = 4-DMAP, 4-MePy, 4-EtPy, 4-OMePy, 3-OMePy and 3-BrPy) and dinuclear *trans*-[PtMe₃(py)I]₂ and *cis*-[PtMe₃LI]₂ (L = 4-EtPy, 4-OMePy, 4-CNPy and 3-ClPy) complexes reveal an octahedral coordination around the platinum(IV) and a *facial* arrangement of the methyl groups. The crystal structure of the dinuclear complexes confirms that the iodide ligand acts as a bridging ligand that holds the two platinum metal ions together. Figures 6.1 and 6.2 illustrates the crystal structures of mononuclear [PtMe₃(4-DMAP)₂I] and dinuclear *trans*-[PtMe₃(py)I]₂, respectively.

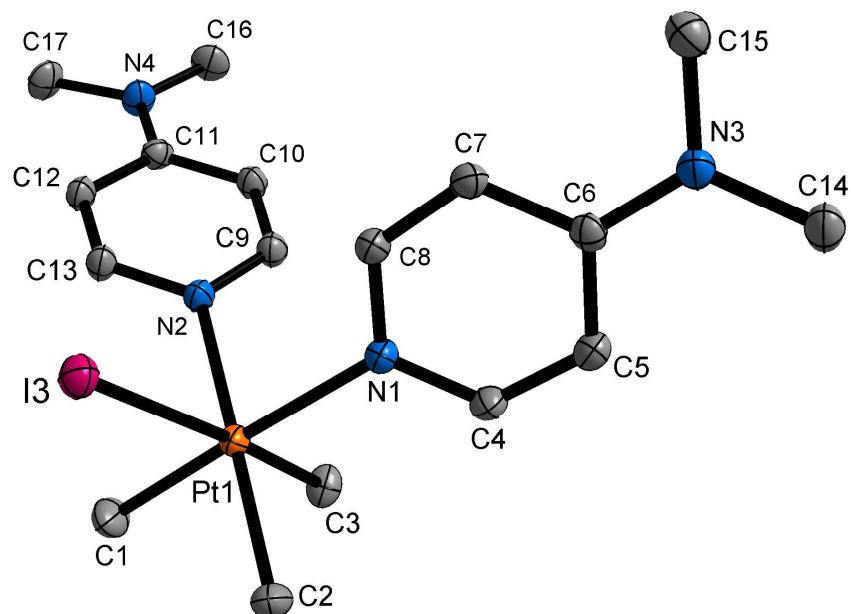


Figure 6.1 Molecular structure of $[\text{PtMe}_3(4\text{-DMAP})_2]\text{I}$ showing the atom labelling scheme. Thermal ellipsoids are at the 50% probability level. Hydrogen atoms are omitted for clarity.

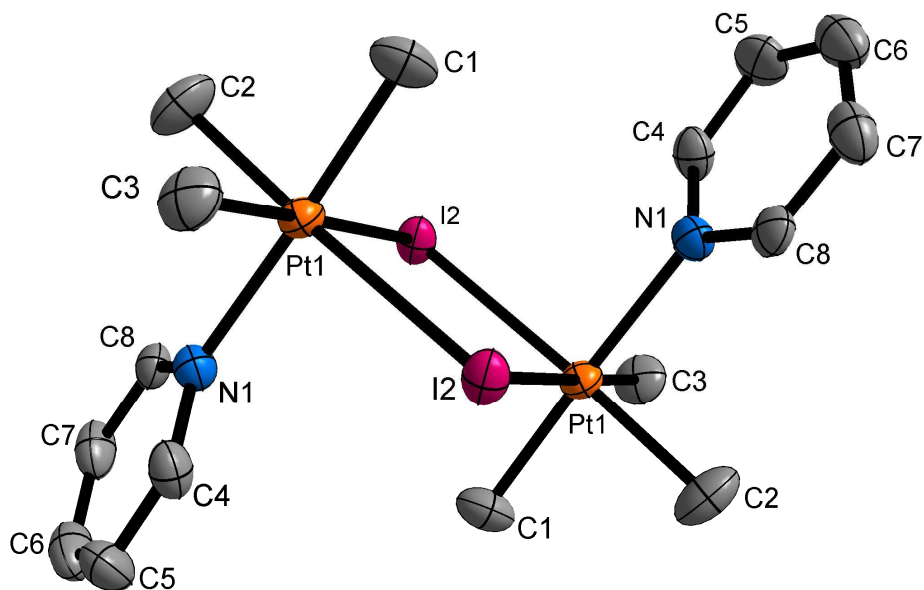
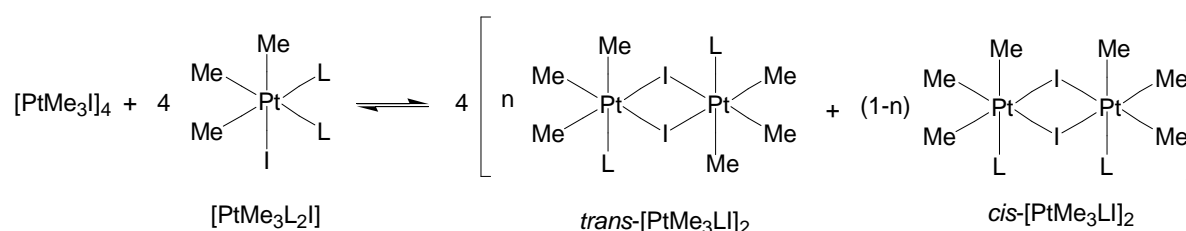


Figure 6.2 Molecular structure of *trans*- $[\text{PtMe}_3(\text{py})]_2\text{I}_2$ showing the atom labelling scheme. Thermal ellipsoids are at the 50% probability level. Hydrogen atoms omitted for clarity.

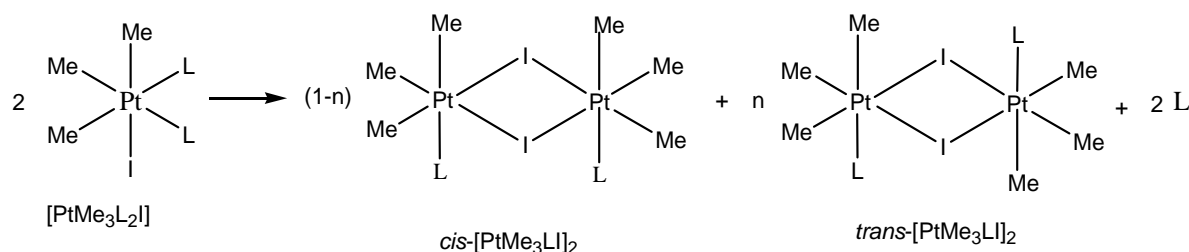
The reaction of the mononuclear $[\text{PtMe}_3\text{L}_2\text{I}]$ ($\text{L} = \text{pyridines}$) complexes with $[\text{PtMe}_3\text{I}]_4$ in chloroform results in the formation of the corresponding dinuclear complexes (both *cis* and *trans* isomers) of pyridines (Scheme 6.2). Although the pyridine substituents have no significant influence on the crystal structures of either the mononuclear or the dinuclear complexes, the equilibrium population of these complexes in solution depends largely on the

electronic effect of the pyridine substituent as well as on the steric bulk of the pyridine substituent. An electron donating substituent such as NMe_2 favours the mononuclear form over the dinuclear form. On the other hand, the dinuclear forms are more stable than the mononuclear forms for pyridines containing electron withdrawing substituents. The *trans* form is more stable than the *cis* form in all the dinuclear complexes of pyridines as the latter exhibit steric interaction among the pyridine ligands which is absent in the former case. With increasing steric bulk of the pyridine substituent the stability of the *cis* isomer also decreases in solution; however, steric interaction among the pyridine ligands in the *cis* dimeric form is less in the case of 3-substituted pyridines than in the case of 4-substituted pyridines.



Scheme 6.2 The reaction of an equimolar mixture of iodotrimethylplatinum and mononuclear $[\text{PtMe}_3\text{L}_2\text{I}]$ ($\text{L} =$ pyridines) leading to the formation of *cis* and *trans* dinuclear complexes.

The weak Pt-N interaction in the mononuclear iodotrimethylplatinum(IV) complexes of electron withdrawing pyridines such as 4-CNPy, 3-BrPy also causes dissociation in solution resulting in the formation of dinuclear complexes and free pyridine ligands, thereby an equilibrium between these species is formed in solution. The extent of dissociation also depends on the concentration of the mononuclear complexes of electron withdrawing pyridines.



Scheme 6.3 The dissociation of mononuclear pyridine complexes of iodotrimethylplatinum(IV), showing the formation of dinuclear complexes. $\text{L} = 4\text{-CNPy}, 3\text{-BrPy}$.

Iodotrimethylplatinum(IV) on treatment with 2,2'-bipyridine and its derivatives gives mononuclear 2,2'-bipyridine complexes (Chapter 3). The EI-Mass spectra analyses of the

complexes gave the highest m/z value for the species $[M-I]^+$, reflecting the mononuclear nature of the complexes. The ^1H NMR spectrum of the complexes shows that the *trans* influence of 2,2'-bipyridine ligand depends on the electronic effect of the substituent. The crystal structure of the complexes, $[\text{PtMe}_3\text{LI}]$ ($L = \text{bipy}, 4\text{Me-bipy}, 5\text{Me-bipy}, \text{OMe-bipy}, \text{Me}_2\text{N-bipy}$ and Cl-bipy) confirms the *fac*-octahedral coordination of the PtMe_3 moiety and the bidentate coordination of the 2,2'-bipyridines. Figure 6.3 shows the crystal structure of $[\text{PtMe}_3(\text{OMe-bipy})\text{I}]$.

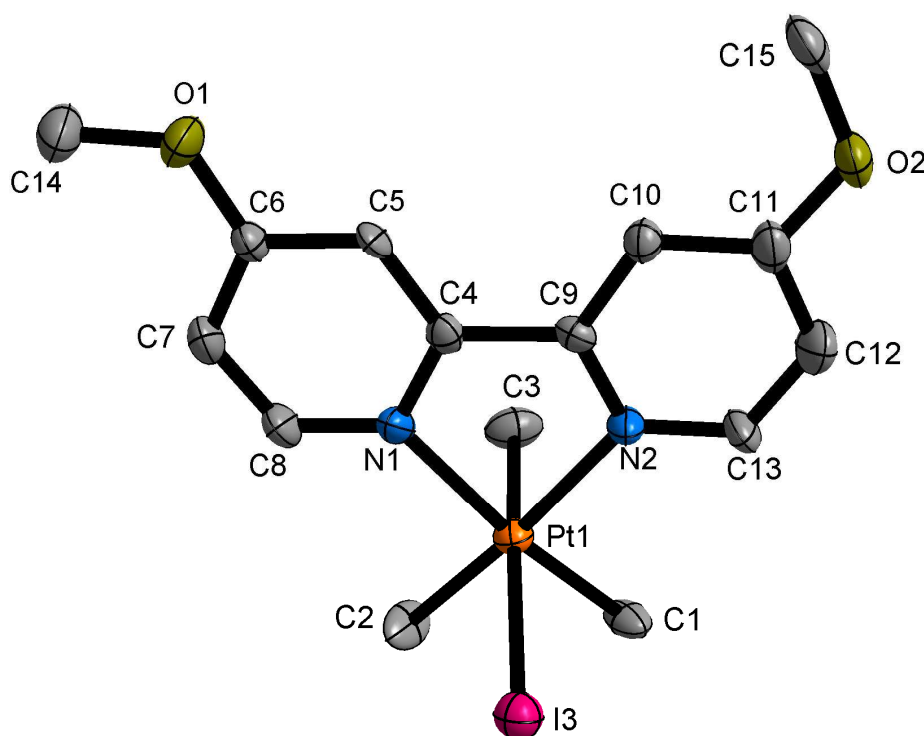


Figure 6.3 Molecular structure of $[\text{PtMe}_3(\text{OMe-bipy})\text{I}]$ showing the atom labelling scheme. Thermal ellipsoids are at the 50% probability level. Hydrogen atoms are omitted for clarity.

Bond length comparison shows that Pt-N bond distances in bipyridine complexes are slightly shorter than in the corresponding pyridine complexes, reflecting the better π -acceptor character of the 2,2'-bipyridines. In addition, the N-Pt-N bite angle in the bipyridine complexes is much lower than in the pyridine complexes. However, the Pt-C, Pt-N and Pt-I bond distances in the complexes do not change significantly. In the crystal packing of $[\text{PtMe}_3(\text{Cl-bipy})\text{I}]$, intermolecular non-covalent interaction between methyl hydrogen and chlorine atom leads to the formation of *zig-zag* chain structures, which are linked through weak π - π interactions to form two-dimensional layer structure (Figure 6.4).

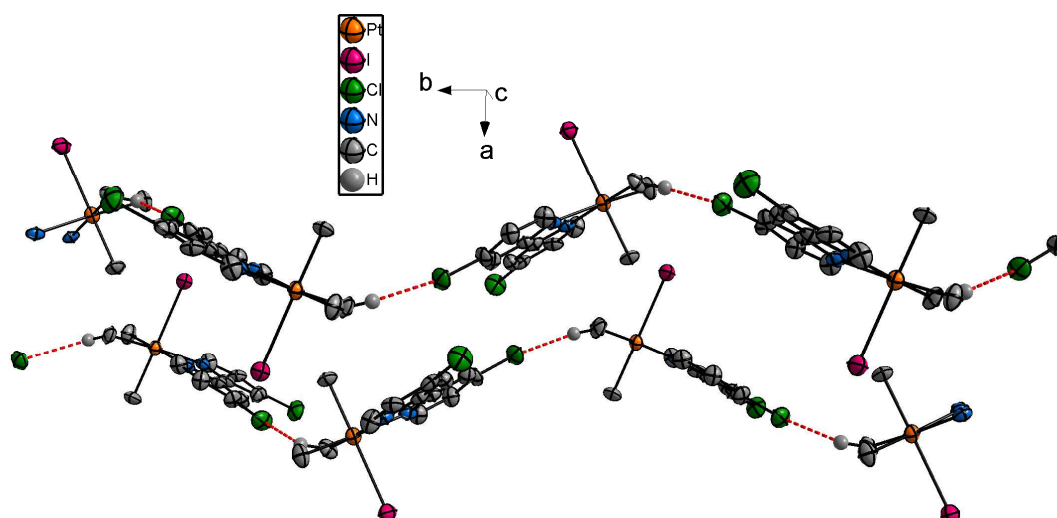
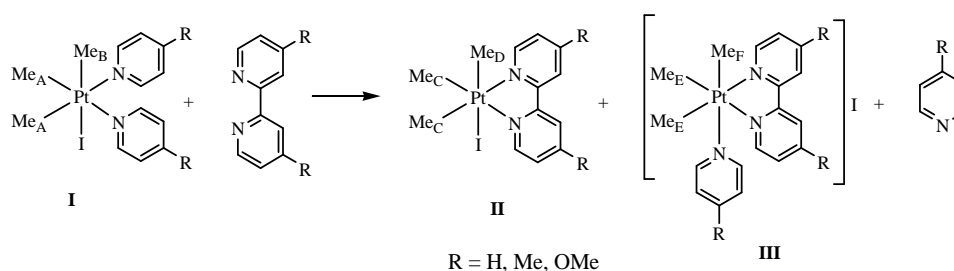
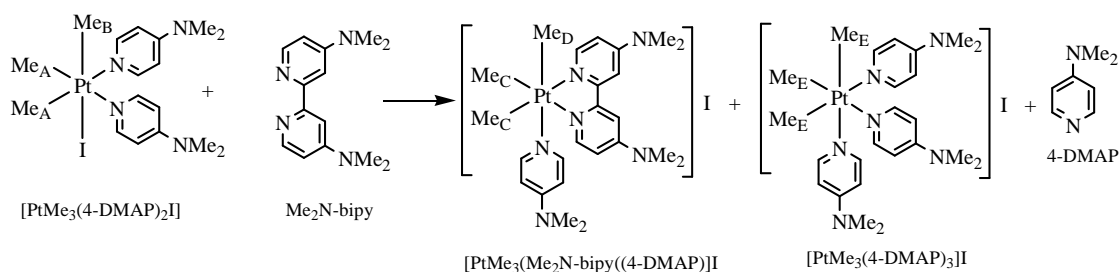


Figure 6.4 A perspective view of a two-dimensional framework structure of $[\text{PtMe}_3(\text{Cl-bipy})\text{I}]$.

The reaction of iodotrimethylplatinum(IV) complexes of pyridines (py, 4-MePy, 4-OMePy, 4-DMAP) with the corresponding 2,2'-bipyridines (bipy, 4Me-bipy, OMe-bipy, $\text{Me}_2\text{N-bipy}$) lead to the substitution of ligands resulting in the formation of chelate bipyridine complexes (described in Chapter 4).



Scheme 6.4 The substitution of pyridine ligands by the corresponding 2,2'-bipyridines in iodotrimethylplatinum(IV) complex.

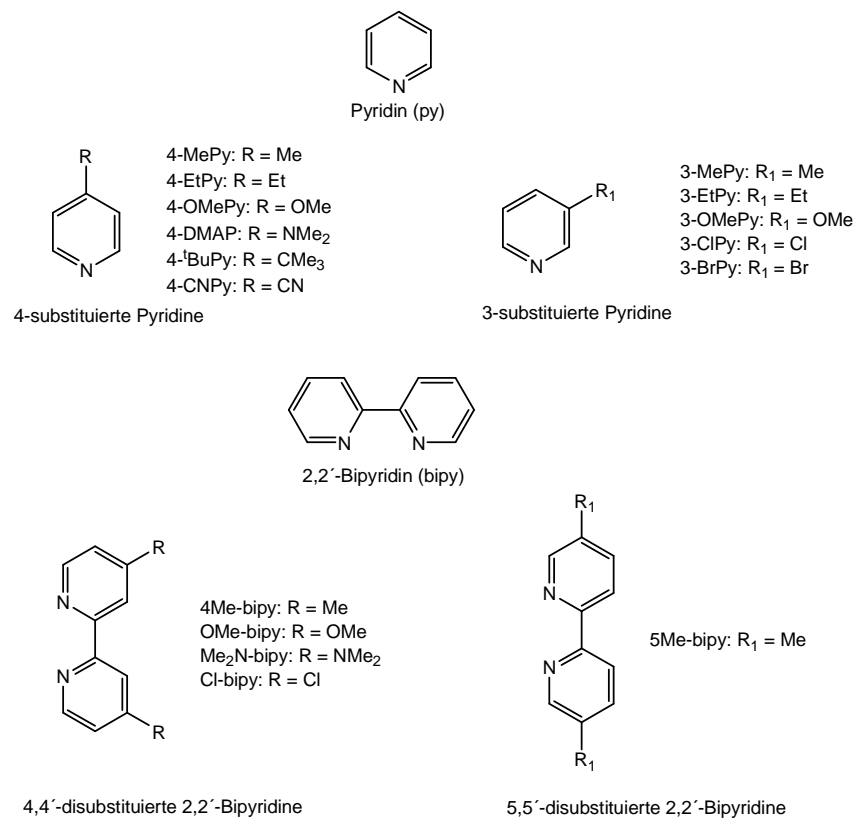


Scheme 6.5 The substitution of 4-DMAP by $\text{Me}_2\text{N-bipy}$ in iodotrimethylplatinum(IV) complex.

The equilibrium for these substitution reactions strongly favours the formation of chelate products. The formation of chelate complexes in solution at equilibrium depends largely on the electronic effect of the substituent as well as on the nature of the solvent.

7 Zusammenfassung

In dieser Arbeit wurden Iodidotrimethylplatin(IV)-Komplexe mit verschiedenen Pyridin- und 2,2'-Bipyridin-Liganden untersucht. Schema 7.1 zeigt eine Übersicht der einzelnen Pyridin und 2,2'-Bipyridin-Liganden.



Schema 7.1 Übersicht der in dieser Arbeit verwendeten Pyridine und 2,2'-Bipyridine.

Iodidotrimethylplatin(IV)-Komplexe von Pyridin und seinen monosubstituierten Derivaten werden in Kapitel 2 behandelt. Die Kristallstrukturen von sowohl mononuklearen $[\text{PtMe}_3\text{L}_2\text{I}]$ ($\text{L} = 4\text{-DMPA}, 4\text{-MePy}, 4\text{-EtPy}, 4\text{-OMePy}, 3\text{-OMePy}$ und 3-BrPy) als auch dinuklearen $\text{trans-}[\text{PtMe}_3(\text{py})\text{I}]_2$ und $\text{cis-}[\text{PtMe}_3\text{LI}]_2$ ($\text{L} = 4\text{-EtPy}, 4\text{-OMePy}, 4\text{-CNPy}$ und 3-ClPy) Komplexen zeigen eine oktaedrische Koordination des Platin(IV) und eine *faciale* Anordnung der Methylgruppen. Die Kristallstrukturen von dinuklearen Komplexen bestätigen, dass der Iodid-Ligand als verbrückender Ligand, der zwei Platin-Ionen zusammenhält, dient. Die Abbildungen 7.1 und 7.2 zeigen beispielhaft die Kristallstrukturen von mononuklearem $[\text{PtMe}_3(4\text{-DMPA})_2\text{I}]$ und dinuklearem $\text{trans-}[\text{PtMe}_3(\text{py})\text{I}]_2$.

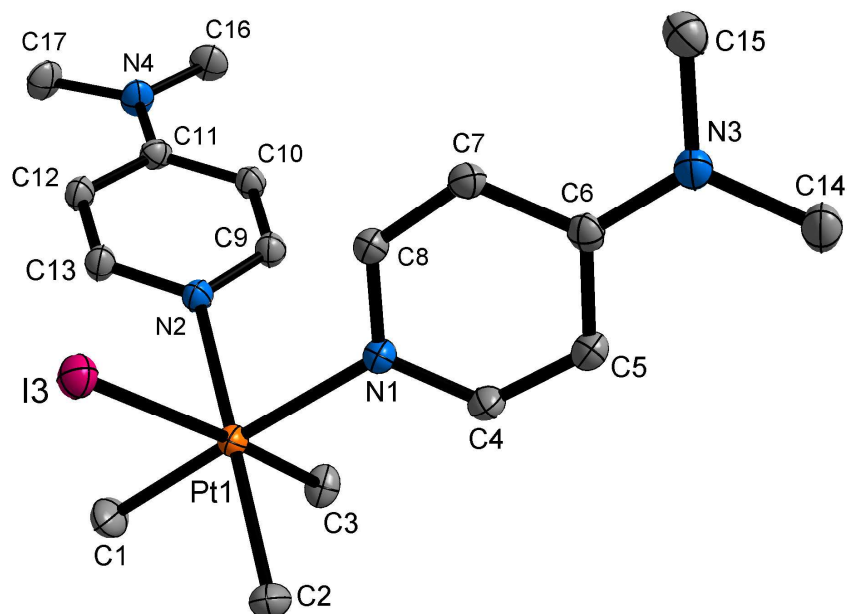


Abb. 7.1 Molekulare Struktur von $[\text{PtMe}_3(4\text{-DMPA})_2]\text{I}$. Thermische Ellipsoide sind am 50% Wahrscheinlichkeitslevel. Wasserstoffatome wurden zur besseren Übersichtlichkeit weggelassen.

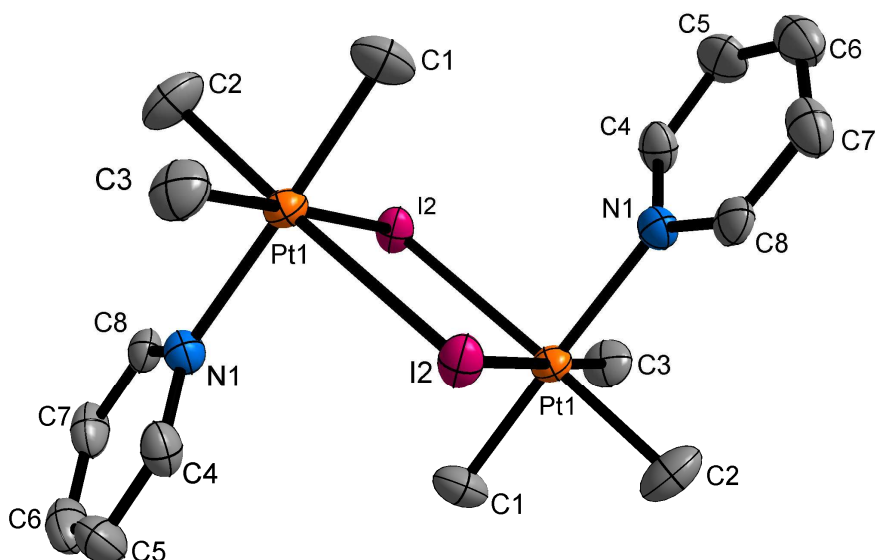
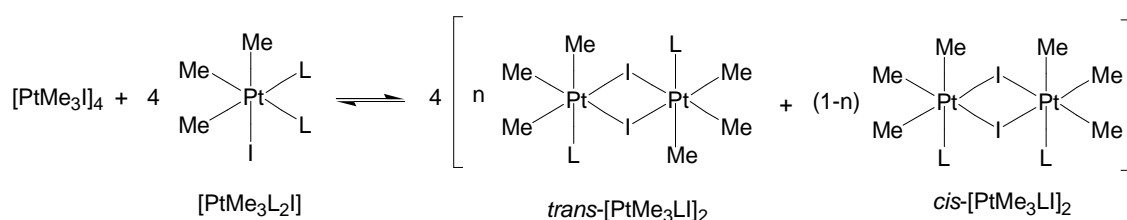


Abb. 7.2 Molekulare Struktur von $\text{trans-}[\text{PtMe}_3(\text{py})\text{I}]_2$. Thermische Ellipsoide sind am 50% Wahrscheinlichkeitslevel. Wasserstoffatome wurden zur besseren Übersichtlichkeit weggelassen.

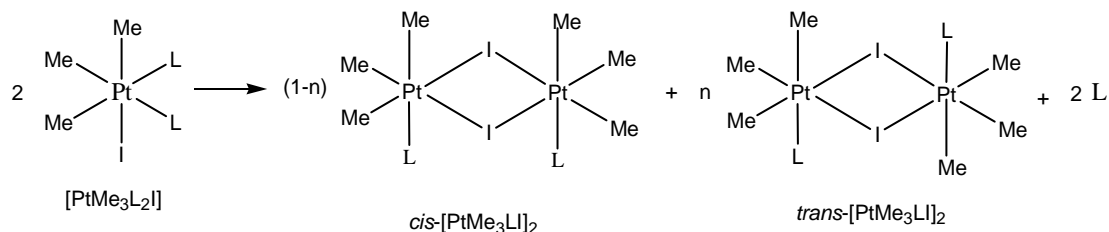
Die Reaktion von mononuklearen $[\text{PtMe}_3\text{L}_2\text{I}]$ -Komplexen ($\text{L} = \text{Pyridin}$) mit $[\text{PtMe}_3\text{I}]_4$ in Chloroform resultiert in der Bildung des entsprechenden dinuklearen Pyridinkomplexes (sowohl *cis*- als auch *trans*-Isomer). Obwohl die Pyridinsubstituenten keinen signifikanten Einfluss auf die Kristallstruktur sowohl von mononuklearen als auch von dinuklearen Komplexen haben, hängt das Gleichgewichtsverhältnis beider Spezies in Lösung zu einem großen Teil von den elektronischen Einflüssen der Substituenten, sowie deren sterischem

Anspruch ab. Ein elektronenschiebender Substituent wie NMe_2 zieht die mononukleare Form der dinuklearen vor. Auf der anderen Seite ist die dinukleare Form für Pyridine mit elektronenziehenden Substituenten stabiler als die mononukleare. Die *trans*-Form ist für alle dinuklearen Pyridinkomplexe stabiler als die *cis*-Form, da letztere sterische Wechselwirkungen zwischen den Pyridinliganden verursacht, die in der *trans*-Form nicht vorkommen. Mit steigendem sterischen Anspruch der Pyridinsubstituenten sinkt auch die Stabilität des *cis*-Isomers in Lösung. Die sterische Wechselwirkung zwischen den Pyridinliganden ist in der dimeren *cis*-Form bei 3-substituierten Pyridinen geringer als bei den 4-substituierten.



Schema 7.2 Die Reaktion einer äquimolaren Mischung aus Iodidotrimethylplatin(IV) und mononuklearem $[\text{PtMe}_3\text{L}_2\text{I}]$ ($\text{L} = \text{Pyridin}$), die zur Bildung von dinuklearen *cis*- und *trans*-Komplexen führt.

Die schwache Pt-N-Wechselwirkung in mononuklearen Iodidotrimethylplatin(IV)-Komplexen mit elektronenziehenden Pyridinen wie 4-CNPy oder 3-BrPy verursacht eine Dissoziation der Komplexe in Lösung, die in der Bildung von dinuklearen Komplexen und freien Pyridinliganden resultiert, wobei ein Gleichgewicht zwischen beiden Spezies in Lösung vorliegt. Der Grad der Dissoziation hängt auch von der Konzentration der mononuklearen Komplexe mit elektronenziehenden Pyridinen ab.



Schema 7.3 Die Dissoziation von mononuklearen Pyridin-Komplexen von Iodidotrimethylplatin zu dinuklearen Komplexen ($\text{L} = 4\text{-CNPy}$, 3-BrPy).

Die Reaktion von Iodidotrimethylplatin(IV) mit 2,2'-Bipyridin und dessen Derivaten erzeugt mononukleare 2,2'-Bipyridin-Komplexe (s. Kap. 3). Die EI-Massenspektren dieser Komplexe

zeigten das höchste m/z Verhältnis für die entsprechenden $[M-I]^+$ Spezies, was die mononukleare Natur dieser Komplexe reflektiert. Die $^1\text{H-NMR}$ Spektren zeigen, dass der *trans*-Einfluss der 2,2'-Bipyridinliganden von den elektronischen Effekten des Substituenten abhängt. Die Kristallstrukturen der Komplexe $[\text{PtMe}_3\text{LI}]$ ($L = \text{bipy}, 4\text{Me-bipy}, 5\text{Me-bipy}, \text{OMe-bipy}, \text{Me}_2\text{N-bipy}$ and Cl-bipy) bestätigen die *fac*-oktaedrische Koordination des PtMe_3 -Rests und die bidentale Koordination der 2,2'-Bipyridine. Die Abbildung 7.3 zeigt die Kristallstruktur von $[\text{PtMe}_3(\text{OMe-bipy})\text{I}]$.

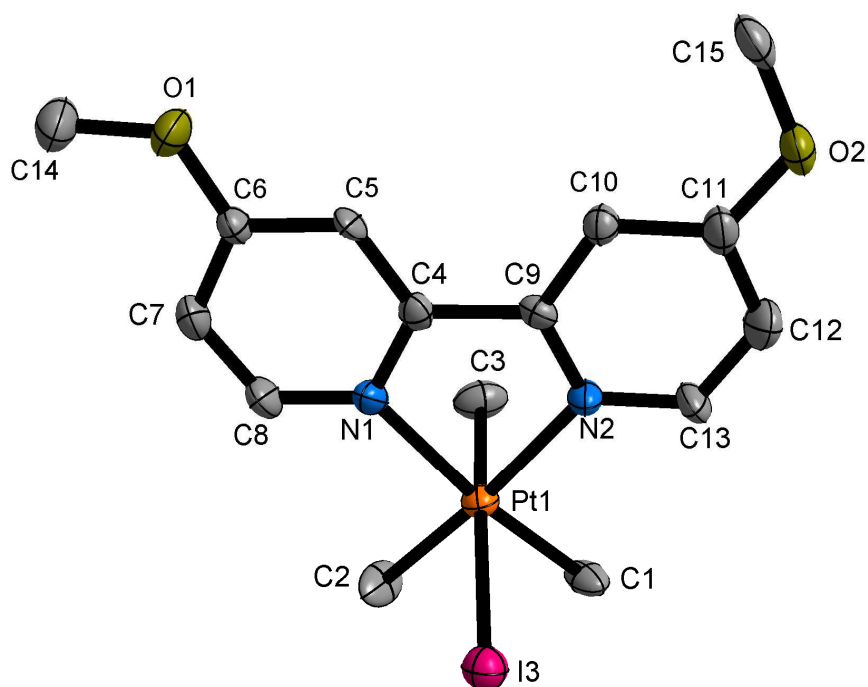


Abb. 7.3 Molekulare Struktur von $[\text{PtMe}_3(\text{OMe-Bipy})\text{I}]$. Thermische Ellipsoide sind am 50% Wahrscheinlichkeitslevel. Wasserstoffatome wurden zur besseren Übersichtlichkeit weggelassen.

Ein Vergleich der Bindungslängen zeigt, dass der Pt-N Bindungsabstand in Bipyridin-Komplexen leicht kürzer ist als in den entsprechenden Pyridin-Komplexen, was die besseren π -Akzeptor Eigenschaften von 2,2'-Bipyridinen zeigt. Des Weiteren ist der N-Pt-N Winkel in Bipyridin-Komplexen wesentlich kleiner als in Pyridin-Komplexen. Die Pt-C, Pt-N und Pt-I Bindungslängen der Komplexe ändern sich hingegen nicht signifikant. In der Kristallpackung von $[\text{PtMe}_3(\text{Cl-bipy})\text{I}]$ führen intermolekulare, nicht kovalente Wechselwirkungen zwischen den Methyl-Wasserstoffatomen und den Chloratomen zu der Ausbildung von kettenartigen Zick-Zack-Strukturen, die über schwache π - π -Wechselwirkungen zur Ausbildung einer zweidimensionalen Schichtstruktur führen (Abb. 7.4).

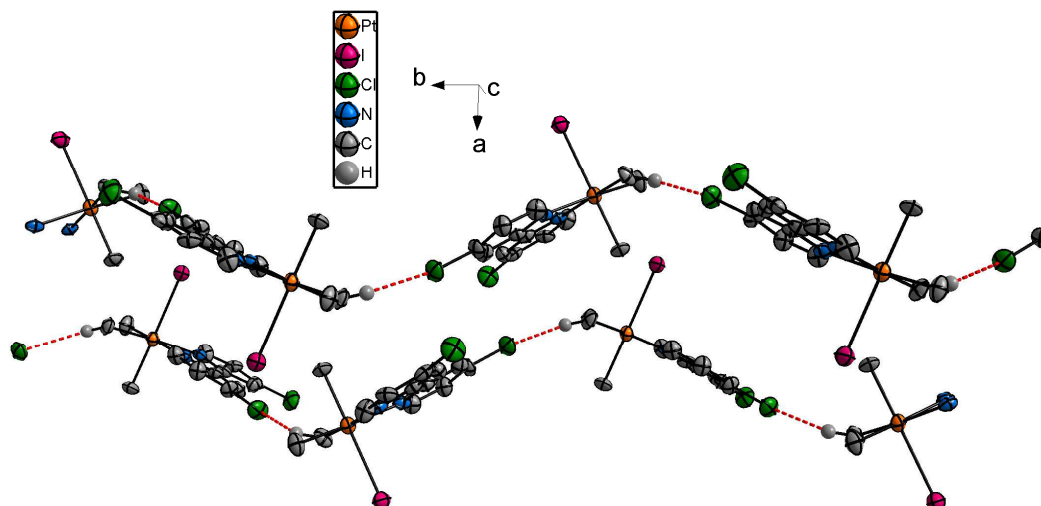
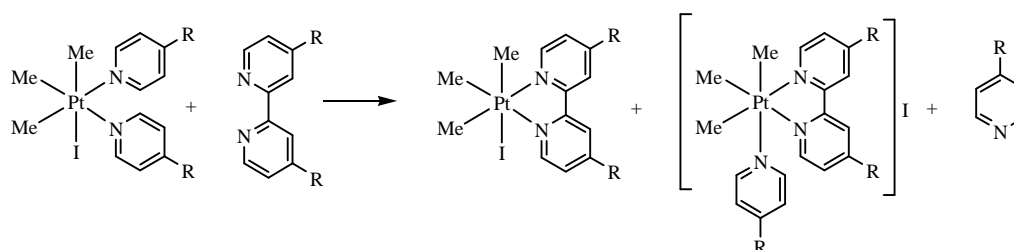
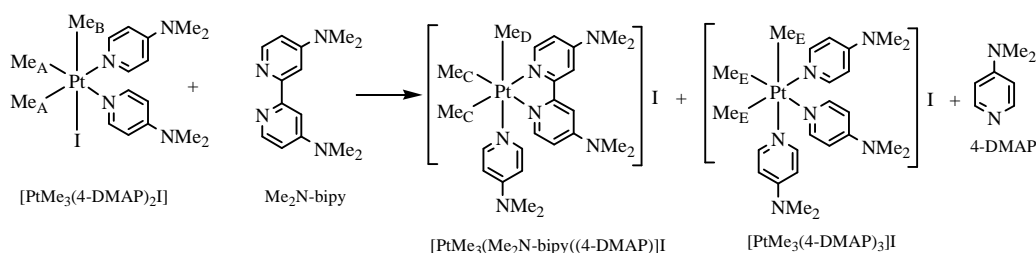


Abb. 7.4 Die zweidimensionale Gerüststruktur von $[\text{PtMe}_3(\text{Cl-bipy})\text{I}]$.

Die Reaktion von Iodidotrimethylplatin(IV)-Pyridinkomplexen (py, 4-MePy, 4-OMePy, 4-DMAP) mit den entsprechenden 2,2'-Bipyridinen (bipy, 4Me-bipy, OMe-bipy, $\text{Me}_2\text{N-bipy}$) führt zu einer Substitution der Liganden, die in der Bildung von Chelat-Bipyridin-Komplexen resultiert (beschrieben in Kapitel 4).



Schema 7.4 Die Substitution von Pyridinliganden durch die korrespondierenden 2,2'-Bipyridine an Iodidotrimethylplatin(IV)-Komplexen ($\text{R} = \text{H}, \text{Me}, \text{OMe}$).



Schema 7.5 Die Substitution von 4-DMAP durch $\text{Me}_2\text{N-bipy}$ an Iodidotrimethylplatin(IV)-Komplexen.

Im Gleichgewicht ist die Bildung des Chelatprodukts bei dieser Substitutionsreaktion stark bevorzugt. Die Bildung von Chelat-Komplexen in Lösung hängt im Gleichgewicht zu einem großen Teil von den elektronischen Effekten der Substituenten sowie von der Natur des Lösungsmittels ab.

8 Appendix

8.1 References

- [1] Wood, I. *The Elements: Platinum*; The Elements, Benchmark Books, **2004**.
- [2] <http://chemistry.about.com/od/elementfacts/a/platinum.htm>.
- [3] Jain, V. K.; Rao, G. S.; Jain, L. *Adv. Organomet. Chem.* **1987**, *27*, 113.
- [4] Peilert, M.; Weißbach, S.; Freisinger, E.; Korsunsky, V. I.; Lippert, B. *Inorg. Chim. Acta* **1997**, *265*, 187.
- [5] Kauffman, G. B.; Thurner, J. J.; Zatzko, D. A. *Inorg. Synth.* **1967**, *9*, 182.
- [6] George, M. W. *2006 Minerals Yearbook: Platinum-Group Metals*; United States Geological Survey, **2007**.
- [7] Vetter, T. A.; Jr. Colombo, D. P. *J. Chem. Educ.* **2003**, *80*, 788.
- [8] Peyrone, M. *Ann. Chemie Pharm.* **1844**, *51*, 1.
- [9] Rosenberg, B.; VanCamp, L.; Trosko, J. E.; Mansour, V. H. *Nature* **1969**, *222*, 385.
- [10] (a) Harrap, K. R. *Cancer Treat. Rev.* **1985**, *12*, 21. (b) Mangioni, C.; Bolis, G.; Pecorelli, S.; Bragman, K.; Epis, A.; Favalli, G.; Gambino, A.; Landoni, F.; Presti, M.; Torri, W.; Vassena, L.; Zanaboni, F.; Marsoni, S. *J. Natl. Cancer Inst.* **1989**, *81*, 1464.
- [11] Extra, J. M.; Espie, M.; Calvo, F.; Ferme, C.; Mignot, L.; Marty, M. *Cancer Chemother. Pharmacol.* **1990**, *25*, 299.
- [12] Periana, R. A.; Taube, D. J.; Gamble, S.; Taube, H.; Satoh, T.; Fujii, H. *Science* **1998**, *280*, 560.
- [13] Johansson, L.; Ryan, O. B.; Tilset, M. *J. Am. Chem. Soc.* **1999**, *121*, 1974.
- [14] For recent comprehensive reviews, see: (a) Goldberg, K. I.; Goldman, A. S. *Activation and Functionalization of C-H Bonds*; Am. Chem. Soc.: Washington, DC, **2004**. (b) Lersch, M.; Tilset, M. *Chem. Rev.* **2005**, *105*, 2471. (c) Labinger, J. A.; Bercaw, J. E. *Nature* **2002**, *417*, 507.
- [15] (a) Puddephatt, R. J. *Angew. Chem. Int. Ed.* **2002**, *41*, 261. (b) Roy, S.; Puddephatt, R. J.; Scott, J. D. *J. Chem. Soc., Dalton Trans.* **1989**, 2121. (c) Brown, M. P.; Puddephatt, R. J.; Upton, C. E. E. *J. Chem. Soc., Dalton Trans.* **1974**, 2457.
- [16] (a) Pawlikowski, A. V.; Getty, A. D.; Goldberg, K. I. *J. Am. Chem. Soc.* **2007**, *129*, 10382. (b) Procelewska, J.; Zahl, A.; Liehr, G.; van Eldik, R.; Smythe, N. A.; Williams, B. S.; Goldberg, K. I. *Inorg. Chem.* **2005**, *44*, 7732. (c) Crumpton-Bregel,

- D. M.; Goldberg, K. I. *J. Am. Chem. Soc.* **2003**, *125*, 9442. (d) Jensen, M. P.; Wick, D. D.; Reinartz, S.; White, P. S.; Templeton, J. L.; Goldberg, K. I. *J. Am. Chem. Soc.* **2003**, *125*, 8614. (e) Williams, B. S.; Goldberg, K. I. *J. Am. Chem. Soc.* **2001**, *123*, 2576. (f) Crumpton, D. M.; Goldberg, K. I. *J. Am. Chem. Soc.* **2000**, *122*, 962. (g) Williams, B. S.; Holland, A. W.; Goldberg, K. I. *J. Am. Chem. Soc.* **1999**, *121*, 252.
- [17] Lindner, R.; Wagner, C.; Steinborn, D. *J. Am. Chem. Soc.* **2009**, *131*, 8861.
- [18] (a) Fekl, U.; Kaminsky, W.; Goldberg, K. I. *J. Am. Chem. Soc.* **2003**, *125*, 15286. (b) Fekl, U.; Goldberg, K. I. *J. Am. Chem. Soc.* **2002**, *124*, 6804.
- [19] (a) Luedtke, A. T.; Goldberg, K. I. *Inorg. Chem.* **2007**, *46*, 8496. (b) Kloek, S. M.; Goldberg, K. I. *J. Am. Chem. Soc.* **2007**, *129*, 3460. (c) Fekl, U.; Kaminsky, W.; Goldberg, K. I. *J. Am. Chem. Soc.* **2001**, *123*, 6423.
- [20] Reinartz, S.; White, P. S.; Brookhart, M.; Templeton, J. L. *J. Am. Chem. Soc.* **2001**, *123*, 6425.
- [21] Zhao, S.-B.; Wu, G.; Wang, S. *Organometallics* **2008**, *27*, 1030.
- [22] Pendyala, L.; Greco, W.; Cowens, J. W.; Madajewicz, S.; Creaven, P. J. *Cancer Chemother. Pharmacol.* **1983**, *11*, 23.
- [23] Casper, E. S.; Smart, T. C.; Hakes, T. B.; Jr. Ochoa, M.; Kaufman, R. J. *Investigational New Drugs* **1988**, *6*, 87.
- [24] Judson, I.; Mckeage, M.; Hanwell, J.; Berry, C.; Mistry, P.; Raynaud, F.; Poon, G.; Murrer, B.; Harrap, K. *Platinum and Other Metal Coordination Complexes in Cancer Chemotherapy 2: The Clinical Development of the Oral Platinum Anticancer Agent JM216*; Plenum Press, New York, **1996**, 83.
- [25] Shamsuddin, S.; Takahashi, I.; Siddik, Z. H.; Khokhar, A. R. *J. Inorg. Biochem.* **1996**, *61*, 291.
- [26] Shamsuddin, S.; Santillan, C. C.; Stark, J. L.; Whitmire, K. H.; Siddik, Z. H.; Khokhar, A. R. *J. Inorg. Biochem.* **1998**, *71*, 29.
- [27] Pope, W. J.; Peachy, S. J. *J. Chem. Soc., Trans.* **1909**, *95*, 571.
- [28] Baldwin, J. C.; Kaska, W. C. *Inorg. Chem.* **1975**, *14*, 2020.
- [29] Ebert, K. H.; Massa, W.; Donath, H.; Lorberth, J.; Seo, B. -S.; Herdtweck, E. *J. Organomet. Chem.* **1998**, *559*, 203.
- [30] Allmann, R.; Kucharczyk, D. *Z. Kristallor.* **1983**, *165*, 227.
- [31] Donnay, G.; Coleman, L. B.; Krieghoff, N. G.; Cowan, D. O. *Acta Cryst. B* **1968**, *24*, 157.

- [32] Rundle, R. E.; Sturdivant, J. H. *J. Am. Chem. Soc.* **1947**, *69*, 1561.
- [33] Massa, W.; Baum, G.; Seo, B. -S.; Lorberth, J. *J. Organomet. Chem.* **1988**, *352*, 415.
- [34] Vance, B. *J. Organomet. Chem.* **1987**, *336*, 441.
- [35] Atam, M.; Müller, U. *J. Organomet. Chem.* **1974**, *71*, 435.
- [36] Schlecht, S.; Magull, J.; Fenske, D.; Dehnicke, K. *Angew. Chem. Int. Ed. Engl.* **1997**, *36*, 1994.
- [37] Lile, W. J.; Menzies, R. C. *J. Chem. Soc.* **1949**, 1168.
- [38] Foss, M. E.; Gibson, C. S. *J. Chem. Soc.* **1951**, 299.
- [39] Clegg, D. E.; Hall, J. R.; Swile, G. A. *J. Organomet. Chem.* **1972**, *38*, 403.
- [40] Orrell, K. G.; Osborne, A. G.; Šik, V.; da Silva, M. W.; Hursthouse, M. B.; Hibbs, D. E.; Malik, K. M. A.; Vassilev, N. G. *J. Organomet. Chem.* **1998**, *555*, 35.
- [41] Gschwind, R. M.; Schlecht, S. *J. Chem. Soc., Dalton Trans.* **1999**, 1891.
- [42] Abel, E. W.; Orrell, K. G.; Platt, A. W. G. *J. Chem. Soc., Dalton Trans.* **1983**, 2345.
- [43] Abel, E. W.; Bhargava, S. K.; Kite, K.; Orrell, K. G.; Šik, V.; Williams, B. L. *J. Chem. Soc., Dalton Trans.* **1982**, 583.
- [44] Abel, E. W.; Khan, A. R.; Kite, K.; Orrell, K. G.; Šik, V. *J. Chem. Soc., Dalton Trans.* **1980**, 2220.
- [45] Abel, E. W.; Khan, A. R.; Kite, K.; Orrell, K. G.; Šik, V. *J. Organomet. Chem.* **1978**, *145*, C18.
- [46] Heard, P. J.; Kite, K.; Aliev, A. E. *Polyhedron* **1998**, *17*, 2543.
- [47] Heard, P. J.; Kite, K. *J. Chem. Soc., Dalton Trans.* **1996**, 3543.
- [48] Abel, E. W.; Heard, P. J.; Kite, K.; Orrell, K. G.; Psaila, A. F. *J. Chem. Soc., Dalton Trans.* **1995**, 1233.
- [49] Appleton, T. G.; Hall, J. R.; Jones, T. G. *Inorg. Chim. Acta* **1979**, *32*, 127.
- [50] Abel, E. W.; Heard, P. J.; Orrell, K. G.; Hursthouse, M. B.; Malik, K. M. A. *J. Chem. Soc., Dalton Trans.* **1995**, 3165.
- [51] Abel, E. W.; Blackwell, E. S.; Heard, P. J.; Orrell, K. G.; Šik, V.; Hursthouse, M. B.; Mazid, M. A.; Malik, K. M. A. *J. Chem. Soc., Dalton Trans.* **1994**, 445.
- [52] Abel, E. W.; Heard, P. J.; Orrell, K. G.; Šik, V. *Polyhedron* **1994**, *13*, 2907.
- [53] Spike, C. G.; Parry, R. W. *J. Am. Chem. Soc.* **1953**, *75*, 2726.
- [54] <http://chem.ch.huji.ac.il/nmr/whatisnmr/whatisnmr.html>.
- [55] <http://nmr-analysis.blogspot.com/2008/07/dosy-nmr.html>.
- [56] (a) Hasenzahl, S.; Hausen, H. -D.; Kaim, W. *Chem. Eur. J.* **1995**, *1*, 95. (b) Bayler, A.; Canty, A. J.; Skelton, B. W.; White, A. H. *J. Organomet. Chem.* **2000**, *595*, 296. (c)

- Baar, C. R.; Carbray, L. P.; Jennings, M. C.; Puddephatt, R. J. *Organometallics* **2000**, *19*, 2482.
- [57] Kavakli, C.; Gabrielsson, A.; Sieger, M.; Schwederski, B.; Niemeyer, M.; Kaim, W. *J. Organomet. Chem.* **2007**, *692*, 3151.
- [58] Freckmann, B.; Tebbe, K.-F. *Acta Cryst. B* **1981**, *37*, 1520.
- [59] Buse, K. D.; Keller, H. J.; Pritzkow, H. *Inorg. Chem.* **1977**, *16*, 1072.
- [60] Clark, H. C.; Ferguson, G.; Jain, V. K.; Parvez, M. *Organometallics* **1983**, *2*, 806.
- [61] Ferguson, G.; Parvez, M.; Monaghan, P. K.; Puddephatt, R. J. *J. Chem. Soc., Chem. Comm.* **1983**, 267.
- [62] Cook P. M.; Dahl, L. F.; Hopgood, D.; Jenkins, R. A. *J. Chem. Soc., Dalton Trans.* **1973**, 294.
- [63] Brawner, S. A.; Lin, I. J. B.; Kim, J. -H.; Jr. Everett, G. W. *Inorg. Chem.* **1978**, *17*, 1304.
- [64] Abel, E. W.; Khan, A. R.; Kite, K.; Hursthouse, M. B.; Malik, K. M. A.; Mazid, M. A. *J. Organomet. Chem.* **1982**, *235*, 121.
- [65] Abel, E. W.; Khan, A. R.; Kite, K.; Orrell, K. G.; Šik, V.; Cameron, T. S.; Cordes, R. *J. Chem. Soc., Chem. Comm.* **1979**, 713.
- [66] Abel, E. W., Beckett, M. A.; Bates, P. A.; Hursthouse, M. B. *J. Organomet. Chem.* **1987**, *325*, 261.
- [67] Frasson, E.; Panattoni, C.; Zannetti, R. *Acta Cryst.* **1959**, *12*, 1027.
- [68] Fletcher, N. C. *J. Chem. Soc., Perkin Trans. I* **2002**, 1831.
- [69] Cook, M. J.; Lewis, A. P.; McAuliffe, G. S. G.; Skarda, V.; Thomson, A. J.; Glasper, J. L.; Robbins, D. J. *J. Chem. Soc., Perkin Trans. II* **1984**, 1293.
- [70] Worl, L. A.; Duesing, R.; Chen, P.; Ciana, L. D.; Meyer, T. J. *J. Chem. Soc., Dalton Trans.* **1991**, 849.
- [71] Holmlin, R. E.; Yao, J. A.; Barton, J. K. *Inorg. Chem.* **1999**, *38*, 174.
- [72] Anderson, P. A.; Deacon, G. B.; Haarmann, K. H.; Keene, F. R.; Meyer, T. J.; Reitsma, D. A.; Skelton, B. W.; Strouse, G. F.; Thomas, N. C.; Treadway, J. A.; White, A. H. *Inorg. Chem.* **1995**, *34*, 6145.
- [73] McInnes, E. J. L.; Farley, R. D.; Rowlands, C. C.; Welch, A. J.; Rovatti, L.; Yellowlees, L. J. *J. Chem. Soc., Dalton Trans.* **1999**, 4203.
- [74] Barqawi, K. R.; Llobet, A.; Meyer, T. J. *J. Am. Chem. Soc.* **1988**, *110*, 7751.
- [75] Araki, K.; Mutai, T.; Shigemitsu, Y.; Yamada, M.; Nakajima, T.; Kuroda, S.; Shima, I. *J. Chem. Soc., Perkin Trans. 2* **1996**, 613.

- [76] Bruce, D.; McCall, J.; Richter, M. M. *Analyst* **2002**, *127*, 125.
- [77] Cheng, K. F.; Drain, C. M.; Grohmann, K. *Inorg. Chem.* **2003**, *42*, 2075.
- [78] Maruyama, K.; Mishima, Y.; Minagawa, K.; Motonaka, J. *Anal. Chem.* **2002**, *74*, 3698.
- [79] Zakeeruddin, S. M.; Grätzel, M.; Fraser, D. M. *Biosensors & Bioelectronics* **1996**, *11*, 305.
- [80] Wrighton, M.; Morse, D. L. *J. Am. Chem. Soc.* **1974**, *96*, 998.
- [81] Casper, J. V.; Sullivan, B. P.; Meyer, T. J. *Inorg. Chem.* **1984**, *23*, 2104.
- [82] Kim, H. -H.; Mano, N.; Zhang, Y.; Heller, A. *J. Electrochem. Soc.* **2003**, *150*, A209.
- [83] Vetter, C.; Bruhn, C.; Steinborn, D. *Acta Cryst. E* **2010**, *66*, m941.
- [84] Vetter, C.; Wagner, C.; Steinborn, D. *Acta Cryst. E* **2010**, *66*, m286.
- [85] Dogan, A.; Kavakli, C.; Sieger, M.; Niemeyer, M.; Sarkar, B.; Kaim, W. *Z. Anorg. Allg. Chem.* **2008**, *634*, 2527.
- [86] Sony, S. M. M.; Ponnuswamy, M. N. *Crystal Growth & Design* **2006**, *6*, 736.
- [87] Janiak, C. *J. Chem. Soc., Dalton Trans.* **2000**, 3885.
- [88] Pan, Y.; Li, K.; Bi, W.; Li, J. *Acta Cryst. C* **2008**, *64*, o41.
- [89] Zeng, Q.; Wu, D.; Ma, H.; Shu, C.; Li, Y.; Wang, C. *CrystEngComm* **2006**, *8*, 189.
- [90] Kondo, Y.; Ishikawa, M.; Ishihara, K. *Inorg. Chim. Acta* **1996**, *241*, 81.
- [91] Hux, J. E.; Puddephatt, R. J. *J. Organomet. Chem.* **1992**, *437*, 251.
- [92] Nakayama, K.; Kondo, Y.; Ishihara, K. *Can. J. Chem.* **1998**, *76*, 62.
- [93] Zhang, D.; Telo, J. P.; Liao, C.; Hightower, S. E.; Clennan, E. L. *J. Phys. Chem. A* **2007**, *111*, 13567.
- [94] Wehman, P.; Dol, G. C.; Moorman, E. R.; Kamer, P. C. J.; van Leeuwen, P. W. N. M.; Fraanje, J.; Goubitz, K. *Organometallics* **1994**, *13*, 4856.
- [95] Stoe & Cie. *STOE IPDS Software*. Stoe & Cie GmbH, Darmstadt, Germany, **1997**.
- [96] Blessing, C. F. R. H. *Acta Cryst. A* **1995**, *51*, 33.
- [97] Bruker. *SAINT*. Bruker AXS Inc., Madison, Wisconsin, USA, **2007**.
- [98] Bruker. *SADABS*. Bruker AXS Inc., Madison, Wisconsin, USA, **2008**.
- [99] Sheldrick, G. M. *Acta Cryst. A* **2008**, *64*, 112.
- [100] Macrae, C. F.; Edgington, P. R.; McCabe, P.; Pidcock, E.; Shields, G. P.; Taylor, R.; Towler, M.; van de Streek, J. *J. Appl. Cryst.* **2006**, *39*, 453.
- [101] Brandenburg, K.; Putz, H. *DIAMOND*. Crystal Impact GbR, Bonn, Germany, **2009**.

8.2 Abbreviations

Å	Angstrom
α	alpha
β	beta
°	degree
°C	degree celsius
δ	chemical shift (NMR)
γ	gyromagnetic ratio
\hbar	reduced Planck constant
λ	X-ray wavelength
^1H	proton
Abb.	Abbildung
abpy	2,2'-azobispyridine
B_0	external magnetic field
BAB	1,2-bis(N-7-azaindoly)benzene
bipy	2,2'-bipyridine
bipy N-Oxide	2,2'-bipyridine N,N'-dioxide
br	broad signal (NMR)
BrPy	bromopyridine
bpym	2,2'-bipyrimidine
CHIP	<i>cis</i> -dichloro- <i>trans</i> -dihydroxy-bis-isopropylamineplatinum(IV)
Cl-bipy	4,4'-dichloro-2,2'-bipyridine
Cl-bipy N-Oxide	4,4'-dichloro-2,2'-bipyridine N,N'-dioxide
ClPy	chloropyridine
cm	centimetre
CNPY	cyanopyridine
COSY	correlation spectroscopy
D	diffusion coefficient
d	doublet(NMR)
dd	doublet of doublets (NMR)
DCM	dichloromethane
DMAP	dimethylaminopyridine
dmas	(dimethylarsino)sulphide

DMF	N,N-dimethylformamide
DMG	dimethylglyoxime
DMSO	dimethyl sulfoxide
DNA	deoxyribonucleic acid
DOSY	diffusion ordered spectroscopy
EI	electron ionisation
en	ethylenediamine
EtPy	ethylpyridine
eV	electron volt
EXSY	exchange spectroscopy
<i>fac</i>	<i>facial</i>
h	hour(s)
Hz	hertz
<i>I</i>	<i>Nuclear Spin</i>
IR	infrared
J	spin-spin coupling constant
JM216	cis-dichloro- <i>trans</i> -diacetato-ammine-cyclohexylamine-platinum(IV)
K	Kelvin
<i>k</i>	Boltzmann Constant
K _{eq}	Equilibrium constant
m	multiplet
4Me-bipy	4,4'-dimethyl-2,2'-bipyridine
5Me-bipy	5,5'-dimethyl-2,2'-bipyridine
Me ₂ N-bipy	4,4'-bis(dimethylamino)-2,2'-bipyridine
MePy	methylpyridine
Me ₂ Pz	3,5-dimethylpyrazole
mg	milligram
MHz	megahertz
mL	millilitre
mmol	millimole
mol	mole
MS	mass spectrometry
m/z	mass to charge ratio

NMR	nuclear magnetic resonance
NOESY	nuclear overhauser effect spectroscopy
OMe-bipy	4,4'-dimethoxy-2,2'-bipyridine
OMePy	methoxypyridine
O ₂ N-bipy N-Oxide	4,4'-dinitro-2,2'-bipyridine N,N'-dioxide
OTf	triflate (trifluoromethanesulfonate)
phen	1,10-phenanthroline
PMDTA	N,N,N',N'',N''-pentamethyldiethylenetriamine
ppdm	1-phenylpropane-1,2-dione 2-oximate
ppm	parts per million
Pt	platinum
PtAs ₂	sperrylite
py	pyridine
pydz	pyridazine
Pz	pyrazole
q	quartet (NMR)
s	singlet (NMR)
t	triplet (NMR)
^t BuPy	tertiarybutylpyridine
TFE	2,2,2-trifluoroethanol
THF	tetrahydrofuran
TMEDA	N,N,N',N'-tetramethylethylenediamine

8.3 Table of Figures

Figure 1.1	Crystal structures of [$\{(o\text{-}^1\text{Pr}_2\text{C}_6\text{H}_3)\text{NC}(\text{CH}_3)\}_2\text{CH}\text{PtMe}_3$ (left); ^[19c] (BAB)PtMe ₃ [BAB = 1,2-bis(<i>N</i> -7-azaindoly)benzene] (right). ^[21]	4
Figure 1.2	Molecular structure of iodotrimethylplatinum(IV). ^[29]	5
Figure 1.3	The basis of NMR in the case of spin ½ nuclei such as ¹ H, ¹³ C, ¹⁵ N, ³¹ P, ¹⁹⁵ Pt, etc. ^[54]	9
Figure 2.1.1	Molecular structure of [PtMe ₃ (4-DMAP) ₂ I] (1) showing the atom labelling scheme. Thermal ellipsoids are at the 50% probability level. Hydrogen atoms are omitted for clarity.	17
Figure 2.1.2	Molecular structure of [PtMe ₃ (3-BrPy) ₂ I] (2) showing the atom labelling scheme. Thermal ellipsoids are at the 50% probability level. Hydrogen atoms are omitted for clarity.	18
Figure 2.1.3	The 400 MHz ¹ H NMR spectrum of [PtMe ₃ (4-DMAP) ₂ I] (1) in CDCl ₃ at a concentration of 0.06 M. For labelling, see inset. X is the solvent peak.	19
Figure 2.1.4	The 400 MHz ¹ H NMR spectrum of [PtMe ₃ (3-BrPy) ₂ I] (2) in CDCl ₃ at 0.06 M at 300 K. X is the solvent peak and Y is the peak for water present in CDCl ₃ . For labelling, see Scheme 2.1.2. Due to close proximity, the signals G and H were not fully resolved and not assigned unambiguously. The signals I and M have virtually identical chemical shifts and not assigned unambiguously.	21
Figure 2.1.5	The 400 MHz ¹ H NMR spectrum of [PtMe ₃ (4-CNPy) ₂ I] (3) in CDCl ₃ at 300 K at 0.06 M. Signals X, Y are the peak for the solvent and water present in CDCl ₃ , respectively. For labelling, see Scheme 2.1.3. Signals K and L were not fully resolved and not assigned unambiguously.	23
Figure 2.1.6	Part of aromatic ligand region of the 600 MHz ¹ H DOSY spectrum of [PtMe ₃ (3-BrPy) ₂ I] (2) in CDCl ₃ at 0.06 M showing the presence of [PtMe ₃ (3-BrPy) ₂ I] (2), <i>cis</i> and <i>trans</i> -[PtMe ₃ (3-BrPy)I] ₂ and 3- bromopyridine (3-BrPy). For labelling, see Scheme 2.1.2.	24
Figure 2.1.7	Part of aromatic ligand region of the 600 MHz ¹ H DOSY spectrum of [PtMe ₃ (4-CNPy) ₂ I] (3) in CDCl ₃ at 0.02 M showing the presence of [PtMe ₃ (4-CNPy) ₂ I] (3), <i>cis</i> and <i>trans</i> -[PtMe ₃ (4-CNPy)I] ₂ and 4- cyanopyridine (4-CNPy). For labelling, see Scheme 2.1.3.	24

Figure 2.2.1	Molecular structure of $[\text{PtMe}_3(4\text{-MePy})_2\text{I}]$ showing the atom labelling scheme. Thermal ellipsoids are at the 50% probability level. Hydrogen atoms are omitted for clarity.	29
Figure 2.2.2	Molecular structure of $[\text{PtMe}_3(4\text{-EtPy})_2\text{I}]$ showing the atom labelling scheme. Thermal ellipsoids are at the 50% probability level. Hydrogen atoms are omitted for clarity.	30
Figure 2.2.3	Molecular structure of $[\text{PtMe}_3(4\text{-OMePy})_2\text{I}]$ showing the atom labelling scheme. Thermal ellipsoids are at the 50% probability level. Hydrogen atoms are omitted for clarity.	31
Figure 2.2.4	Molecular structure of $[\text{PtMe}_3(3\text{-OMePy})_2\text{I}]$ showing the atom labelling scheme. Thermal ellipsoids are at the 50% probability level. Hydrogen atoms are omitted for clarity.	31
Figure 2.2.5	The 400 MHz ^1H NMR spectrum for the reaction of $[\text{PtMe}_3(4\text{-OMePy})_2\text{I}]$ with $[\text{PtMe}_3\text{I}]_4$ in equimolar mixture at equilibrium in CDCl_3 at 300 K. For labelling, see Scheme 2.2.2. (t) = <i>trans</i> - $[\text{PtMe}_3(4\text{-OMePy})\text{I}]_2$. (c) = <i>cis</i> - $[\text{PtMe}_3(4\text{-OMePy})\text{I}]_2$. (m) = $[\text{PtMe}_3(4\text{-OMePy})_2\text{I}]$. X is the solvent peak and Y is the peak for water present in CDCl_3	34
Figure 2.2.6	The 400 MHz ^1H NMR spectrum for the reaction of $[\text{PtMe}_3(3\text{-ClPy})_2\text{I}]$ with $[\text{PtMe}_3\text{I}]_4$ in equimolar mixture at equilibrium in CDCl_3 at 300 K. For labelling, see Scheme 2.2.2. (t) = <i>trans</i> - $[\text{PtMe}_3(3\text{-ClPy})\text{I}]_2$. (c) = <i>cis</i> - $[\text{PtMe}_3(3\text{-ClPy})\text{I}]_2$. (m) = $[\text{PtMe}_3(3\text{-ClPy})_2\text{I}]$. X is the solvent peak and Y is the peak for water present in CDCl_3	35
Figure 2.3.1	Molecular structure of <i>trans</i> - $[\text{PtMe}_3(\text{py})\text{I}]_2$ showing the atom labelling scheme. Thermal ellipsoids are at the 50% probability level. Pt---Pt distance is 4.07 Å. Hydrogen atoms omitted for clarity.	45
Figure 2.3.2	Molecular structure of <i>cis</i> - $[\text{PtMe}_3(4\text{-EtPy})\text{I}]_2$ showing the atom labelling scheme. Thermal ellipsoids are at the 50% probability level. Pt---Pt distance is 4.05 Å. Hydrogen atoms omitted for clarity.	45
Figure 2.3.3	Molecular structure of <i>cis</i> - $[\text{PtMe}_3(4\text{-OMePy})\text{I}]_2$ showing the atom labelling scheme. Thermal ellipsoids are at the 50% probability level. Pt---Pt distance is 4.06 Å. Hydrogen atoms omitted for clarity.	46
Figure 2.3.4	Molecular structure of <i>cis</i> - $[\text{PtMe}_3(4\text{-CNPy})\text{I}]_2$ showing the atom labelling scheme. Thermal ellipsoids are at the 50% probability level. Pt---Pt distance is 4.06 Å. Hydrogen atoms omitted for clarity.	47

Figure 2.3.5	Molecular structure of <i>cis</i> -[PtMe ₃ (3-ClPy)] ₂ showing the atom labelling scheme. Thermal ellipsoids are at the 50% probability level. Pt---Pt distance is 4.03 Å. Hydrogen atoms omitted for clarity.	47
Figure 3.1	The 400 MHz ¹ H NMR spectrum of [PtMe ₃ (OMe-bipy)]I in CDCl ₃ at 300 K. For labelling, see inset. X is the solvent peak and Y is the peak for water present in CDCl ₃	52
Figure 3.2	Molecular structure of [PtMe ₃ (bipy)]I showing the atom labelling scheme. Thermal ellipsoids are at the 50% probability level. Hydrogen atoms are omitted for clarity.	54
Figure 3.3	Molecular structure of [PtMe ₃ (4Me-bipy)]I showing the atom labelling scheme. Thermal ellipsoids are at the 50% probability level. Hydrogen atoms are omitted for clarity.	55
Figure 3.4	Molecular structure of [PtMe ₃ (5Me-bipy)]I showing the atom labelling scheme. Thermal ellipsoids are at the 50% probability level. Hydrogen atoms are omitted for clarity.	55
Figure 3.5	Molecular structure of [PtMe ₃ (OMe-bipy)]I showing the atom labelling scheme. Thermal ellipsoids are at the 50% probability level. Hydrogen atoms are omitted for clarity.	56
Figure 3.6	Molecular structure of [PtMe ₃ (Me ₂ N-bipy)]I showing the atom labelling scheme. Thermal ellipsoids are at the 30% probability level. Hydrogen atoms are omitted for clarity.	56
Figure 3.7	Unit cell structure of [PtMe ₃ (bipy)]I. Thermal ellipsoids are at the 50% probability level. Hydrogen atoms are omitted for clarity.	57
Figure 3.8	Unit cell structure of [PtMe ₃ (4Me-bipy)]I showing solvent benzene. Thermal ellipsoids are at the 50% probability level. Hydrogen atoms are omitted for clarity.	57
Figure 3.9	Molecular structure of [PtMe ₃ (Cl-bipy)]I showing the atom labelling scheme. Thermal ellipsoids are at the 50% probability level. Hydrogen atoms are omitted for clarity.	60
Figure 3.10	A perspective view of [PtMe ₃ (Cl-bipy)]I showing the intermolecular interaction (red colour dotted bond) between the hydrogen atom (H) and chlorine atom (Cl1).	61
Figure 3.11	A perspective view of an infinite chain of one dimensional <i>zig-zag</i> structure of [PtMe ₃ (Cl-bipy)]I.	62

Figure 3.12	A perspective view of a two-dimensional framework structure of [PtMe ₃ (Cl-bipy)I].	62
Figure 4.1	The platinum-methyl region in the ¹ H NMR spectrum of an equimolar mixture of [PtMe ₃ (py) ₂ I] and bipy in nitrobenzene-d ₅ at equilibrium at 300 K showing presence of three platinum(IV) complexes [PtMe ₃ (py) ₂ I] (I), [PtMe ₃ (bipy)I] (II) and [PtMe ₃ (bipy)(py)]I (III). For labelling, see Scheme 4.2.	66
Figure 4.2	The methoxy region in the ¹ H NMR spectrum of an equimolar mixture of [PtMe ₃ (4-OMePy) ₂ I] and OMe-bipy in CDCl ₃ at equilibrium at 300 K. I = [PtMe ₃ (4-OMePy) ₂ I]. II = [PtMe ₃ (OMe-bipy)I]. III = [PtMe ₃ (OMe-bipy)(4-OMePy)]I. The signal at the left correspond to the methoxy group of OMe-bipy in complex III, while the signal at the utmost right corresponds to the methoxy group of the 4-OMePy in complex III.	66
Figure 6.1	Molecular structure of [PtMe ₃ (4-DMAP) ₂ I] showing the atom labelling scheme. Thermal ellipsoids are at the 50% probability level. Hydrogen atoms are omitted for clarity.	107
Figure 6.2	Molecular structure of <i>trans</i> -[PtMe ₃ (py)I] ₂ showing the atom labelling scheme. Thermal ellipsoids are at the 50% probability level. Hydrogen atoms omitted for clarity.	107
Figure 6.3	Molecular structure of [PtMe ₃ (OMe-bipy)I] showing the atom labelling scheme. Thermal ellipsoids are at the 50% probability level. Hydrogen atoms are omitted for clarity.	109
Figure 6.4	A perspective view of a two-dimensional framework structure of [PtMe ₃ (Cl-bipy)I].	110
Abb. 7.1	Molekulare Struktur von [PtMe ₃ (4-DMPA) ₂ I]. Thermische Ellipsoide sind am 50% Wahrscheinlichkeitslevel. Wasserstoffatome wurden zur besseren Übersichtlichkeit weggelassen.	112
Abb. 7.2	Molekulare Struktur von <i>trans</i> -[PtMe ₃ (py)I] ₂ . Thermische Ellipsoide sind am 50% Wahrscheinlichkeitslevel. Wasserstoffatome wurden zur besseren Übersichtlichkeit weggelassen.	112
Abb. 7.3	Molekulare Struktur von [PtMe ₃ (OMe-Bipy)I]. Thermische Ellipsoide sind am 50% Wahrscheinlichkeitslevel. Wasserstoffatome wurden zur besseren Übersichtlichkeit weggelassen.	114
Abb. 7.4	Die zweidimensionale Gerüststruktur von [PtMe ₃ (Cl-bipy)I].	115

8.4 Tables

Table 2.1.1	Selected bond lengths [Å] and angles [°] for [PtMe ₃ (4-DMAP) ₂ I] (1).....	18
Table 2.1.2	Selected bond lengths [Å] and angles [°] for [PtMe ₃ (3-BrPy) ₂ I] (2).....	18
Table 2.1.3	¹ H NMR data ^a of 4-DMAP, 3-BrPy and 4-CNPY complexes of iodotrimethylplatinum(IV) in CDCl ₃ at 300 K	25
Table 2.1.4	Concentration-dependent solution behaviour of [PtMe ₃ L ₂ I] complexes (L = 4-DMAP, 3-BrPy, 4-CNPY).....	26
Table 2.2.1	Selected bond lengths [Å] and angles [°] for [PtMe ₃ L ₂ I] (L = 4-MePy, 4-EtPy, 4-OMePy, 3-OMePy) complexes	32
Table 2.2.2	¹ H NMR data ^a for the reaction of [PtMe ₃ I] ₄ with [PtMe ₃ L ₂ I] at equilibrium at 300 K (L = 4-substituted pyridines) in CDCl ₃	36
Table 2.2.3	¹ H NMR data ^a for the reaction of [PtMe ₃ I] ₄ with [PtMe ₃ L ₂ I] at equilibrium at 300 K (L = 3-substituted pyridines) in CDCl ₃	38
Table 2.2.4	Population ratios of different Pt(IV) species for the reaction of an equimolar mixture of [PtMe ₃ L ₂ I] (L = 4-substituted pyridines) with iodotrimethylplatinum(IV) in CDCl ₃ at equilibrium at 300 K	40
Table 2.2.5	Population ratios of different Pt(IV) species for the reaction of an equimolar mixture of [PtMe ₃ L ₂ I] (L = 3-substituted pyridines) with iodotrimethylplatinum(IV) in CDCl ₃ at equilibrium at 300 K.....	40
Table 2.3.1	Selected bond lengths [Å] and angles [°] for <i>trans</i> -[PtMe ₃ (py)I] ₂	48
Table 2.3.2	Selected bond lengths [Å] and angles [°] for <i>cis</i> -[PtMe ₃ (4-EtPy)I] ₂	48
Table 2.3.3	Selected bond lengths [Å] and angles [°] for <i>cis</i> -[PtMe ₃ (4-OMePy)I] ₂	48
Table 2.3.4	Selected bond lengths [Å] and angles [°] for <i>cis</i> -[PtMe ₃ (4-CNPY)I] ₂	49
Table 2.3.5	Selected bond lengths [Å] and angles [°] for <i>cis</i> -[PtMe ₃ (3-ClPY)I] ₂	49
Table 3.1	¹ H NMR data ^a for the [PtMe ₃ (L-L)I] (L-L = 2,2'-bipyridine and its derivatives) complexes in CDCl ₃ at 300 K	53
Table 3.2	Selected bond lengths [Å] and angles [°] for [PtMe ₃ (bipy)I].....	59
Table 3.3	Selected bond lengths [Å] and angles [°] for [PtMe ₃ (L-L)I] (L-L = 4Me-bipy, 5Me-bipy, OMe-bipy, Me ₂ N-bipy) complexes	59
Table 3.4	Selected bond lengths [Å] and angles [°] for [PtMe ₃ (Cl-bipy)I].....	61
Table 4.1	¹ H NMR data ^a for the reaction of an equimolar mixture of [PtMe ₃ L ₂ I] (L = pyridines) and corresponding 2,2'-bipyridines at equilibrium at 300 K in CDCl ₃ and in nitrobenzene-d ₅	68

Table 4.2	The reaction of an equimolar mixture of [PtMe ₃ L ₂ I] (L = pyridines) and corresponding 2,2'-bipyridines (L-L) at equilibrium at 300 K in CDCl ₃ and in nitrobenzene-d ₅ ^{a, b}	69
Table 5.4.1	Crystal data and structure refinement for [PtMe ₃ (4-DMAP) ₂ I].....	89
Table 5.4.2	Crystal data and structure refinement for [PtMe ₃ (3-BrPy) ₂ I].....	90
Table 5.4.3	Crystal data and structure refinement for [PtMe ₃ (4-MePy) ₂ I].....	91
Table 5.4.4	Crystal data and structure refinement for [PtMe ₃ (4-EtPy) ₂ I].....	92
Table 5.4.5	Crystal data and structure refinement for [PtMe ₃ (4-OMePy) ₂ I].....	93
Table 5.4.6	Crystal data and structure refinement for [PtMe ₃ (3-OMePy) ₂ I].....	94
Table 5.4.7	Crystal data and structure refinement for <i>trans</i> -[PtMe ₃ (py)I] ₂	95
Table 5.4.8	Crystal data and structure refinement for <i>cis</i> -[PtMe ₃ (4-EtPy)I] ₂	96
Table 5.4.9	Crystal data and structure refinement for <i>cis</i> -[PtMe ₃ (4-OMePy)I] ₂	97
Table 5.4.10	Crystal data and structure refinement for <i>cis</i> -[PtMe ₃ (4-CNPy)I] ₂	98
Table 5.4.11	Crystal data and structure refinement for <i>cis</i> -[PtMe ₃ (3-ClPy)I] ₂ . [PtMe ₃ I] ₄	99
Table 5.4.12	Crystal data and structure refinement for [PtMe ₃ (bipy)I].....	100
Table 5.4.13	Crystal data and structure refinement for [PtMe ₃ (4Me-bipy)I]. 0.5 C ₆ H ₆	101
Table 5.4.14	Crystal data and structure refinement for [PtMe ₃ (5Me-bipy)I].....	102
Table 5.4.15	Crystal data and structure refinement for [PtMe ₃ (OMe-bipy)I].....	103
Table 5.4.16	Crystal data and structure refinement for [PtMe ₃ (Me ₂ N-bipy)I].....	104
Table 5.4.17	Crystal data and structure refinement for [PtMe ₃ (Cl-bipy)I].....	105

8.5 Table of Schemes

Scheme 1.1	Platinum(II) compounds exhibit anti-cancer activity.	2
Scheme 1.2	Proposed mechanism for the oxidation of methane to methanol. ^[12,14b]	3
Scheme 1.3	Mechanism for the reductive elimination of ethane from [PtMe ₃ L ₂ I] (L = tertiary phosphane ligand). ^[15a, 15c]	3
Scheme 1.4	Bulky anionic N,N-chelating ligands (I-III) and neutral N,N-chelating ligand (IV) which stabilize five-coordinate platinum(IV) species.	4
Scheme 1.5	Effect of different bases on trimethylplatinum(IV) triflate complex. TMEDA = N,N,N',N'-tetramethylethylenediamine, PMDTA = N,N,N',N'',N'''-pentamethyldiethylenetriamine). ^[36]	6
Scheme 1.6	Effect of nitrogen ligands on iodotrimethylplatinum(IV) complex. py = pyridine, bipy = 2,2'-bipyridine, en = ethylenediamine. ^[37-39]	6
Scheme 1.7	The fluxional behaviour of [PtMe ₃ (TMEDA)OTf] (OTf = OSO ₂ CF ₃). ^[41]	6
Scheme 1.8	The fluxional behaviour of [PtMe ₃ (ppdm)(H ₂ O)] where ppdm = 1-phenylpropane-1,2-dione 2-oximate. ^[47]	7
Scheme 1.9	Effect of 1,2-metallotropic shift in [PtMe ₃ (pydz) ₂ X] (where X = Cl, Br, I; pydz = pyridazine) complexes. ^[51]	7
Scheme 1.10	[Mg(EDTA)] ²⁻ chelate complex.	8
Scheme 1.11	Different pyridines used for the solution behaviour study of [PtMe ₃ L ₂ I] (L = pyridines) complexes.	12
Scheme 1.12	Different pyridines (4- and 3-substituted) used for the reaction of [PtMe ₃ L ₂ I] with iodotrimethylplatinum(IV).	13
Scheme 1.13	Different 2,2'-bipyridines.	14
Scheme 2.1.1	Different substituted pyridines.	15
Scheme 2.1.2	The dissociation of [PtMe ₃ (3-BrPy) ₂ I] (2) into <i>cis</i> and <i>trans</i> -[PtMe ₃ (3-BrPy)I] ₂ and 3-bromopyridine (3-BrPy) in CDCl ₃ (showing the labelling).	20
Scheme 2.1.3	The dissociation of [PtMe ₃ (4-CNPy) ₂ I] (3) into <i>cis</i> and <i>trans</i> -[PtMe ₃ (4-CNPy)I] ₂ and 4-cyanopyridine (4-CNPy) in CDCl ₃ (showing the labelling).	22
Scheme 2.2.1	Different substituted pyridines used for the reaction of [PtMe ₃ L ₂ I] with [PtMe ₃ I] ₄	28

Scheme 2.2.2	The reaction of an equimolar mixture of iodotrimethylplatinum(IV) and mononuclear [PtMe ₃ L ₂ I] (L = 4- and 3-substituted pyridines) complexes in chloroform showing the proton labelling.	33
Scheme 3.1	2,2'-Bipyridine and its derivatives.	50
Scheme 3.2	Reaction of iodotrimethylplatinum(IV) with 2,2'-bipyridine and its derivatives in benzene.	51
Scheme 4.1	Different pyridines and corresponding 2,2'-bipyridines used for the chelation reaction in trimethylplatinum(IV) system.	64
Scheme 4.2	The substitution of pyridine ligands by the corresponding 2,2'-bipyridines in iodotrimethylplatinum complexes.	65
Scheme 4.3	The substitution of 4-DMAP by Me ₂ N-bipy in iodotrimethylplatinum(IV) complex.	67
Scheme 6.1	The pyridine and 2,2'-bipyridine ligands used in this doctoral work.	106
Scheme 6.2	The reaction of an equimolar mixture of iodotrimethylplatinum and mononuclear [PtMe ₃ L ₂ I] (L= pyridines) leading to the formation of <i>cis</i> and <i>trans</i> dinuclear complexes.	108
Scheme 6.3	The dissociation of mononuclear pyridine complexes of iodotrimethylplatinum(IV), showing the formation of dinuclear complexes. L = 4-CNPy, 3-BrPy.	108
Scheme 6.4	The substitution of pyridine ligands by the corresponding 2,2'-bipyridines in iodotrimethylplatinum(IV) complex	110
Scheme 6.5	The substitution of 4-DMAP by Me ₂ N-bipy in iodotrimethylplatinum(IV) complex.	110
Schema 7.1	Übersicht der in dieser Arbeit verwendeten Pyridine und 2,2'-Bipyridine. ...	111
Schema 7.2	Die Reaktion einer äquimolaren Mischung aus Iodidotrimethylplatin(IV) und mononuklearem [PtMe ₃ L ₂ I] (L = Pyridin), die zur Bildung von dinuklearen <i>cis</i> - und <i>trans</i> - Komplexen führt.	113
Schema 7.3	Die Dissoziation von mononuklearen Pyridin-Komplexen von Iodidotrimethylplatin zu dinuklearen Komplexen (L = 4-CNPy, 3-BrPy).	113
Schema 7.4	Die Substitution von Pyridinliganden durch die korrespondierenden 2,2'-Bipyridine an Iodidotrimethylplatin(IV)-Komplexen (R = H, Me, OMe).	115
Schema 7.5	Die Substitution von 4-DMAP durch Me ₂ N-bipy an Iodidotrimethylplatin(IV)-Komplexen.	115

8.6 Acknowledgements

I am grateful to many for the support and encouragement they provided me throughout the course of this study, without them, it would have never been possible. I would specially like to acknowledge the following:

I would like to express my heartfelt gratitude to Prof. Dr. Sabine Schlecht for giving me the opportunity and the facilities to carry out this thesis work in her working group, for all her ideas, scientific discussions and enormous encouragement.

I am thankful to Prof. Dr. Siegfried Schindler for the second supervision of this doctoral work.

I thank Deutsche Forschungsgemeinschaft (SFB 765) for the financial support.

I am thankful to Dr. Michael Serafin, Dr. Christian Würtele, Alexander Beitat, Günter Koch and Prof. Dr. Dieter Lentz for the X-ray crystallographic measurements.

I convey my sincere thanks to Dr. Heike Hausmann for the ^1H DOSY NMR measurements, G. Stammer and A. Pospiech for ^1H NMR and IR measurements, Dr. E. Röcker for the EI-MS measurements, R. Meurer for CHN analyses, E. Reitz for installing TOPSPIN NMR software. Special thanks to Bernadette Landschreiber for translating the summary and proof reading, Gwyneth Schulz, Christian Rohner and Isabella Tavernaro for proof reading this work.

I wish to thank all my colleagues in Giessen and in Berlin, Dr. Christoph Erk, Christian Rohner, Bernadette Landschreiber, Isabella Tavernaro, Weizhe Meng, Dr. Michael Serafin, Gwyneth Schulz, Marcel Nebe, Dr. Meike Roskamp, Denis Petri, Dr. Marina Artamonova, Christian Uhlig, Marc Loeh, Ekrem Güneş, Dr. Wolfgang Herrendorf, Günter Koch, Hubert Wörner, Michaela Jakubowski, Petra Grundmann, Rita Freise, Dr. Ivan Angelov, Sven Kroker, for creating friendly atmosphere in the laboratory.

I would also like to thank David Ley, Dr. Attila Farkas and all the members of Prof. Schindler's working group for their help.

I thank Dr. Krishnendu Mukherjee, Dr. Chandan Maity, Hari, Subrata, Susnata, Ankit, Minidi, Indranil and all other friends for making my life much easier in Germany. Finally, I am indebted to my family, for the love, affection, blessings and inspiration.

8.7 Publications

- Biswa Nath Ghosh, Heike Hausmann, Dieter Lentz and Sabine Schlecht
“A Comparative Study of the Solution Behaviour of Some Iodotrimethylplatinum(IV) Complexes of Pyridines. Crystal structure of Iodotrimethylbis-(4-dimethylaminopyridine)platinum(IV)” Submitted to *J. Organomet. Chem.*, **2011**.
- Biswa Nath Ghosh, Dieter Lentz and Sabine Schlecht
“Substituent Effects on the Reaction of Trimethylplatinum(IV) iodide Complexes of Pyridines with Tetrameric Iodotrimethylplatinum(IV)” *to be submitted*.
- Biswa Nath Ghosh, Michael Serafin and Sabine Schlecht
“Ligand-Exchange Study on Trimethylplatinum(IV) Complexes of Pyridines” *in preparation*.
- Biswa Nath Ghosh, Michael Serafin and Sabine Schlecht
“Crystallographic Characterization of Dinuclear Iodotrimethylplatinum(IV) Complexes Containing Pyridine Ligands” *in preparation*.

Poster Presentation

- Biswa Nath Ghosh, Dieter Lentz and Sabine Schlecht
Title: “Multivalent Binding at Noble Metal Centers”, ‘1st Molecular Science Workshop in Berlin, Germany, **2009**.

Oral Presentations

- “Synthesis, Structure and Solution Behaviour of Iodotrimethylplatinum(IV) Complexes”, *Nanotage 2010*, Bad Herrenalb, Germany, **2010**.
- “Iodotrimethylplatinum(IV) Complexes of Pyridines”, *Nanotage 2011*, Altenberg, Germany, **2011**.

Der Lebenslauf wurde aus der elektronischen Version der Arbeit entfernt.

The curriculum vitae was removed from the electronic version of the paper.